Charles University

Faculty of Science

Study program: Biology
Field of study: Cell and Developmental Biology

Patrik Hohoš

Charakterizace uzavřené mitózy u kvasinky *Schizosaccharomyces pombe* s narušeným metabolismem lipidů

Characterization of closed mitosis in the fission yeast *Schizosaccharomyces pombe* with perturbed lipid metabolism

Diploma thesis

Supervisor: RNDr. Martin Převorovský, Ph.D.

Prague, 2022

Čestné prohlášení

Prohlašuji, že svou diplomovou práci " Charakterizace uzavřené mitózy u kvasinky Schizosaccharomyces pombe s narušeným metabolismem lipidů" jsem vypracoval samostatně pod vedením vedoucího diplomové práce a s použitím odborné literatury a dalších informačních zdrojů, které jsou citovány v práci a uvedeny v seznamu použitých zdrojů na konci práce. Jako autor uvedené diplomové práce dále prohlašuji, že jsem v souvislosti s jejím vytvořením neporušil autorská práva třetích osob.

V Praze dne 26.04.2022 _____

Aknowledgements

I would like to thank my supervisor RNDr. Martin Převorovský for the support, patience and his overall engagement in the study. I am grateful to all of the current and former members of the research group. I wish to namely thank Akshay Vishwanatha for the establishment of methods used in this study and preliminary data leading to this study, Viacheslav Zemlianski for his tremendous help with the technical aspects of the methods used in this study (mainly microscopic methods), Anna Marešová for her encouragement, help with the cultivations and detailed protocols of methods, Jarmila Princová for her help with cultivations and fruitful discussions and Kateřina Jelínková for her encouragement and technical support of the experiments. Last but not least, I would love to thank my family, friends and my fiancée for their relentless support during my whole studies and Michal Bogdan for the language corrections.

Abstract [EN]

The division of an eukaryotic cell is mediated by the process of mitosis. It is a complex cellular process which needs to be highly regulated. In contrast to the mammalian open type of mitosis when nuclear envelope is disassembled, fission yeast *Schizosaccharomyces pombe* undergoes closed mitosis inside the intact nuclear compartment. Cell nucleus undergoes morphological changes as a common sphere-shaped nucleus stretches upon mitotic spindle activity forming typical dumbbell structure. Further tension results in the separation of two daughter nuclei. Such extensive changes in the nuclear envelope surface demand a sufficient supply of membrane phospholipids. Cells with perturbed lipid metabolism are unable to meet such a demand and the mitotic division in these cells usually results as a catastrophic mitotic event or CUT (Cell Untimely Torn) phenotype. Moreover, recent studies show genetic interactions between the deletions of the lipid gene regulator *cbf11* and factors maintaining the centromere chromatin structure. Surprisingly, rescue of CUT phenotype has been recently reported after the deletion of several factors contributing to the centromeric H3K9 epigenetic modifications in the cells lacking the transcription factor Cbf11. Here we show no rescue of CUT phenotype after the deletion of histone deacetylases in *cbf11Δ* cells contrasting with the previous unpublished results. We also show consistent changes in mitotic parameters through all of the used *cbf11Δ* mutant strains. To achieve the results, we have successfully optimised the live-cell imaging method and subsequent data analysis. We anticipate this study to be a starting point for deeper research of the connection between lipid metabolism and mitotic fidelity in *Schizosaccharomyces pombe*.

Key words: Fission yeast, closed mitosis, defect, lipid metabolism, transcription factor, microscopy

Abstrakt [SK]

Delenie eukaryotických buniek spočíva v procese mitózy. Ide o komplexný bunkový proces, ktorý je potrebné správne regulovať. Na rozdiel od cicavčieho otvoreného typu mitózy, kedy sa jadrový obal rozpadá, mitóza kvasinky *Schizosaccharomyces pombe* prebieha vo vnútri neporušeného jadrového obalu. Takýto typ mitózy sa nazýva uzavretá mitóza. Bunkové jadro však prechádza morfologickými zmenami. Vplyvom aktivity mitotického vretienka sa bunkové jadro počas delenia sa naťahuje a vytvára typickú činkovitú štruktúru. Zvyšovanie pnutia vplyvom mitotického vretienka má za následok rozdelenie dvoch dcérskych jadier. Takéto rozsiahle zmeny povrchu jadrového obalu vyžadujú dostatočný prísun membránových fosfolipidov. Bunky s narušeným metabolizmom lipidov nie sú schopné vytvoriť dostatočnú zásobu lipidov a mitotické delenie v týchto bunkách zvyčajne vedie ku katastrofickej mitotickej udalosti inak nazývanej CUT (Cell Untimely Torn) fenotyp. Nedávne štúdie zároveň popisujú genetické interakcie medzi deléciami *cbf11* a faktormi zodpovednými za údržbu štruktúry chromatínu prítomného v oblastiach centromér. Bolo dokonca ukázané vymiznutie fenotypu CUT po delécii niektorých faktorov prispievajúcich k centromerickým epigenetickým modifikáciám H3K9 v bunkách s deléciou transkripčného faktoru Cbf11. Táto diplomová práca vyvracia predošlé nepublikované závery a ukazuje prítomnosť fenotypu CUT aj po delécii histónových deacetyláz v bunkách *cbf11Δ*. Práca tiež poukazuje na konzistentné zmeny v mitotických parametroch naprieč všetkými použitými mutantnými kmeňmi *cbf11Δ*. Úspešná optimalizácia metódy mikroskopie živých buniek a následná analýza dát nám poskytla nástroj pre dosiahnutie vytýčených cieľov. Predpokladáme, že táto práca bude východiskovým bodom pre hlbší výskum spojenia medzi metabolizmom lipidov a presnosťou mitózy u *Schizosaccharomyces pombe*.

Kľúčové slová: Štiepna kvasinka, uzavretá mitóza, defekt, metabolizmus lipidov, transkripční faktor, mikroskopia

Table of contents

List of abbreviations

ACC Acetyl coenzyme A carboxylase
CENP-A Centromere protein A
ChIP-seq Chromatin immunoprecipitation assay with sequencing
CLRC CRL4-like Clr4 complex
CSL CBF1/RBP-Jκ/Suppressor of Hairless/LAG-1
Ctrl Control
CUT Cell Untimely Torn
DAG Diacylglycerol
DAPI 4′,6-diamidine-2′-phenylindole dihydrochloride
dH2O Deionised water
DMSO Dimethylsulfoxide
EDTA Ethylenediaminetetraacetic acid
EMM Edinburgh Minimal Medium
FAS Fatty Acid Synthase
FD FastDigest
gDNA genomic DNA
GFP Green Fluorescent Protein
H3K9 Lysine 9 of histone H3
H3K9ac Acetylated lysine 9 of histone H3
H3K9me2 Dimethylated lysine 9 of histone H3
H3K9me2/3 Dimethylated or trimethylated lysine 9 of histone H3
H3K9me3 Trimethylated lysine 9 of histone H3
H3S10 Serine 10 of histone H3
HAT Histone acetyltransferase
HDAC Histone deacetylase
Hyg Hygromycin B
Kan Kanamycin
LiAc Lithium acetate
LSD Large and Small Daughter nuclei
M Marker
ME Malt Extract
MS Microsoft
NAD Nicotinamide adenine dinucleotide
Nat Nourseothricine
NCBI National Center of Biotechnology Information
ncRNA non-coding RNA
NICD Notch intracellular domain
OD_{600} Optical density
ORF Open Reading Frame
PA Phosphatidic acid
PCR Plymerase Chain Reaction
PDMS Polydimethylsiloxane
PEG Polyethylene glycol
PFS Perfect Focus System
PKC Protein kinase C
PL Phospholipid
rDNA DNA encoding ribosomal RNA
RDRC RNA-directed RNA polymerase complex
RITS RNA-induced transcriptional silencing
RNAi RNA interference
SAC Spindle Assembly Checkpoint
SAGA Spt-Ada-Gcn5 acetyltransferase
SDS Sodium dodecyl sulfate
SHREC Snf2/Hdac-containing Repressor Complex
siRNA silencing RNA
TAE Tris, acetic acid and EDTA
TAG Triacylglycerol
TE Tris and EDTA
UV Ultra violet
WT Wild type
YES Yeast Extract Supplemented

1 Introduction

Mitosis is a complex process crucial for cell reproduction. During the mitotic progression, it is crucial to equally distribute the genetic information into the daughter cells. Defects in the genetic information distribution can result in aneuploidy or catastrophic mitosis. To avoid the mitotic failure, the mitotic process must be controlled and regulated. The fission yeast, *Schizosaccharomces pombe*, is a widely used model microorganism for studies of cell cycle progression and regulation. However, *S. pombe* undergoes closed mitosis different to mammalian open mitosis. The process chromosome segregation during the closed mitosis occurs inside the intact nuclear compartment. Only after the sister chromatid segregation, the nucleus is pushed to the opposite poles of the cell during the anaphase and start to divide. Failures in the coordination and regulation of this process lead to intersection of undivided nucleus by the developing septum. Such catastrophic mitotic event is called CUT (Cell Untimely Torn) phenotype and is considered lethal. Intriguingly studies of lipid metabolism show a connection between the lipid metabolism and mitotic fidelity. Inhibition of the fatty acid synthase or downregulation of acetylcoenzyme A carboxylase function results in high frequencies of CUT phenotype incidence (Převorovský et al., 2009, 2016; Zach et al., 2018). The crucial role of lipid metabolism in the nuclear envelope expansion during anaphase was highlighted by the recent study of nuclear surface dynamics during the mitosis (Takemoto et al., 2016). The process of nuclear expansion requires an adequate supply of membrane phospholipid, which is impaired in the cells with perturbed lipid metabolism (Zach et al., 2018). Failure to expand the nucleus during anaphase is coupled with mitotic spindle bending and subsequent breaking, chromosome segregation defects and the CUT phenotype (Převorovský et al., 2016; Takemoto et al., 2016).

Cbf11 is a transcription factor from the CSL (CBF1/RBP-Jκ/Suppressor of Hairless/LAG-1) family regulating several lipid metabolism genes in fission yeast. It has been shown that cells lacking Cbf11 display morphological defects, altered cell adhesion and catastrophic mitosis or CUT phenotype (Převorovský et al., 2015, 2016). A recent study also showed decreased content of storage lipid droplets in *cbf11Δ* cells supporting the hypothesis of a requirement for adequate capacity of membrane phospholipid production for a successful mitotic division (Zach et al., 2018). However, Cbf11 is also expected to be involved in the process of proper chromosome segregation as negative genetic interaction between the

deletion of *cbf11* and mutations in cohesion loaders and chromatin modification enzymes have been shown (Z. Chen et al., 2012).

Even though, the mitotic process in *S.pombe* is different than in mammalian cells, it's centromere structure is similar. The centromeric chromatin is strongly heterochromatinized for proper kinetochore formation and correct attachment to the mitotic spindle. The correct chromosome segregation is ensured by the mitotic spindle attached to kinetochore of sister chromatids held together by the cohesin rings. Yet, cohesin must be removed during the mitotic progression for the proper segregation of chromatids.

Unpublished data by Akshay Vishwanatha from our laboratory show altered cohesin occupancy and histone H3K9 modifications at the centromeres and aberrant mitotic timing in the cells lacking Cbf11. Strikingly, the rescue of CUT phenotype was also observed after the deletion of several histone deacetylases in cells with perturbed lipid metabolism. However, the experiments were done using strains auxotrophic for various nutrients. As auxotrophic mutations were found to alter a number of cellular processes, we set out to validate some of the experiments using prototrophic strains. We also desired to observe whether the mitotic dynamics change in the HDACΔ *cbf11Δ* cells with reported rescue of CUT phenotype.

2 Hypothesis and thesis objectives

2.1 Hypothesis

Deletion of histone deacetylases can rescue the catastrophic mitosis of the prototrophic *Schizosaccharomyces pombe* cells with perturbed lipid metabolism through yet-to-be-defined mechanisms.

2.2 Thesis objectives

In this study, we aim to analyse the mitotic progression in the HDACΔ *cbf11Δ* deletion mutant fission yeast strains. To achieve this objective we need to:

- Create the prototrophic strains
    - With fluorescently tagged chromatin and spindle components
    - With fluorescently tagged chromatin and spindle components together with deletion mutations of all non-essential fission yeast HDACs
    - With fluorescently tagged chromatin and spindle components together with the *cbf11* deletion mutation
    - With fluorescently tagged chromatin and spindle components together with deletion mutations of all non-essential fission yeast HDACs and *cbf11*
- Optimize the live-cell imaging method
- Establish and optimize the live-cell imaging data analysis
- Characterise the mitotic parameters of the strains of interest

3 Materials and methods

3.1 *Schizosaccharomyces pombe* strains used in this study and their cultivation

3.1.1 List of strains

Strain ID	Genotype	Source
JB32	*h⁺ WT*	Lab stock
JB710	*h⁻ ura4-D18*	Juan Mata
JB959	*h⁻ sir2Δ::KanMX4*	Babis Rallis
MP207	*h⁻ hst2Δ::KanMX4*	Karl Ekwall lab, Hu1251
MP208	*h⁻ hst4Δ::KanMX4*	Karl Ekwall lab, Hu1481
MP209	*h⁻ hos2Δ::leu2 leu1-32*	Karl Ekwall lab, Hu1026
MP210	*h⁻ clr3Δ::KanMX4*	Karl Ekwall lab, Hu1024
MP739	*h⁻ hos2Δ::LEU2 leu1-32 cbf11Δ::NatR*	Akshay Vishwanatha (unpublished)
MP741	*h⁻ sir2Δ::KanMX4 cbf11Δ::NatR*	Akshay Vishwanatha (unpublished)
MP752	*h⁺ mCherry-atb2-HygR hht2-GFP:ura4+ ade6-21? Leu1-32 ura4-D18*	(Lin et al., 2017)
MP807	*h⁺ mCherry-atb2-HygR hht2-GFP:ura4+ ura4-D18*	This study
MP808	*h⁻ mCherry-atb2-HygR hht2-GFP:ura4+ ura4-D18*	This study
MP843	*mCherry-atb2-HygR hht2-GFP:ura4+ ura4-D18 cbf11Δ::NatR* (clone 1)	This study
MP844	*mCherry-atb2-HygR hht2-GFP:ura4+ ura4-D18 cbf11Δ::NatR* (clone 2)	This study
MP847	*mCherry-atb2-HygR hht2-GFP:ura4+ ura4-D18? Sir2Δ::KanMX4* (clone 1)	This study
MP848	*mCherry-atb2-HygR hht2-GFP:ura4+ ura4-D18? Sir2Δ::KanMX4* (clone 2)	This study
MP849	*mCherry-atb2-HygR hht2-GFP:ura4+ ura4-D18? Hst2Δ::KanMX4* (clone 1)	This study
MP850	*mCherry-atb2-HygR hht2-GFP:ura4+ ura4-D18? Hst2Δ::KanMX4* (clone 2)	This study
MP851	*mCherry-atb2-HygR hht2-GFP:ura4+ ura4-D18? Hst4Δ::KanMX4* (clone 1)	This study

MP852	*mCherry-atb2-HygR hht2-GFP:ura4+ ura4-D18? Hst4Δ::kanMX4* (clone 2)	This study
MP853	*mCherry-atb2-HygR hht2-GFP:ura4+ ura4-D18? Clr3Δ::KanMX4* (clone 1)	This study
MP854	*mCherry-atb2-HygR hht2-GFP:ura4+ ura4-D18? Clr3Δ::KanMX4* (clone 2)	This study
MP861	*mCherry-atb2-HygR hht2-GFP:ura4+ ura4-D18? Sir2Δ::KanMX4 cbf11Δ::NatR* (clone 1)	This study
MP862	*mCherry-atb2-HygR hht2-GFP:ura4+ ura4-D18? Sir2Δ::KanMX4 cbf11Δ::NatR* (clone 2)	This study
MP868	*mCherry-atb2-HygR hht2-GFP:ura4+ ura4-D18? Hst2Δ::KanMX4 cbf11Δ::NatR*	This study
MP870	*mCherry-atb2-HygR hht2-GFP:ura4+ ura4-D18? Clr3Δ::KanMX4 cbf11Δ::NatR* (clone 1)	This study
MP871	*mCherry-atb2-HygR hht2-GFP:ura4+ ura4-D18? Clr3Δ::KanMX4 cbf11Δ::NatR* (clone 2)	This study
MP884	*mCherry-atb2-HygR hht2-GFP:ura4+ ura4-D18? Hst4Δ::KanMX4 cbf11Δ::NatR* (clone 1)	This study
MP885	*mCherry-atb2-HygR hht2-GFP:ura4+ ura4-D18? Hst4Δ::KanMX4 cbf11Δ::NatR* (clone 2)	This study
MP886	*mCherry-atb2-HygR hht2-GFP:ura4+ ura4-D18? Hst4Δ::KanMX4 cbf11Δ::NatR* (clone 3)	This study
MP887	*mCherry-atb2-HygR hht2-GFP:ura4+ ura4-D18? Hst4Δ::KanMX4 cbf11Δ::NatR* (clone 4)	This study
MP888	*mCherry-atb2-HygR hht2-GFP:ura4+ ura4-D18? Hst4Δ::KanMX4 cbf11Δ::NatR* (clone 5)	This study
MP943	*mCherry-atb2-HygR hht2-GFP:ura4+ ura4-D18? Hos2Δ::leu2 leu1-32* (clone 1)	This study
MP944	*mCherry-atb2-HygR hht2-GFP:ura4+ ura4-D18? Hos2Δ::leu2 leu1-32* (clone 2)	This study
MP945	*mCherry-atb2-HygR hht2-GFP:ura4+ ura4-D18? Hos2Δ:: leu2 leu1-32* (clone 3)	This study
MP959	*mCherry-atb2-HygR hht2-GFP:ura4+ ura4-D18? Hos2Δ:: leu2 leu1-32 cbf11Δ::NatR* (clone 1)	This study
MP960	*mCherry-atb2-HygR hht2-GFP:ura4+ ura4-D18? Hos2Δ:: leu2 leu1-32 cbf11Δ::NatR* (clone 2)	This study
MP961	*mCherry-atb2-HygR hht2-GFP:ura4+ ura4-D18? Hos2Δ:: leu2 leu1-32 cbf11Δ::NatR* (clone 3)	This study

3.1.2 List of used antibiotics

Antibiotic	Abbreviation	Stock concentration	Working concentration	Manufacturer
Hygromycin B	hygB	100 mg/ml	100 µg/ml	Invivogen
G418 Geneticin	G-418	100 mg/ml	100 µg/ml	Life technologies
Nourseothricin	cloNat	100 mg/ml	100 µg/ml	Jena Bioscience

Table 1 – List of used antibiotics in this study

3.1.3 Cultivation methods

All *Schizosaccharomyces pombe* strains used in this study were cultivated in the same manner unless stated otherwise. Yeast cells were withdrawn from the -80°C freezer and plated (small amount of biomass) on solid Yeast Extract Supplemented (YES) medium before every experiment. Plates were then incubated at 32°C for 2-3 days. In the morning the day before the experiment small fraction of biomass was inoculated into 5 ml of liquid YES medium and cultured for approximately 8 hours at 32°C with shaking (180 rpm). The volume of the Erlenmeyer flask used for the cultivation should be at least 10 times bigger than the volume of the cultivated culture. Fulfilment of this condition is crucial for the correct aeration of the culture during the whole cultivation process. After the time frame of approximately 8 hours, the yeast cells are assumed to overcome potential lag phase of growth resulting from the change of the medium state. The growth of the liquid culture was measured based on the optical density at 600 nm (OD_{600}) using WPA Biowave CO8000 Cell Density Meter (Biochrom). An OD_{600} of 1.0 corresponds to approximately 10^7 cells per 1 ml of the culture. Cultures were then diluted with fresh YES medium and grow further to reach the exponential phase of growth corresponding OD_{600} 0.3 – 1.5 in the beginning of the experiment.

There are three types of cultivation media used during this study. Each of the media were sterilised by autoclaving.

- Malt Extract (ME) medium
    - 30 g/l Bacto-Malt Extract
    - 20 g/l bacteriological agar (only solid form of media was prepared) (Oxoid, LP0011)
- Edinburgh Minimal Medium (EMM)

- 12.3 g/l EMM Broth without dextrose (Formedium)
- 20 g/l glucose (Sigma-Aldrich)

- Yeast Extract Supplemented (YES) medium
  - 5 g/l yeast extract (Formedium)
  - 0.25 g/l SP supplements (Formedium, Adenine 50 mg/l, L-Histidine HCl 50 mg/l, L-Leucine 50 mg/l, L-Lysine HCl 50 mg/l, Uracil 50 mg/l)
  - 20 g/l bacteriological agar (if solid medium is prepared) (Oxoid, LP0011)
  - 30 g/l glucose (Sigma-Aldrich)

Aliquote of the Glucose solution (200 g/l) to be added to the YES and EMM media was sterilized by autoclaving separately before adding to the medium to prevent the caramelization in the medium. Glucose is therefore added to the YES and EMM media after autoclaving.

3.1.4 Preparation of glycerol stocks

The yeast strain cultures were stored at -80°C as the glycerol stocks. For the glycerol stocks preparation yeast cells were cultured in the YES medium to the stationary phase of growth (usually for 1-2 days) at 32°C. 600 µl of the cell culture in stationary phase of growth was collected and mixed with 600 µl of sterile 60% glycerol solution. Before storing at -80°C, samples were incubated in ice for 20 minutes.

3.1.5 *Schizosaccharomyces pombe* ethanol fixation

Fixation methods are widely used to halt the internal contents of cells in the particular phase of growth for further microscopy and analysis or other experiments. In this study, the performed fixation method uses 70% (v/v) ethanol. 1 ml of the cell culture grown to exponential phase of growth (exactly as described in the sub-chapter 3.1.3 was transferred to 1.5 ml microcentrifuge tube and collected (1 000 *g*, 3 min). Supernatant was carefully removed, and pellet was resuspended in the 70% (v/v) ethanol. Ethanol fixed cell culture can be stored for several months at 4°C.

3.1.6 *Schizosaccharomyces pombe* genetic crossing

Mating type of the *Schizosaccharomyces pombe* is determined by the occurrence of two possible alleles of the *mat1* locus. Therefore, there are two possible mating types of the

fission yeast: h^+ and h^- (Egel et al., 1984). Fission yeast strains used in the research are heterothallic, which means they are unable to switch between these two mating types. To induce the mating and sporulation of *S. pombe*, h^+ and h^- strains must be mixed and starved for nitrogen. Two cells of opposite mating type then conjugate and sporulate forming an ascus containing four spores (Egel, 2004). Segregants having the desired genotype are then selected using antibiotic resistance cassettes, auxotrophic mutations or other selectable traits (Sabatinos & Forsburg, 2010).

A small amount of biomass was picked from two glycerol stocks of strains with opposite mating type, plated separately on solid YES medium and incubated at 32°C for 2-3 days. A small amount of biomass from both strains was then mixed in 30 µl of sterile deionized water (dH_2O) in a microcentrifuge tube by pipetting. Properly mixed cell suspension was plated on the ME plate and allowed to dry before inverting. The plate was sealed with parafilm and incubated at 25°C for 2-3 days. The success of mating was proved by the presence of asci visualised using differential interference contrast microscopy (Leica DM750). A tiny amount of biomass was transferred to 300 µl β-glucuronidase solution (Sigma-Aldrich, G7017, stock diluted 100X for working solution) in a microcentrifuge tube using a sterile pipette tip and the sample was incubated at 37°C over night. β-glucuronidase solution exterminates all the vegetative cells, digests the ascus wall, and leaves spores in a dormant state. At this stage, spores can be stored at 4°C for several weeks. 50 and 150 µl of the solution was spread on two respective selective plates and incubated at 32°C until sufficient size monocolonies formed

(3-5 days). Monocolonies were picked, plated on fresh selective plates and incubated at 32°C for another 1-2days (until sufficient biomass formed). The desired genotype was finally verified by PCR.

3.1.7 Growth curve measurement and doubling time estimation

The knowledge of the doubling time of the cultures helps to find the right cultivation methods for the future experiments and to describe the phenotype of newly created strains. The doubling time is estimated based on the measurement of the growth curves using microplate reader VarioSkan Flash (Thermo Scientific).

The strains to be measured were cultivated in 5 ml of liquid YES medium at 32°C. As the method observes the overall growth of the cultures, cells do not need to be pre-cultured as

described in the sub-chapter 3.1.3. After approximately 7 hours (2-3 generation times) the amount of the cell suspension corresponding to 0.1 OD_{600} was directly transferred to 12-well plate. To every well of the plate, fresh liquid YES medium was added up to 1.4 ml. Prepared plate was cultivated in the VarioSkan Flash at 32°C with shaking (180 rpm, amplitude 20 mm). Optical density (OD_{600}) of the cultivated cultures in the 12-well plate was measured every 10 minutes. The data were visualised in MS Excel to form a scatterplot, where the x axis represents the time and y axis represents the $\log_2$ of the measured OD_{600} in the particular time point. The doubling time (T) is estimated based on the exponential phase of growth of the culture. Therefore, the exponential phase of growth was extracted from the chart and trend lines of the data were inserted. The doubling time was derived from the equation of the trendlines as follows:

Equation of the trendline: $y = kx + q$

$$\boldsymbol{T = 1/k}$$

3.2 DNA manipulation methods

3.2.1 Plasmids

In this study, there was one plasmid used for *Schiozosaccharomyces pombe* transformation to construct the strains with desired genotype. It was the plasmid for knock-out of the *cbf11* gene based on the pCloneNat1 (Gregan et al., 2006) (Figure 1). This plasmid was edited and modified with the restriction sites to specifically knock-out the *cbf11* gene (Převorovský et al., 2009).

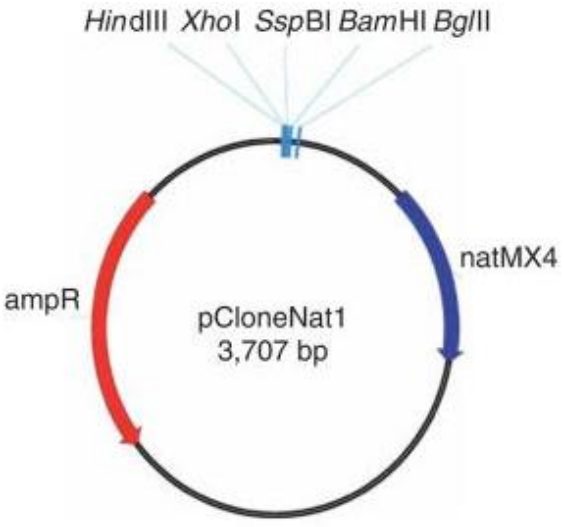

Figure 1 – Map of vector pCloneNat1. Adapted from (Gregan et al., 2006)

In this study, the plasmid was used for the lithium-acetate transformation method by Gregan *et al.* (Gregan et al., 2006) (described in the sub-chapter 3.2.3). It is based on the homologous recombination of the gene of interest with the specific antibiotic resistance cassette. The transformation plasmid ends are designed to be homologous with the upstream and downstream flanking regions of the desired gene. The homologous recombination is triggered by the presence of linear DNA fragment (linearised transformation plasmid).

3.2.2 Plasmid linearization

Plasmids are usually produced and stored in their natural circular form. However, for efficient integration into the genome, linearized form of the plasmid is required. Commonly used technique for plasmid linearization is the reaction with the restriction endonuclease enzymes.

The plasmid used in this study was obtained from Anna Marešová (other member of the group). The circular plasmid was isolated from 10 ml of bacterial culture using alkaline lysis method (Bimboim & Doly, 1979). For concentration estimation, aliquot of the isolated plasmid was loaded on a gel (detailed description of agarose electrophoresis in a sub-chapter 3.2.6). The concentration of the plasmid was estimated to be 2 µg/µl. Plasmid was further linearized using FastDigest XbaI (Thermo Scientiofic, FD0684) restriction endonuclease. The detailed information about the reaction mixture is stated in the Table 2 for reaction volumes of 20 µl or 40 µl used in this study. Prepared samples were incubated for 15 minutes at 37°C. Next, restriction endonuclease reaction was inactivated by incubation for 10 minutes at 65°C. The samples were then cooled on ice and stored at -20°C for further use. To confirm the plasmid linearization, aliquot was loaded on a gel (Agarose electrophoresis described in the sub-chapter 3.2.6). The desired outcome of the agarose electrophoresis is one band visible on the gel corresponding the length of the plasmid (Figure 2).

	V = 20 µl	**V = 40 µl**
Plasmid DNA	2 µl	4 µl
FD XbaI	2 µl	4 µl
FD Buffer	2 µl	4 µl
dH_2O	14 µl	28 µl

Table 2 – Plasmid linearization mixture for 20 µl and 40 µl reaction volume

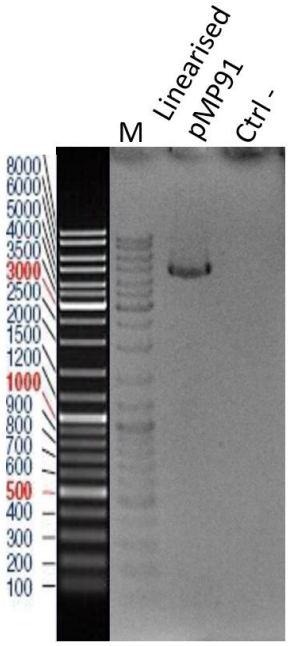

Figure 2 – Verification of plasmid linearisation. Plasmid for fission yeast transformation, pMP91, was linearised using FD XbaI restriction endonuclease enzyme. The aliquot of the reaction was loaded on a 1% agarose gel. The resulting band confirms the linearisation of a plasmid. The size around 5000 bp corresponds with the size of the plasmid. Reaction without template was used as negative control (Ctrl-).

3.2.3 Transformation of *Schizosaccharomyces pombe* using lithium-acetate method

Deletion of the *cbf11* gene in this study was performed by transformation using lithium-acetate method (Gregan et al., 2006). Strains to be transformed were grown to exponential phase of growth as described in the sub-chapter 3.1.3. 5 ml of the culture was collected by centrifugation (1 000 *g*, 3 min) in the 15 ml falcon tube and washed with 5 ml of sterile dH_2O (collecting and washing stands for centrifugation and removal of the supernatant). Washed fission yeast cells were resuspended in 1 ml of sterile dH_2O and transferred to a microcentrifuge tube. Cells were collected once more (1 000 *g*, 3 min) and washed with 1 ml of LiAc/TE solution (1 000 *g*, 3 min). At this stage, we can be sure to completely wash away remaining residues of cultivation medium and yeast cells are ready to be transformed with the transforming DNA. Washed cells were resuspended in 100 µl of LiAc/TE solution and transforming DNA was added (linearized plasmid DNA; 1-3 µg) together with 2 µl of denatured salmon sperm DNA (10 mg/ml; Sigma-Aldrich). Contents were mixed gently and incubated at room temperature for 10 minutes. Then, 260 µl of 40% PEG/LiAc/TE solution was added, the suspension was again gently mixed and incubated at 30°C without shaking for 2-3 hours. Next, 43 µl of dimethylsulfoxide (DMSO) was added and the cell suspension

was incubated at 42°C for 10 minutes. The sample was centrifuged (1 000 *g*, 3 min) and approximately 200 µl of the supernatant was removed. Cells were then resuspended in the rest of the supernatant and spread on two solid YES plates (50 and 150 µl respectively). These non-selective plates were incubated for 1 day at 32°C and then replica plated on selective plates (could be antibiotics or nutrient deficiency). In case of this study, the selective agent was the Nourseothricin antibiotic. Selective plates were incubated at 32°C until monocolonies formed (3-5 days). The replica plating after initial growth in the non-selective environment is necessary for the transformation involving integration into genomic locus. In case of transformation with no genomic integration, the initial non-selective growth step can be skipped. Transformed cells can be plated on the selective plates directly after the transformation procedure.

10x LiAc solution = 1 M lithium acetate; pH 7.5 ; sterilized by autoclaving
10x TE solution = 0.1 M Tris-HCl, 10 mM EDTA; pH 7.5 ; sterilized by autoclaving
LiAc/TE solution = 150 µl 10x LiAc + 150 µl 10x TE + 1200 µl dH_2O
40% PEG/LiAc/TE solution = 400 µl 50% PEG 4000 + 50 µl 10x LiAc + 50 µl 10x TE

3.2.4 Quick chromosomal DNA isolation from *Schizosaccharomyces pombe*

There are many methods for the genomic DNA extraction from *Schizosaccharomyces pombe*. For the routine Polymerase Chain Reaction (PCR) verification, when the Colony PCR method is not sufficient, the most convenient method is the isolation of the chromosomal DNA using lithium acetate, SDS, heat and alcohol precipitation (Lõoke et al., 2011). A small amount of biomass from YES plate prepared as described in the sub-chapter 3.1.3 was added to 60 µl of dH_2O in the microcentrifuge tube. 60 µl of the 2x LiAc + SDS solution was added to the solution and the sample was incubated for 10 minutes at 75°C. After the incubation, 120 µl of isopropanol was quickly added to the sample, contents were vortexed and centrifuged (14 000 *g*, 3 min). The supernatant was removed completely and the tube with the sample was left open to dry for approximately 5-10 minutes. Residues of the isopropanol could cause the inefficiency of the PCR reaction. Pellet was then resuspended in 200 µl of dH_2O. At this stage, samples can be stored at -20°C for further use, or directly used for the PCR. DNA isolated using the lithium-acetate method must be centrifuged (14 000 *g*, 3 min) and 5 µl of the supernatant can be used for the PCR. This is

done to reduce the possibility of the reaction inhibition by cellular debris, which sediments at the bottom of the tube after the centrifugation. Physical characteristics of DNA do not allow its sedimentation in the water, so DNA stays dissolved in the supernatant.

2x LiAc + SDS solution = 0.4 M lithium acetate, 2% SDS

3.2.5 Polymerase Chain Reaction (PCR)

The polymerase chain reaction was used for strain genotype verification by DNA fragments amplification in this study. The reaction itself was performed in three different configurations which will be specified in the next sub-chapters. However, the components of the reactions were shared for every PCR setup as follows:

Reaction component	Final concentration	Volume used for 20 µl reaction
10x Reaction NH_4^- based buffer (NEB)	1X	2 µl
dNTPs, each	0.25 mM	1.6 µl
Primers	0.5 µM each	1 µl each
Taq DNA Polymerase (NEB)	0.4 U	0.12 µl
Template DNA	depends on the configuration	depends on the configuration
dH_2O	-	up to 20 µl

Table 3 – Components of the polymerase chain reaction

A negative control without template DNA was used in each PCR performed during this study for reactions of every primer pair.

3.2.5.1 Mating type identification colony PCR

For the identification of the mating type of newly created strains (if needed), a colony PCR method was performed in this study. The components of the reaction were used as stated in the Table 3. The distinctive features of the mating type identification PCR method used in this study was in usage of three different primers, instead of usual pair, in each PCR reaction as described in the Table 4.

Description	Primer name	Sequence	Product length
Mating locus, universal	MT1	AGAAGAGAGAGTAGTTGAAG	-
Mating locus, h-	MM	TACGTTCAGTAGACGTAGTG	729 bp with MT1
Mating locus, h+	MP	GGTAGTCATCGGTCTTCC	987 bp with MT1

Table 4 – Mating type identification primers

The template for the reaction was added as a small amount of fresh biomass (approximately 1 µg) from a plate using sterile pipette tip. Cells are disrupted and DNA released from the nucleus in the first step of the PCR cycle. The cycling parameters according to the primers used and the length of amplified regions were as described in the Table 5.

Step	Repeats	Temperature	Time
1	1x	94 °C	5 min
2	35x	94 °C	30 s
		56 °C	30 s
		72 °C	1 min
3	1x	72 °C	5 min

Table 5 – Colony PCR cycling parameters

The known mating type strain was used as a positive control for this PCR method.

3.2.5.2 Verification of plasmid integration by colony PCR

Lithium-acetate transformation method by Gregan *et al.* (Gregan et al., 2006) (described in the sub-chapter 3.2.3) is based on the homological recombination of the gene of interest with the specific resistance cassette. The success of lithium-acetate transformation method was verified by the presence of the upstream and downstream plasmid end regions in the genomic DNA of transformants.

In this study, the lithium-acetate transformation method was used to create the cbf11 deletion mutant strains. For the verification of the transformation method, colony PCR method was performed. The components of the reaction were used as stated in the Table 3. The primers used for the reaction amplify the upstream and downstream junction regions between the integrated plasmid and the target chromosomal locus (Table 6).

Primer pair	Primer name	Sequence	Product length
Upstream	MP144	GTCGTTAGAACGCGGCTACA	953 bp
	MP150	AGGGATCGAAAGACATCCGC	
Downstream	MP54	GCGCACGTCAAGACTGTC	823 bp
	MP53	GCTTGTACACACGGCCTTCAA	

Table 6 – Primers used for the verification of lithium-acetate transformation method.

The template for the reaction was added as a small amount of fresh biomass (approximately 1 μg) from a plate using sterile pipette tip. The cycling parameters according to the primers used and the length of amplified regions were as described in the Table 5.

3.2.5.3 *cbf11* deletion verification using panel of primers

During the deletion of *cbf11* gene by various techniques, random reintegration of the *cbf11* locus and DNA rearrangement can occur (recent unpublished experience of the research group). Verification of the successful transformation by integration of recombinogenic regions is not sufficient in this scenario.

To verify complete *cbf11*deletion, four different pairs of primers were designed to amplify four different regions inside the *cbf11* open reading frame. Primers used for this verification are described in the Table 7.

Primer pair	Primer name	Sequence	Product length
1	MP63	CCTAGTCAGCTGGTAACAG	286 bp
	MaP176	CCAGAGAAAGCCGTAAGT	
2	MP54	TTAGTATTGTCTCCAAACC	190 bp
	MP53	AGGTTAATACGCAATGG	
3	MP69	TAAATATGGCTCCATCG	198 bp
	AJ18	GCCAGTGAACTATGCTCAG	
4	MP35	ATTTGGCTAGGTGTTCATGG	195 bp
	MP45	TGACGTTAGCAAAATCTCGC	
5	MP37	GTAAACGATACCAGGTCCGC	210 bp
	MP38	GGTACCACTATGTATCCCGG	
Positive control (*act1*)			

Table 7 – Primers used for *cbf11* deletion verification

As a template for this verification, the isolated fission yeast gDNA was used in this study (the best DNA template selected in the sub-chapter **Error! Reference source not found.** in the Figure 16). The isolation method used in this study was the quick chromosomal DNA isolation described in the sub-chapter 3.2.4. The cycling parameters according to the primers

used and the length of amplified regions are stated in the Table 8. As a positive control to exclude the PCR failure, wild type strain was used with a cbf11 locus present in the genome.

Step	Repeats	Temperature	Time
1	1x	95 °C	5 min
2	30x	95 °C	30 s
		65 °C	30 s
		72 °C	30 s
3	1x	72 °C	5 min

Table 8 – Cycling parameters for *cbf11* deletion verification

3.2.5.4 *hos2* deletion verification

hos2 is a non-essential gene encoding the histone deacetylase Hos2 in *S. pombe* (Rundlett et al., 1996). The deletion of the *hos2* gene was not introduced by the author of the study, because the strains collection of the research group already contained such mutant strains. The deletion of *hos2* gene, however, must have been verified by the colony PCR. The components of the reaction were used as stated in the Table 3. The primers for this PCR verification were designed to amplify a DNA fragment located inside the *hos2* open reading frame. The best pair of primers was designed using NCBI Primer-BLAST tool (https://www.ncbi.nlm.nih.gov/tools/primer-blast/) described in the Table 9. The template for the reaction was added as a small amount of fresh biomass (approximately 1 µg) from a plate using sterile pipette tip. The cycling parameters for the colony PCR were used as described in the Table 5.

Primer name	Sequence	Product length
PH01	TCAATTGGAGCGGTGGTCTC	405 bp
PH02	CAAGCGAATCAGCACCACAC	

Table 9 – *hos2* ORF region primers

Based on the design of this verification, the desired outcome is the absence of the amplified region in the tested sample. For the PCR validity control, two positive controls were used. As a positive control to exclude the PCR failure, wild type strain was used with a *hos2* locus present in the genome. The second positive control used in this experiment was a previously confirmed *hos2*Δ strain from the research groups´ strain collection.

3.2.6 Agarose gel electrophoresis

Agarose gel electrophoresis was used for visualisation and separation of the amplified DNA fragments in this study. 1% or 2% (2% gel was used for the *cbf11* deletion verification using panel of primers) agarose gel was prepared using 1x TAE (2 M Tris, 1 M acetic acid, 0.1 M EDTA; pH = 8.5) buffer and microbiological agarose (Serva). The agarose was properly melted and dissolved in the microwave oven. Melted agarose gel was left to cool down to be able to hold the flask by hand. To the cooled but still liquid agarose gel, MIDORI Green (Elisabeth Pharmacon) intercalation dye was added (5µl/100ml), mixed and the gel was poured into the prepared agarose gel preparation apparatus. DNA samples (20 µl) were mixed with 4 µl of the 6x DNA Loading Dye (ThermoScientific). Solidified gel was transferred into the horizontal electrophoretic apparatus (Scie Plas) filled with the 1x TAE buffer. Prepared DNA samples were loaded into the wells of the gel. For the estimation of the DNA fragments sizes, GeneRuler DNA ladders (1 kb and Mix; ThermoScientific) were loaded into the gel together with the DNA samples. During the agarose gel electrophoresis, DNA fragments are separated by applying the electrical field with constant voltage. For this purpose, Bio Rad PowerPac (Bio Rad) power supply was used with the voltage set to 5 V per 1 cm of gel length. 80 V was used for the short gels and 170 V for the large gels in this study. The proper fragment separation using this voltage setup takes around 45 minutes. After the separation, the gel was visualised using UV transilluminator (Azure biosystems c150).

3.3 Microscopic methods

3.3.1 4′,6-diamidine-2′-phenylindole dihydrochloride (DAPI) staining and microscopy

4′,6-diamidine-2′-phenylindole dihydrochloride (DAPI) is an intercalation dye incorporating in the major groove of the DNA (Tarnowski et al., 1991) widely used to visualise DNA molecules.

300 µl of the ethanol fixed cell culture was transferred to a new 1.5 ml microcentrifuge tube. The cell suspension was collected (3 000 *g*, 3 min) and supernatant removed. The tube was left open on the bench for 5 minutes to let the residues of the ethanol evaporate. Then, 300 µl of dH_2O was added and the suspension was vortexed. Cell suspension was incubated at room temperature for 10 minutes to rehydrate the cells. DAPI (Sigma-Aldrich) was added

to the rehydrated cell suspension to final concentration of 1 µg/ml. The suspension was centrifuged (3 000 *g*, 3 min) and 150 µl of the supernatant removed. Then, the suspension was vortexed and centrifuged again (3 000 *g*, 3 min). 100 µl of the supernatant was removed, suspension vortexed and centrifuged (3 000 *g*, 3 min) for the last time.

2 µl of the pelleted cell suspension was layered onto a microscopic slide for further microscopy.

Microscopy of the cells fixed with ethanol and stained with DAPI intercalation dye was performed on the Leica microscope (Leica DM750 with Leica ICC50 W camera) in two light conditions. The same position on the slide was photographed in the bright field as well as in the UV illuminated condition to allow the DAPI excitation (maximal excitation wavelength – 358 nm; maximal emission wavelength – 461 nm). Images were further processed and analysed (described in the sub-chapter 3.3.3.1).

3.3.2 Live-cell imaging

To observe the course of the mitotic events in particular cells, live-cell imaging method was performed. It is a widely used method to study the cell cycle progression in the living cells. The method is based on the image acquisition during specified time interval to produce the time-lapse imaging data of the studied sample. Usually, the imaging is done in a brightfield and one or two fluorescent channels to combine the morphological and intracellular dynamics in time. The setup used in this study was based on the publication by Tran *et al.* (Tran et al., 2004) and Akshay Vishwanatha (former member of the group) with some adjustment described in this sub-chapter.

3.3.2.1 Slide preparation

Fission yeast cells are cultivated on the solid YES medium containing 4% microbiological agarose (Serva) during the live-cell microscopy. YES medium with addition of microbiological agarose was preferred over standard agar medium because of the better optical properties of the agarose. 0.4 g of microbiological agarose was melted in 10 ml of liquid YES medium using microwave oven. The content was aliquoted to 1.5 ml microcentrifuge tubes for better further manipulation and stored at 4°C.

Silicone Slide Spacer represents another specific component used for the live-cell microscopy method. It was created by Viacheslav Zemlianski (other member of the research group) from a solidified PDMS (Lukoporen N 1000; Lučební závody Kolín) with two

separate chambers cut out for the samples. The thickness of the Silicone Slide Spacer was 2 mm and the dimensions of the chambers were roughly 1 x 1 cm. The Spacer is then placed directly on the microscopic glass slide to stick to the surface of the slide.

Aliquot of the YES medium containing 4% microbiological agarose was melted at 94°C. Approximately 350 µl of the melted medium is quickly split to both chambers of the prepared microscopic glass slide with the Silicone Slide Spacer. The chambers were quickly covered with 40 x 22 mm cover glass to equally distribute the medium in the chambers and create a flat surface for the cells to grow on. The medium in the chambers was left to solidify at room temperature. The redundant bits of the medium were removed from the slide using the detached cover glass after its´ complete solidification. Two cell cultures for the live cell microscopy were cultivated as described in the sub-chapter 3.1.3. 1 ml of both exponentially growing cell cultures (corresponding OD_{600} 0.3 – 1.5) was transferred to a 1.5 ml microcentrifuge tube separately and collected (1 000 *g*, 3 min, RT). 2 µl of the pelleted cell suspension of each culture was transferred onto the solid YES medium containing 4% microbiological agarose in the chamber of prepared slide. The cell suspension in the chambers was left to dry and both chambers were covered with the 40 x 22 mm cover-glass. The cover-glass was taped to the slide from sides with the common office adhesive tape without obstructing the field of the chambers.

3.3.2.2 Microscopy setup

Nikon H-TIRF 2 microscope equipped with the cultivation chamber (Okolab h301-k-frame) was used for the live-cell microscopy in this study. The cultivation chamber with thermostat and air flow features was used to ensure the right growth conditions for the cells throughout the experiment. The environmental settings inside the chamber were set to 32°C and ambient CO_2 (0% addition of CO_2) for the whole duration of the live-cell imaging.

The fission yeast cells were imaged for 3.5 hours every 2 minutes in three different channels: Differential Interference Contrast (DIC), green channel (GFP; maximal excitation wavelength – 395 nm; maximal emission wavelength – 509 nm) and red channel (mCherry; maximal excitation wavelength – 587 nm; maximal emission wavelength – 610 nm). Two lasers of 460 and 580 nm wavelengths were used to excite the GFP and mCherry fluorescent marks respectively. Nikon Perfect Focus System (PFS) was used together with imaging of 5 focal planes in Z stack (0.5 µm steps between the focal planes of Z-stack) to ensure the best

focus of the images. Obtained large image files were further processed and analysed (described in the sub-chapter 3.3.3.2).

3.3.3 Image processing and analysis

The processing and further analysis was done using ImageJ software (v1.53q) (Schneider et al., 2012). It is important to have the version including all Fiji plug-ins installed to be able to open the .nd2 format imaging files and proceed with the analysis (https://imagej.net/software/fiji/).

3.3.3.1 Image analysis for CUT phenotype screening

For the CUT phenotype screening, brightfield images were overlayed with the fluorescent images of blues channel (DAPI emission) to properly recognize the cell boundaries, septa and nuclei. Transparency of 75% was applied to brightfield images during the overlay. Cells were counted using "Multi-point" ImageJ function. The data was visualised using bar charts in MS Excel.

3.3.3.2 Live-cell imaging data processing and analysis

During the live-cell imaging, big .nd2 files are created containing time-course. ImageJ software with Fiji plug-ins installed is capable of opening this type of file. The files are opened as big multi-layer stacks containing 3 channels (DAPI, green and red), 5 focal planes of Z-stack and time points. To further process and analyse acquired data, an image processing pipeline was developed and optimized (in collaboration with Viacheslav Zemlianski, other member of the research group).

The Z-stack planes were merged together based on the maximal projection of the layers. Colour channels were split and background extracted from each channel. As mCherry and GFP fluorescent marks tend to bleach during the longer exposure to the light of their excitation wave length, the bleach correction (included adjustment toll in the ImageJ software) was applied to each channel. Also, to eliminate any micromovements of the sample during the live-cell imaging, Linear Alignment with SIFT image stabilization plug-in was run for each channel. Processed colour channels were then re-merged for further analysis and montage creation.

4 Theoretical background

4.1 CSL transcription factors

The focus of this study is on the proteins from the CSL (CBF1/RBP-Jκ/Suppressor of Hairless/LAG-1) transcription factor family. The CSL transcription factors are conserved through opisthokont organisms from fungi to metazoans including humans (Gazave et al., 2009). As the effectors of the Notch signalling pathway in animals (Bray, 2006; Hori et al., 2013), they play a crucial role in cellular processes such as proliferation (VanDussen et al., 2012), differentiation (Nguyen et al., 2006) or apoptosis (Yang et al., 2004). The defects in the Notch signalling pathway can cause many human development syndromes or cancer (Louvi & Artavanis-Tsakonas, 2012; Penton et al., 2012).

The Notch signalling pathway is activated upon ligand binding to the transmembrane Notch receptor. The active receptor is then proteolytically cleaved releasing the Notch intracellular domain (NICD) (Kopan & Ilagan, 2009; Schroeter et al., 1998). The released NICD is translocated to the cell nucleus to form a complex with the DNA bound CSL transcription factor. Together with other co-activators, the NICD-CSL complex promotes the transcription of Notch-target genes containing the CSL response element (Kopan & Ilagan, 2009; Tun et al., 1994). Without NICD binding, CSL binds transcriptional co-repressors to repress the expression of the Notch-target genes (Hori et al., 2013). The schematic overview of the core Notch signalling pathway is shown in the Figure 3.

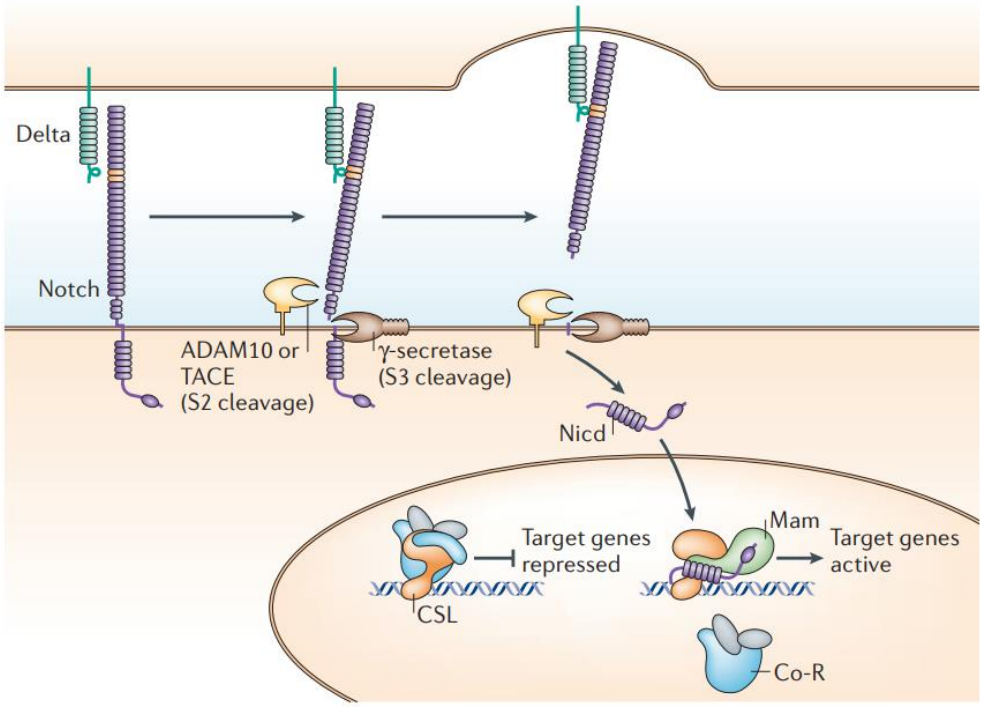

Figure 3 – The core Notch signalling pathway (Bray, 2006). Delta ligand (green) on one cell binds the Notch receptor (purple) on the other cell. Upon ligand binding, the Notch receptor is cleaved by two proteolytic enzymes. The ADAM10 or TACE metalloprotease (yellow) catalyses the S2 cleavage generating the substrate for S3 cleavage by the γ-secretase complex (brown). After the cleavage, Notch intracellular domain (Nicd) is released from the membrane and translocates to the nucleus. In the nucleus, Nicd interacts with the DNA-binding CSL protein (orange). The Nicd-CSL binding promotes the release of Co-repressor complex (Co-R, blue and grey) and binding of the Mastermind (Mam, green) co-activator together with other transcriptional regulator. This activation complex then activates the transcription of a number of target genes.

4.2 CSL transcription factors in the Notch-less fission yeast *Schizosaccharomyces pombe*

Transcription factors belonging to the CSL family were identified even in organisms lacking Notch, including the unicellular fission yeast, *Schizosaccharomyces pombe* (Převorovský et al., 2007). The fission yeast genome encodes two CSL paralogs, Cbf11 and Cbf12 (Oravcová et al., 2013; Převorovský et al., 2009). Cbf11 and Cbf12 are not essential, meaning that mutants with the deletion of one or both CSL genes remain viable (Převorovský et al., 2009). The functions and expression of the two fission yeast CSL transcription factors during the life cycle of the fission yeast differ (Převorovský et al., 2009). Transcription of *cbf12* is upregulated upon entering the stationary phase, whereas *cbf11* transcription is relatively constant (Převorovský et al., 2009). *Cbf12* deletion mutants show lower surface adhesion,

but no other morphological or growth phenotypical defects. On the other hand, *cbf11*Δ strains display many disorders including aberrant cellular shapes and sizes, nuclear fragmentation, multi-septation, catastrophic mitotic events and a significant growth defect (Převorovský et al., 2009, 2015, 2016). There is also evidence of the Cbf11 involvement in the oxidative stress response regulation. *Cbf11* deletion mutants show up-regulation of the oxidative stress response genes and are resistant to H_2O_2 treatment (Daněk, 2015; Tvarůžková, 2015). Moreover, the Cbf11 transcription factor seems to be also involved in the response to nutrients. Deletion of the genes encoding the major nutrient response regulator, Pka1, rescues the phenotypic defects of the *cbf11*Δ strains (Převorovský et al., 2015). The role of Cbf11 in lipid metabolism regulation was also described. The expression of lipid-metabolism-related genes was lower in c*bf11*Δ strains suggesting its broad involvement in fission yeast lipid metabolism regulation (Převorovský et al., 2015). Also, *cbf11* deletion mutants display a dramatically lower content of lipid droplets (Zach et al., 2018), the main fission yeast lipid storage bodies (Meyers et al., 2017). The schematic overview of the known targets of Cbf11 is shown in the Figure 4.

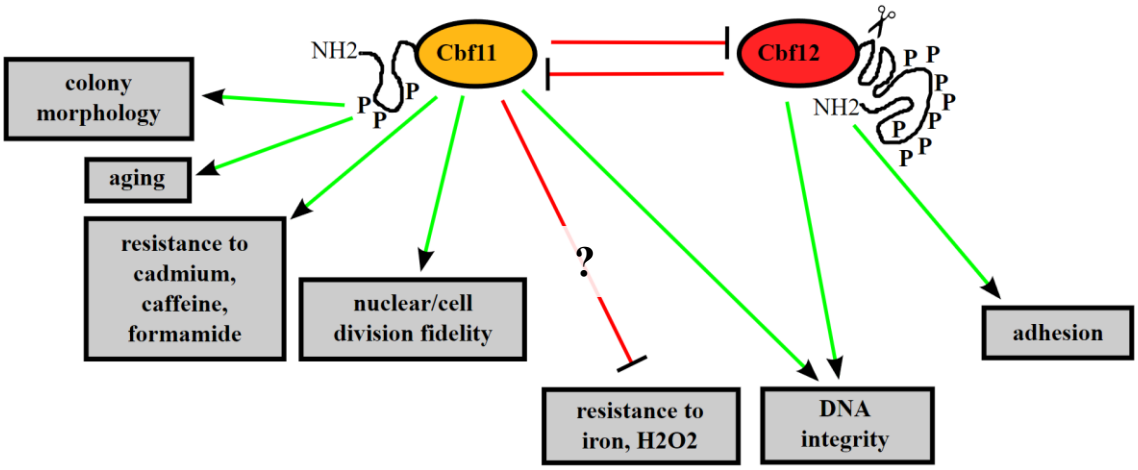

Figure 4 – Overview of the identified functions of Cbf11 and Cbf12 transcription factors in *Schizosaccharomyces pombe* (Převorovský, unpublished). The Cbf12 transcription factor plays a major role in cell-surface adhesion and DNA integrity maintenance in fission yeast (Převorovský et al., 2009). The Cbf11 transcription factor also helps to maintain the DNA integrity, but also secures the successful nuclear and cell division (Převorovský et al., 2016), ensures the right colony morphology (Převorovský et al., 2015) and promotes cellular aging (Romila et al., 2021) and resistance to various stressors. The Cbf11 transcription factor represses the resistance to oxidative stress, but the exact mechanism remains unclear (Převorovský et al., 2015). Moreover, Cbf11 and Cbf12 transcription factors function antagonistically and disruption in a balance of their function leads to many cellular defects (Převorovský et al., 2009).

4.3 Mitosis and lipid metabolism in *Schizosaccharomyces pombe*

4.3.1 Closed mitosis in *Schizosaccharomyces pombe*

The majority of cells present in higher eukaryotic organisms undergo open mitosis coupled with the nuclear envelope breakdown (Güttinger et al., 2009). Mitotic kinases drive the process of nuclear pore complex disassembly and the nuclear envelope is retracted into the endoplasmic reticulum membrane system during the prometaphase of mitosis. Condensed chromosomes are released from the nuclear environment, bound by the mitotic spindles, and segregated. The nuclear envelope starts to reform during the anaphase through the attraction of endoplasmic reticulum tubules to the chromatin surface. Subsequently, nuclear pore complexes and nuclear lamina are reformed during telophase (Güttinger et al., 2009).

However, the mitotic event differs in many fungal species including *Saccharomyces cerevisiae* and *Schizosaccharomyces pombe*. Chromosome segregation during the mitosis of these organisms occurs inside the intact nuclear compartment. This is called "closed mitosis" (Arnone et al., 2013). Even though the nuclear envelope during the closed mitosis does not disassemble, the nucleus undergoes some morphological changes in *S. pombe*. The common sphere-shaped nucleus is stretched to form a spherocylindrical compartment by the mitotic apparatus during the anaphase. The still intact nuclear compartment is drawn to the opposite poles of the cell together with chromatin to form a dumbbell structure. The distance between the two emerging nuclear bodies extends to form two sphere-shaped daughter nuclei (Castagnetti et al., 2015; Yam et al., 2011; Zhu et al., 2016). The schematic comparison of different types of mitosis is described in the Figure 5.

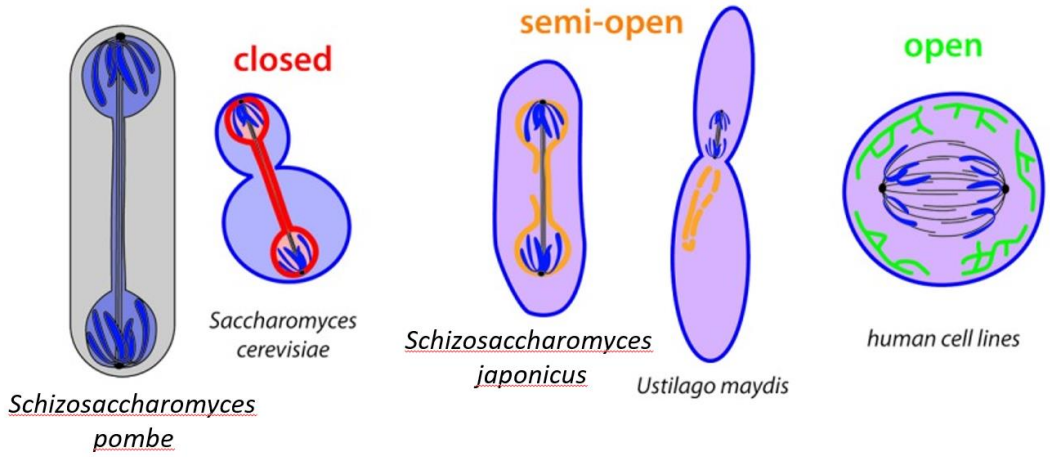

Figure 5 – Comparison of the closed mitosis present in *Schizosaccharomyces pombe* with semi-open and open mitosis. Adapted from (Boettcher & Barral, 2013).

As mentioned above, the nuclear transformation and chromosome segregation are driven by the mitotic spindle apparatus. It originates from two opposite spindle pole bodies equivalent to metazoan centrosomes. So, the structure of the fission yeast mitotic spindle resembles the structure of metazoan mitotic spindle, however, it´s localisation is different. Unlike the metazoan mitotic spindle, the fission yeast mitotic spindle is localised inside the nucleus (Castagnetti et al., 2015; Zhu et al., 2016). Also, the activity of the fission yeast mitotic spindle is rather pushing than towing in comparison to metazoan mitotic spindle. The closed mitotic karyokinesis is also coupled with an increase of the nuclear envelope surface. Some studies show a mitotic nuclear surface increase by 33% (± 4%) in *S. pombe* (Takemoto et al., 2016; Yam et al., 2011). Biomechanical attributes of the lipid bilayers do not allow such an expansion by simple stretching. Thus, the nuclear expansion present during the fission yeast closed mitosis must be coupled with an incorporation of new phospholipids to the enlarging nuclear membrane (Jorgensen et al., 2007).

4.3.2 Nuclear membrane biogenesis during mitosis in *Schizosaccharomyces pombe*

The *S. pombe* nuclear envelope area is constantly increasing during the interphase (Jorgensen et al., 2007). However, the rapidness (minutes) and scale (around 33%) of the nuclear expansion during the fission yeast karyokinesis suggest the presence of other mechanisms involved in *S. pombe* mitotic nuclear expansion than membrane stretching.

The main lipidic components of cell membranes are phospholipids. For phospholipid production, phosphatidic acid (PA) presence is required in the cell. There are several known ways cells utilize for PA production (Raben & Barber, 2017):

- De-novo synthesis
- Acylation of lyso-PA
- Phosphorylation of diacylglycerol (DAG)
- Phospholipase D-mediated phospholipid hydrolysis

Cells can then utilize PA either for production of storage triacylglycerols (TAGs) or structural phospholipids (PLs). For TAGs production, PA undergoes dephosphorylation to DAG performed by PA phosphatase lipin (Raben & Barber, 2017). This enzymatic reaction is considered to be the decision point in the question of which lipidic molecules will be further produced in the cell.

The pathway regulating lipin activity was described for the budding yeast *Saccharomyces cerevisiae*. The budding yeast lipin Smp2p/Pah1p is activated upon dephosphorylation by the phosphatase complex Nem1p-Spo7p (Siniossoglou et al., 1998). Active Smp2/Pah1 dephosphorylates PA to start the TAGs synthesis (O'Hara et al., 2006; Santos-Rosa et al., 2005). The opposite effect of this molecular switch is achieved by negative regulation of Smp2p/Pah1p through phosphorylation by several protein kinases including PKA (Su et al., 2012), TORC1 (Dubots et al., 2014) or Cdc28 (CDK1) (Choi et al., 2011). Inactive Smp2p/Pah1p cannot catalyse the PA dephosphorylation to DAG, leading the PA for PLs synthesis. The schematic overview of the budding yeast lipid synthesis pathways is described in the Figure 6. *smp2/pah1*, *nem1* or *spo7* deletion mutant budding yeast strains display aberrantly shaped nuclei with many protrusions (Santos-Rosa et al., 2005; Siniossoglou et al., 1998). The same phenotype was achieved by overexpressing the gene coding *DGK1* diacylglycerol kinase, the antagonist of the Smp2p/Pah1p (Han et al., 2008). On the other hand, the aberrant nucleus phenotype was rescued by disruption of phospholipid synthesis (Santos-Rosa et al., 2005). These findings suggest that the nuclear membrane synthesis is dependent on phospholipid synthesis and incorporation. Moreover, lipin phosphorylation (i.e., inactivation) by CDK1 during the first stages of M phase was shown in both *S. cerevisiae* and *S. pombe* (Makarova et al., 2016; Santos-Rosa et al., 2005).

Schizosaccharomyces pombe contains the lipin activity regulation pathway that is homologous to the budding yeast pathway. Also, the corresponding allele mutants display similar phenotypes – *Δnem1*, *Δspo7* and *Δned1* (lipin homolog) mutants show elongated nuclei and overdeveloped endoplasmic reticulum (Tange et al., 2002).

All mentioned findings suggest the necessity of an elevated rate of phospholipid synthesis for successful nuclear division.

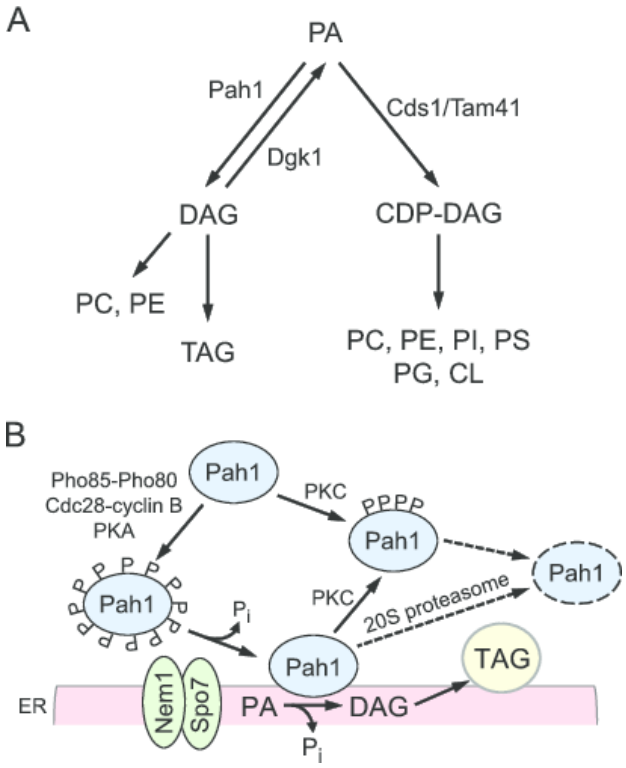

Figure 6 – Lipid synthesis pathways in S. cerevisiae (Hsieh et al., 2015). (A) Branch point of phosphatidic acid (PA) fate. PA is used either for production of storage triacylglycerols (TAGs) or membrane phospholipids. **(B)** Pah1 is phosphorylated in the cytoplasm by Pho85-Pho80/Cdc28-cyclin B. Phosphorylated Pah1 translocates to the ER membrane through its dephosphorylation by the Nem1-Spo7 phosphatase complex. Dephosphorylated Pah1 associated with the ER membrane becomes active and catalyses the conversion of PA to DAG. DAG is further acylated to form storage lipid molecule TAG. Dephosphorylated Pah1 is degraded by 20S proteasome either directly or through PKC phosphorylation. Phosphorylation by PKC takes place on different phosphorylation sites than the Pho85-Pho80/Cdc28-cyclin B phosphorylation. This phosphorylation pattern is recognized by the 20S proteasome.

4.3.3 Cell Untimely Torn (CUT) phenotype

Cell Untimely Torn (CUT) phenotype describes the phenomenon of *Schizosaccharomycess pombe* cells failing to divide the nucleus properly during the progression of mitosis. The undivided nucleus is then intersected by the developing septum (Pérez et al., 2016; Samejima et al., 1993) (Figure 7). Mechanically cleaved chromosomes are grossly damaged and are not segregated equally to daughter nuclei. CUT phenotype is considered as a terminal defect, although, some infrequent viability of aneuploid CUT cells was shown (Syrovatkina & Tran, 2015). Two major groups of mutants manifesting CUT phenotype are being studied. The first group includes strains mutated in genes responsible for chromosome segregation and anaphase progression. Corresponding mutant strains are defective in genes for securin and

separase (Funabiki et al., 1996; Nagao & Yanagida, 2006; Yuasa et al., 2004), cohesin or condensin (Saka et al., 1994), APC/cyclosome complex (Yamashita et al., 1999), topoisomerase II (Uemura et al., 1987; Uemura & Tanagida, 1986) or mitotic spindle (Syrovatkina & Tran, 2015) functions. The CUT phenotype occurrence was also described for a second, less understood group of mutants defective in lipid metabolism (Makarova et al., 2016; Převorovský et al., 2015, 2016). Moreover, the CUT phenotype occurrence was recently shown to be sensitive to nutrient availability (Zach et al., 2018). After supplying cells with a good nitrogen source (ammonium chloride), Zach *et al*. observed significantly lower CUT phenotype incidence in *cbf11Δ* and cut6–621 mutants (Zach et al., 2018). This study is trying to describe other possible factors involved in the CUT phenotype manifestation.

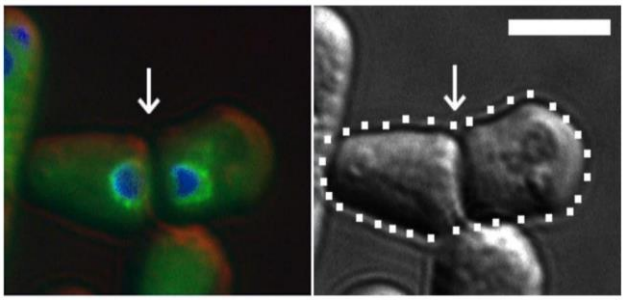

Figure 7 – CUT phenotype in the fission yeast (Zach, 2018). Left panel: nuclear envelope in green (Cut11-GFP) (West et al., 1998), DNA in blue (DAPI); right panel: DIC. The arrows show the position of the division septum. Scale bar represents 5 μm.

4.3.3.1 Lipid metabolism linked CUT phenotype

The first study describing the potential crosstalk between the lipid metabolism and CUT phenotype was done in 1996 by Saitoh *et al*. During the characterisation of genes encoding the acetyl coenzyme A carboxylase (ACC) and the fatty acid synthase (FAS) alpha subunit (*cut6* and *lsd1/fas2* respectively) Saitoh *et al.* described two different mitotic defects (Saitoh et al., 1996). When using temperature sensitive *cut6* and *lsd1* mutants with deficient ACC or FAS function under certain temperature conditions, catastrophic mitotic events occurred with two different mechanisms (Saitoh et al., 1996):

- Nucleus was intersected by septum = CUT phenotype
- Chromosomes were unequally segregated to two daughter nuclei resulting in different daughter nuclei size = Large and Small Daughter LSD phenotype

More recent studies show other linkage between the disruption of fission yeast lipid metabolism and catastrophic mitotic events. Deletion of *cbf11*, gene coding the transcription factor Cbf11 (described in the subchapter 4.2) leads to severe morphological and physiological abnormalities, further resulting in frequent CUT phenotype occurrence (Převorovský et al., 2015, 2016). As described before, Cbf11 regulates many downstream target genes including *cut6* and *vht1*. Vht1 stands for biotin/vitamin H transmembrane transporter, the main fission yeast biotin provider. Biotin is needed for fatty acid synthesis as the essential prosthetic group of ACC (in *S. pombe* Cut6) (Stolz, 2003). Interestingly, decreased expression of *cut6* or deletion of the *vht1* gene individually do not result in nuclear defects (Převorovský et al., 2016). However, the combination of mutation in the Cbf11-binding element in *cut6* promoter (*Pcut6MUT*) and *vht1* deletion does result in significant CUT phenotype development (Převorovský et al., 2016). Therefore, Převorovský *et al.* suggest that the *cbf11*Δ and *Pcut6MUT vht1*Δ mutants both produce fewer ACC/Cut6 molecules, of which only a small fraction is enzymatically active due to insufficient biotin supply caused by perturbed biotin uptake (Převorovský et al., 2016). The described mutations can result in down-regulation of fatty acid synthesis leading to mitotic defects analogous to those reported by Saitoh *et al.* in cells deficient in ACC or FAS (Saitoh et al., 1996).

4.3.3.2 Role of nuclear expansion in CUT phenotype

As described in the sub-chapter 4.3.2, nuclear expansion plays a crucial role during the process of closed mitosis. Insufficient PL production due to lipid metabolism mutations can thus lead to the development of CUT phenotype. The proof of this hypothesis was provided the study with FAS inhibitor Cutin-1 (Takemoto et al., 2016). *S. pombe* cells treated with Cutin-1 show perturbed fatty acid synthesis resulting in the inability to expand the nuclear surface during mitosis. Morphological transformations of the mitotic nucleus do not occur, and the nucleus is intersected by the developing septum (Takemoto et al., 2016).

Even more interesting, and for this study crucial, are the effects of defective nuclear expansion on the mitotic spindle. The nucleus unable to expand constraint the elongation of intranuclear mitotic spindle. However, the mitotic spindle still elongates resulting in bending and eventual breaking of the mitotic spindle (Takemoto et al., 2016). Similar spindle

behaviour during mitosis was observed in *S. pombe* cells treated with cerulenin (inhibitor of a different FAS subunit) (Yam et al., 2011).

4.4 Epigenetic regulation of chromatin structure in *Schizosaccharomyces pombe*

4.4.1 Chromatin structures regulated by acetylation of histones

The DNA is stored in a chromatin form inside the eukaryotic cell nucleus. Chromatin structure is formed by the octamer histone protein complexes binding DNA. Five types of histones conserved through eukaryotic organisms have been identified. Histones H1, or homologous H5, serves as a linker of the future solenoid structure. Histones H2A, H2B, H3 and H4 are the core components associating with the DNA. They form a hetero-octamer containing two pairs of histones H2A-H2B and two pairs of histones H3-H4 binding negatively charged DNA by positively charged histone tails containing lysine and arginine residues. The structure of DNA bound with histones is called a nucleosome. Six or more nucleosomes can form a more condensed solenoid coil structure. Chromosomes are then formed by this supercoiled chromatin fibre (Olins & Olins, 2003; Park & Kim, 2020). This supercoiled chromatin structure is not accessible to the replication or transcription machinery. Therefore, regulation of the affinity of nucleosome structure must be present to facilitate the replication or transcription process. The main regulation mechanism to control the affinity of the chromatin structure is acetylation or deacetylation of the lysine residues of histone N-terminal tails. Enzymes catalysing the histone acetylation and deacetylation are called histone acetyl-transferases (HATs) and histone deacetylases (HDACs). Acetylation of the lysine residues of histone tails neutralizes their positive charge loosening the nucleosome structure. Loosened nucleosome structure is called euchromatin. In contrast, deacetylation recovers the positive charge of lysine residues of histone tails compacting the nucleosome structure. This structure is called heterochromatin and is less accessible for the replication or transcription machinery. Histone acetylation and deacetylation is one of the major epigenetic gene expression regulation systems in many eukaryotes as the gene expression can be influenced by the type of chromatin surrounding the gene (Park & Kim, 2020).

Generally, HDACs can be divided into three main classes based on the presence of a conserved deacetylase domain and their dependence on specific cofactors. The class I and class II enzymes are distinguished by the sequence of histone deacetylase domain, whereas class III HDACs are NAD-dependent sirtuins.

According to the current database, there are six known HDACs (or HDAC complexes) present in *Schizosaccharomyces pombe* (PomBase – Ontology Term - Histone Deacetylase Activity) out of which only one, Clr6, is essential (Grewal et al., 1998). Fission yeast HDAC classes:

1. Class I
    a. Clr6 – main fission yeast HDAC maintaining the heterochromatin through the cell cycle progression (Grewal et al., 1998)
    b. Hos2/Had1 – regulating cytokinesis (C. Grewal et al., 2012)
2. Class II – Clr3 – involved in the regulation of the mating type locus (Bjerling et al., 2002) and rDNA heterochromatin assembly (Bjerling et al., 2002)
3. Class III – NAD-dependent sirtuins Sir2, Hst2 and Hst4 (Alper et al., 2013; Durand-Dubief et al., 2007; Imai et al., 2000) ; Hst2 is also involved in the rDNA heterochromatin assembly (Durand-Dubief et al., 2007); Hst4 is also involved in the regulation of DNA repair (Haldar & Kamakaka, 2008) and subtelomeric heterochromatin assembly (Freeman-Cook et al., 1999)

The described process of histone deacetylation reveals the positively charged lysin residues of histone N-terminal tail to be recognised by the histone methyltransferase enzymes mediating the histone methylation process. Methylation of histone N-terminal tails is typical for heterochromatinised chromatin regions. Lysine residues of histones H3 and H4 N-terminal tails represent the main sites of epigenetic posttranslational modifications. Probably the most important epigenetic modifications of histone N-terminal tails in *S. pombe* are the modifications of lysine 9 of histone H3 (H3K9) N-terminal tail (Allshire & Ekwall, 2015).

4.4.2 Fission yeast centromeric heterochromatin

Heterochromatin is present in two functionally distinct forms in eukaryotes: facultative heterochromatin and constitutive heterochromatin. Facultative heterochromatin is present in the gene-dense regions of chromosomes. It is responsible for silencing genes active during the specific stages of cell cycle or environmentally regulated genes (Tashiro et al., 2013).

The maintenance of facultative heterochromatin seems to be mediated by the HDAC activity (Watts et al., 2018), but the exact mechanisms are not well understood. Constitutive heterochromatin is, on the other hand, present in the gene-poor chromosome regions such as centromeres and telomeres, but also mating type loci and rDNA regions (Egel, 2004). The exact role of the constitutive heterochromatin in the rDNA regions is not clear. However, there are suggestions of constitutive heterochromatin involvement in the maintenance of rDNA stability by preventing recombination between rDNA repeat sequences originating from the research of *S. cerevisiae* (Grunstein & Gasser, 2013). In the mating type loci, it regulates mating type switching (Egel, 2004). In telomeric regions it plays a major role during the meiotic chromosome segregation (Kanoh et al., 2005). The constitutive heterochromatin presence in centromeric regions ensures normal chromosome segregation (Ekwall et al., 1995).

The fission yeast centromere consists of two distinctive major parts. A central core and inner repeats where canonical H3 is replaced with the CENP-A histone variant and outer *dh* and *dg* repeats. These repeats consist of constitutive heterochromatin with strong H3K9 methylation epigenetic marks (Clarke et al., 1986; Kniola et al., 2001; Pidoux & Allshire, 2004).

After the deacetylation of H3K9 over the centromeric outer repeats by HDACs such as Clr6 or Sir2, H3K9 becomes the target for the activity of Clr4, key cellular histone methyl transferase (Allshire & Ekwall, 2015). The Clr4 protein functions as a part of the CLRC complex. It is responsible for creation of H3K9me2 and H3K9me3, main heterochromatin histone marks (Nakayama et al., 2001). Clr4 molecule contains a chromodomain suggesting its sequential activity mediated through the ability to bind H3K9me2/3 (Zhang et al., 2008). Other proteins containing chromodomain binding H3K9me2/3 are heterochromatin family proteins Swi6, Chp1 and Chp2 (Allshire & Ekwall, 2015). Swi6 and Chp2 proteins bind methylated H3K9 and contribute to the formation of heterochromatin over the centromere outer repeats (Bannister et al., 2001). Swi6 is also responsible for cohesion recruitment to outer repeats(Bernard et al., 2001). Chp1 is a member of the RNA-induced transcriptional silencing complex. By its ability to bind methylated H3K9, it is able to target the RNAi machinery also required for complete H3K9 methylation (Sadaie et al., 2004) The RNAi machinery functions in fission yeast are however complex and not yet fully understood

(Allshire & Ekwall, 2015). The schematic overview of the fission yeast centromere structure and proteins involved in its assembly and maintenance is presented in the Figure 8.

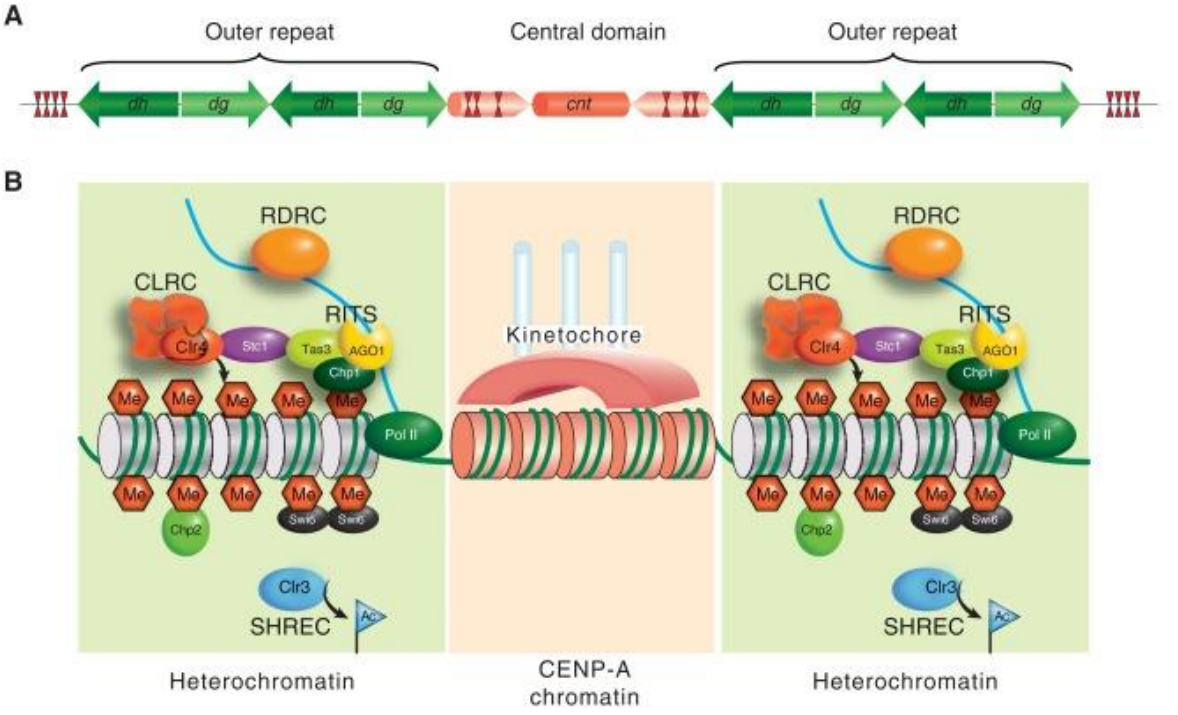

Figure 8 – Schematic overview of the *S. pombe* centromere structure (Allshire & Ekwall, 2015). (A) DNA arrangement of the *S. pombe* centromere. **(B)** Detailed schematic overview of the *S. pombe* centromere structure. Outer repeats (green) are packed in nucleosomes as heterochromatin with H3K9 methylated by Clr4 as part of the CLRC complex. H3K9 methylation allows the binding of the chromodomain proteins Chp1 (a component of the RNAi RITS complex), Swi6 and Chp2. RNAi activity is also maintained by the activity of RNA-directed RNA polymerase complex (RDRC). Clr3 HDAC acts as a part of the SHREC complex. All of these complexes act together to assemble and maintain the centromeric heterochromatin in fission yeast. Centromere central domain consists of DNA wrapped around specialised nucleosome complexes and inner and outer kinetochore multiprotein structures (pink arc). Specialised kinetochore nucleosomes consists of CENP-A histones replacing the majority of histones H3.

Chromodomain containing proteins have different affinities for methylated H3K9 when H3K4 residue is acetylated suggesting the mechanism of heterochromatin maintenance during the cell cycle. After DNA replication, Clr4 and Chp1 proteins with higher affinity for methylated H3K9 while H3K4 is deacetylated are recruited. On acetylation of H3K4 by the Mst1 histone lysine acetyltransferase, binding of Chp2 and Swi6 proteins is favoured as the cell cycle progresses and heterochromatin is fully reassembled (Xhemalce & Kouzarides, 2010). Protein Swi6 plays also a major role during the mitosis through its cohesin recruitment activity. Cohesin mediates tight physical cohesion of sister centromeres.

Therefore, kinetochores are tightly held together for the correct attachment of spindle microtubules (Bernard et al., 2001). Protein Swi6 is however released from chromatin during the division of sister chromatids after the H3S10 phosphorylation suggesting lower heterochromatin stability during the mitotic division (E. S. Chen et al., 2008). It is essential to reestablish the stability of heterochromatin by re-binding the Swi6 protein during the S phase of fission yeast cell cycle. This window of partly loosened heterochromatin structure allows the transcription of noncoding repetitive sequences playing crucial role in the heterochromatin maintenance (E. S. Chen et al., 2008). Such transcriptional activity is considered to result in a boost of siRNA production leading to recruitment of heterochromatin assembly factors described before.

4.4.3 Connection between histone acetylation and lipid metabolism in fission yeast

It was shown that the perturbation of centromeric heterochromatin leads to mitotic defects (Allshire et al., 1995; Roche et al., 2016). Guo *et al.* showed negative genetic interaction between the deletions of *cbf11* and *sgf73* and higher frequency of catastrophic mitosis in *cbf11Δ sgf73Δ* strain (Guo et al., 2014). *Sgf73* encodes a deubiquitinating submodule subunit of SAGA acetyltransferase complex (Guo et al., 2014). Sgf73 is directly involved in the centromeric RNAi-dependent heterochromatin maintenance by its contribution in the RITS complex assembly (Deng et al., 2015). *Sgf73* deletion mutants show decreased histone acetylation at H3K9 and H3K16 (Guo et al., 2014).

This (together with the results of ChIP-seq analysis of centromeric chromatin marks in *cbf11Δ* strain described in sub-chapter 5.4) prompted us to the formulation of the hypothesis, that the disruption of HDAC activity could lead to the rescue of catastrophic mitotic events in the *cbf11Δ* mutant.

5 Preliminary data

This study builds on the unpublished data provided by Akshay Vishwanatha, a former member of our research group. He managed to establish the first generation of live-cell imaging method together with imaging data analysis pipelines and obtain some crucial data to build on during this study. Unpublished data by Akshay Vishwanatha will be presented in this chapter to provide context.

5.1 List of strains used for preliminary experiments

Strain ID	Genotype	Source
JB22	*h⁻ wt*	Lab stock
JB32	*h⁺ s*	Lab stock
MP44	*h⁺ cbf11Δ::KanMX4*	Lab stock
JB710	*h⁻ ura4-D18*	Lab stock
MP660	*h⁺ clr4Δ::KanMX4*	(Vishwanatha et al., unpublished)
MP691	*h⁺ clr4Δ::KanMX4 cbf11Δ::NatR*	(Vishwanatha et al., unpublished)
MP207	*h⁻ hst2Δ::KanMX4*	Karl Ekwal
MP738	*h⁻ hst2Δ::KanMX4 cbf11Δ::NatR*	(Vishwanatha et al., unpublished)
MP208	*h⁻ hst4Δ::KanMX4*	Karl Ekwal
MP793	*h⁻ hst4Δ::KanMX4 cbf11Δ::NatR*	(Vishwanatha et al., unpublished)
MP209	*h⁻ hos2Δ::LEU2 leu1-32*	Karl Ekwal
MP739	*h⁻ hos2Δ::LEU2 leu1-32 cbf11Δ::NatR*	(Vishwanatha et al., unpublished)
MP210	*h⁻ clr3Δ::KanMX4*	Karl Ekwal
MP743	*h⁻ clr3Δ::KanMX4 cbf11Δ::NatR*	(Vishwanatha et al., unpublished)
JB959	*h⁻ sir2Δ::KanMX4*	Babis Rallis

MP741	*h- sir2Δ::KanMX4 cbf11Δ::NatR*	(Vishwanatha et al., unpublished)
MP726	*h- bub1Δ::KanMX4 leu1*	Yeast Genetic Resource Center National BioResource Project, FY18581
MP784	*h- bub1Δ::KanMX4 cbf11Δ::NatR leu1*	(Vishwanatha et al., unpublished)
MP730	*h- pds5Δ::ura4 leu1 ura4D18*	Yeast Genetic Resource Center National BioREsource Project, FY31429
MP787	*h- pds5Δ::ura4 cbf11Δ::NatR leu1 ura4D18*	(Vishwanatha et al., unpublished)
MP731	*h- wpl1Δ::Hyg leu1*	Yeast Genetic Resource Center National BioREsource Project, FY31430
MP789	*h- wpl1Δ::Hyg cbf11Δ::NatR leu1*	(Vishwanatha et al., unpublished)
MP732	*h- mad2Δ leu1*	Yeast Genetic Resource Center National BioREsource Project, FY9228
MP790	*h- mad2Δ cbf11Δ::NatR leu1*	(Vishwanatha et al., unpublished)
MP322	*h- leu1 psm1-GFP:LEU2*	Yeast Genetic Resource Center National BioREsource Project, FY11280
MP745	*h- leu1 psm1-GFP:LEU2 cbf11Δ::NatR*	(Vishwanatha et al., unpublished)
MP752	*h+ mCherry-atb2-HygR hht2-GFP:Ura4+ ade6-21? Leu1-32 ura4-D18*	(Lin et al., 2017)
MP758	*h+ mCherry-atb2-HygR hht2-GFP:Ura4+ cbf11Δ::NatR ade6-21? Leu1-32 ura4-D18*	(Vishwanatha et al., unpublished)
JB814	*h+ ura4-D18 leu1-32 ade6-M210 Ch16-RMGAH arg3-D4 his3-D1*	(Tinline-Purvis et al., 2009)
MP194	*h+ ura4-D18 leu1-32 ade6-M210 Ch16-RMGAH cbf11Δ::NatR his3? Arg3?*	(Vishwanatha et al., unpublished)

5.2 Live-cell imaging and data analysis

Akshay Vishwanatha introduced the live-cell imaging method based on the published methodology by Tran *et al.*(Tran et al., 2004). For his experiments, he used an Olympus CellR inverted fluorescent microscope together with the cultivation chamber (Okolab h301-k-frame). To observe and compare the process of mitosis, wild type and *cbf11*Δ strains were used with fluorescently tagged histone H3 (Hht2-GFP) and alpha-tubulin (mCherry-Atb2) in order to visualize chromatin and mitotic spindle respectively. Cells were cultivated in the cultivation chamber for 6 – 8 hours at 32°C during the experiment and images were acquired every 4 minutes in 10-step Z-stack (of 0.5 μm sections) for DIC, green and red fluorescent channels. Three different mitotic outcomes were observed (Vishwanatha et al., unpublished):

1. Normal successful mitosis resulting in the formation of two daughter cells with equally segregated chromosomes.
2. Catastrophic CUT phenotype mitotic events with intersected nuclei and unequal chromosome segregation. If nuclear displacement from the centre of the cell occurs prior to septum formation, this can lead to the formation of a viable diploid daughter cell and a non-viable anucleate daughter cell.
3. The LSD phenotype with unequal chromosome segregation but no visible nuclear intersection.

Akshay Vishwanatha also established the image processing and data analysis pipeline for the live-cell imaging data using ImageJ software (Schneider et al., 2012). Examples of the different mitotic outcomes that were observed are shown in Figure 9. The data analysis pipeline will be further described in the subsequent sub-chapters.

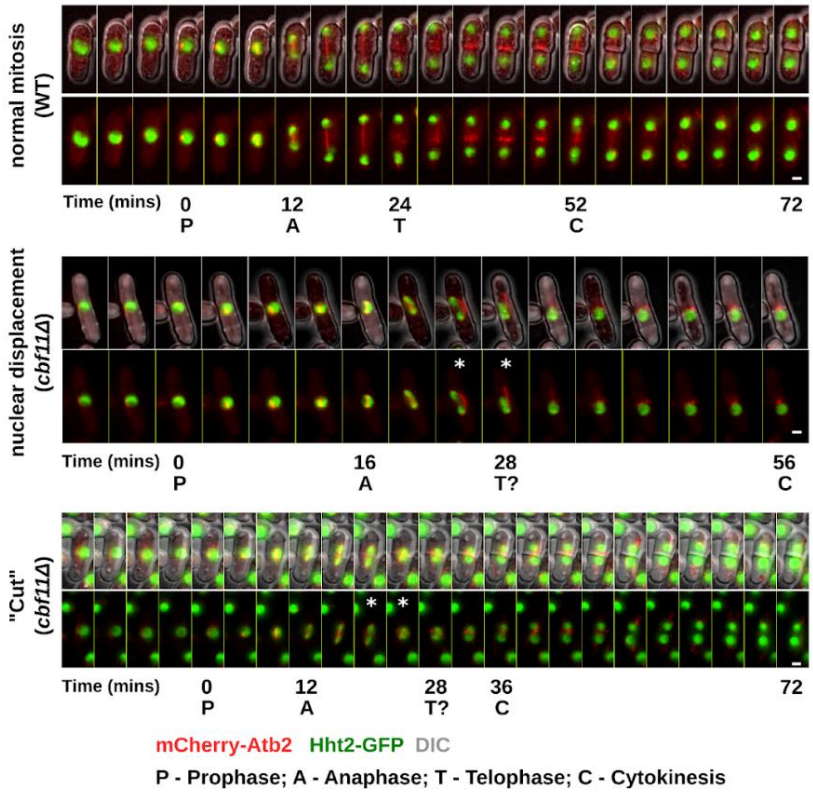

Figure 9 Comparison of normal and catastrophic mitotic events in the wild type and *cbf11*Δ cells. Adapted from (Vishwanatha et al., unpublished). Examples of normal and catastrophic mitotic events in wild type and *cbf11Δ* genetic background. Bottom panels show chromosomes in green and microtubules in red; top panels show an overlay with DIC images to visualize cell boundaries and septa. The beginning of individual mitotic phases is indicated below the respective frame together with the timestamp of the respective frame. White scale bars in the lower right corner represent 1 µm. Asterisks indicate spindle defects.

5.3 Aberrant mitotic timing and spindle dynamics in *cbf11*Δ cells

Deeper analysis of acquired data from live-cell imaging was done to better understand the defective mitotic process and it´s attributes in *cbf11*Δ cells. The first and maybe the most obvious attribute analysed was the timing of the mitotic process. 10 cells from each identified mitotic outcome (described in the sub-chapter 5.2) were randomly selected for further analysis.

*Cbf11*Δ cells that have undergone normal mitotic division displayed longer and more variable mitotic duration compared to the wild type cells. Interestingly, *cbf11*Δ cells displayed also more variable and longer intervals between the spindle formation and anaphase onset compared to wild type cells, suggesting problems with the attachment of the spindle to chromosomes.

Aberrantly divided *cbf11*Δ showed even more variability in both parameters and significantly slower spindle elongation rate. Also, the mitotic spindle was shorter in its maximum length than in either successfully divided *cbf11*Δ or wild type cells.
Another common behaviour observed during the defective mitosis of *cbf11*Δ cells was bending of the mitotic spindle in anaphase with subsequent detachment of one of the daughter chromatin masses from the spindle. The spindle then breaks and the dividing nucleus becomes spherical again. These findings correspond with the published data of spindle bending upon chemical inhibition of fatty acid synthesis, presented in the sub-chapter 4.3.2 (Takemoto et al., 2016).

5.4 Perturbation of centromeric chromatin in *cbf11*Δ cells

There are indications of correlation between the lipid metabolism perturbation and centromeric structure changes during the chromosome segregation, as described in the sub-chapter 4.4.3. To confirm previous published data and investigate the centromeric epigenetic pattern, ChIP-seq analysis of H3K9 acetylation and methylation was performed in wild type and *cbf11Δ* strains. Cbf11 deficient strains showed hypermethylated centromeric regions with altered H3K9me2 pattern compared to the wild type. Also, the expression of centromeric *dh* and *dg* repeats was lower in *cbf11Δ* strains compared to the wild type. However, the results were questionable to some extent as the expression of centromeric repeats is generally very low. The analysis was therefore repeated in the heterochromatin-disrupted *clr4Δ* and *clr4Δ cbf11Δ* double-mutant strains. The *dh/dg* expression levels in these mutants are high and can provide a more robust readout (Allshire & Ekwall, 2015). The *dh* repeat expression was also lower in the *clr4Δ cbf11Δ* double-mutant strain compared to the *clr4Δ* mutant, suggesting Cbf11 role in heterochromatin biology.

5.5 Histone deacetylases deficiency rescue the mitotic defects of *cbf11Δ* cells

The comparison between *dh* repeats expression data in the heterochromatin-disrupted *clr4Δ cbf11Δ* double-mutant and the *clr4Δ* mutant suggests Cbf11 involvement in the histone acetylation. Disruption of the histone acetylation would result in the imbalance of HAT and HDAC activities leading to the lower number of pronounced euchromatin marks and

chromatin more prone to forming heterochromatin. Hypothetically, the deletion of HDACs could reestablish this balance and rescue the catastrophic mitosis phenotype in *cbf11Δ* mutant strains. Strikingly, with the exception of *hst4Δ*, all tested HDAC mutations dramatically decreased the incidence of catastrophic mitosis in the *cbf11Δ* background (Figure 10). All HDACs whose deletion was indicating the rescue of catastrophic mitosis phenotype in *cbf11Δ* background are directly or indirectly required for H3K9 deacetylation and subsequent methylation (Alper et al., 2013; Bjerling et al., 2002; Durand-Dubief et al., 2007; Wirén et al., 2005). The only HDAC whose deletion was unable to rescue the catastrophic mitosis phenotype in *cbf11Δ* background was Hst4, which regulates the acetylation status of H3K56 in DNA repair (Haldar & Kamakaka, 2008). Also, it was never reported to alter the acetylation of H3K9.

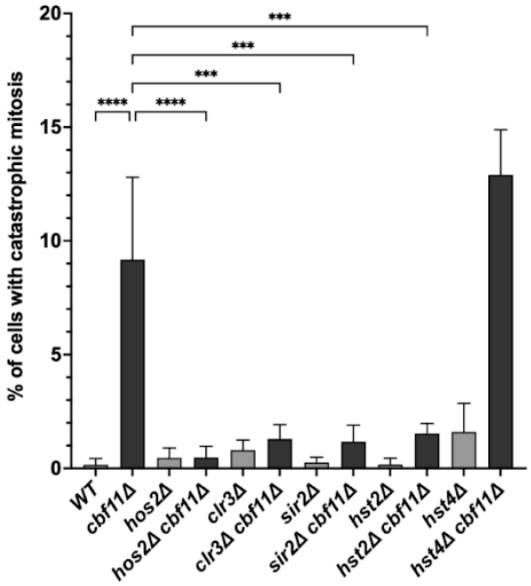

Figure 10 – Catastrophic mitosis in HDAC and Cbf11 mutants. (Vishwanatha et al., unpublished). Incidence of catastrophic mitosis in the indicated strains. At least 400 cells were scored per sample. Values represent means and error bars standard deviation from 3 independent experiments. The significance of suppression of catastrophic mitosis in the respective double mutants compared to the *cbf11Δ* strain was determined by one-way ANOVA followed by Bonferroni multiple comparison test. ** - p <0.001,*** - p < 0.0001, **** - p < 0.00001 (Vishwanatha et al., unpublished).

In conclusion, data provided by Vishwanatha *et al.* strongly suggest that altered H3K9 posttranslational modifications have a strong negative effect on the successful mitotic progression in *cbf11Δ* cells.

6 Results

6.1 Strain creation

To reach the main goal of this study and observe the mitotic dynamics in different HDAC mutant strains in wild type and *cbf11Δ* genetic backgrounds, a library of suitable strains was created using different genetic manipulation methods described in the subsequent sub-chapters.

The preliminary live-cell imaging experiments by Akshay Vishwanatha were performed on *S. pombe* strains auxotrophic for uracil, adenine and leucine. These auxotrophic mutations can cause different phenotypical changes in the fission yeast cells like increased flocculation (Kwon et al., 2012), disrupted cell wall integrity (Matsuo et al., 2013) or altered respiratory apparatus (Malecki et al., 2016). Therefore, the data obtained using auxotrophic strains can be biased by possible genetic or metabolic interactions.

As a parental fission yeast strain, the *h^+ mCherry-Atb2-HygR Hht2-GFP:Ura4+ ade6-21? Leu1-32 ura4-D18* (MP752) strain that was created by Lin *et al.* (Lin et al., 2017) and used by Akshay Vishwanatha for preliminary experiments. The strain features the mCherry tagged alpha-tubulin (Atb2) coupled with a hygromycin resistance cassette and GFP tagged histone H3 (Hht2) coupled with an *ura4* gene as a selective marker. However, the genome of the strain contains also undesired auxotrophic mutations.

For the creation of new strains, genetic crossing and transformation were used in this study. The schematic overview of every crossing and transformation is depicted in the Figure 11.

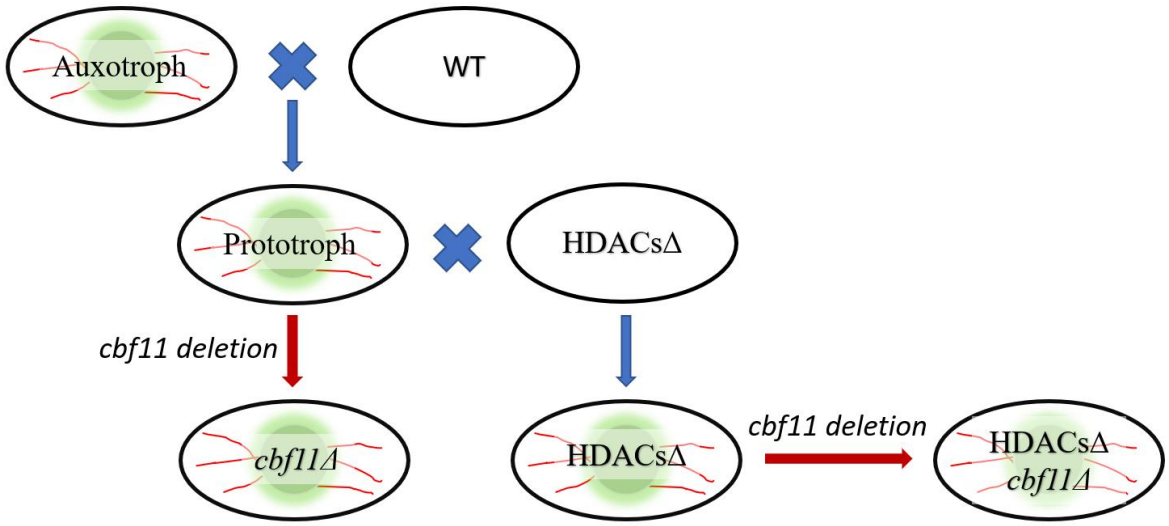

Figure 11 – Schematic overview of genetic crosses and transformations of *Schizosaccharomyces pombe* in this study.

6.1.1 Genetic crossing

To remove the undesired auxotrophic mutations from the MP752 strain, the *Schizosaccharomyces pombe* genetic crossing method was performed as described in the sub-chapter 3.1.6. The h^+ MP752 strain was crossed with the h^- *ura4-D18* (JB710) strain. The uracil auxotrophic mutation at the endogenous *ura4* locus was kept because of the GFP coupling with an ectopic copy of the *ura4* gene as a selective marker. The correct genotype of daughter cells after the crossing, *mCherry-atb2-HygR hht2-GFP:Ura4+ ura4-D18* (double-tagged), was ensured by cultivation on selective EMM + Hyg plates and subsequent microscopy. Two strains with opposite mating types were picked for further experiments. The mating type was identified by colony PCR method for 8 picked monocolonies (described in the sub-chapter 3.2.5.1) with subsequent agarose gel electrophoresis (described in the sub-chapter 3.2.6). A small amount of biomass (approximately 1 µg) of the h^+ wild type strain was used as a positive control for this PCR experiment. The resulting gel is shown in the Figure 12.

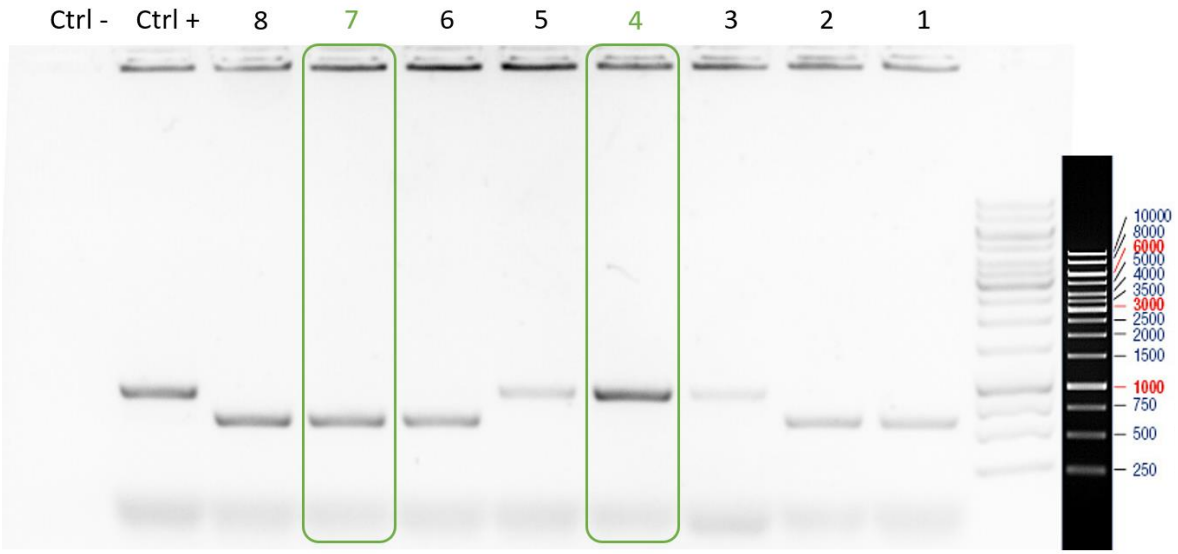

Figure 12 – Mating type identification. Mating type was identified for 8 different strains created by genetic crossing. The presence of 987 bp PCR product indicates h^+ mating type and 729 bp PCR product indicates h^- mating type of a tested strain. Reaction without template was used as negative control (Ctrl-) and wild type strain with defined h^+ mating type as a positive control (Ctrl+). PCR products were separated in 1% agarose gel and visualised by UV light (illuminator Azure biosystems c150). GeneRuler 1kb DNA Ladder (ThermoScientific) was loaded in the gel together with the PCR reactions. The DNA ladder is aligned to correctly estimate the size of desired DNA fragments. Numbers indicate the order of the colonies on the plate. Picked colonies for further use are marked with a green colour.

Strains numbered 4 and 7 with mating types h^+ and h^-, respectively, were picked for glycerol stocks creation (described in sub-chapter 3.1.4) and added to the database as MP807 and MP808 respectively.

The *Schizosaccharomyces pombe* genetic crossing method was also performed to create the desired HDAC deletion mutant strains in the double-tagged genetic background. The previously created h^+ prototrophic double-tagged strain MP807 was crossed together with the h^- *sir2Δ::KanMX4* (JB959), *hst2Δ::KanMX4* (MP207), *hst4Δ::KanMX4* (MP208), *clr3Δ::KanMX4* (MP210) and *hos2Δ::LEU2 leu1-32* (MP209) strains. All genetic crossings were performed as described in the sub-chapter 3.1.7. The correct genotype (double-tagged HDACΔ) of daughter cells was ensured by subsequent cultivation on selective YES + geneticin and YES + hygromycin plates. Two clones of every crossed genotype were picked for stock creation and further experiments. The only exception in this procedure was crossing the double-tagged strain with *hos2Δ::LEU2 leu1-32* strain. The *hos2* deletion cassette complelemts leucine auxotrophy instead of any antibiotic selection as before. In this case, the selection by PCR and subsequent microscopy was chosen to ensure the right genotype

of daughter cells. The PCR detection of hos2 presence was performed for 23 picked monocolonies as described in the sub-chapter 3.2.5.4 and visualised by the agarose gel electrophoresis method (described in the sub-chapter 3.2.6).

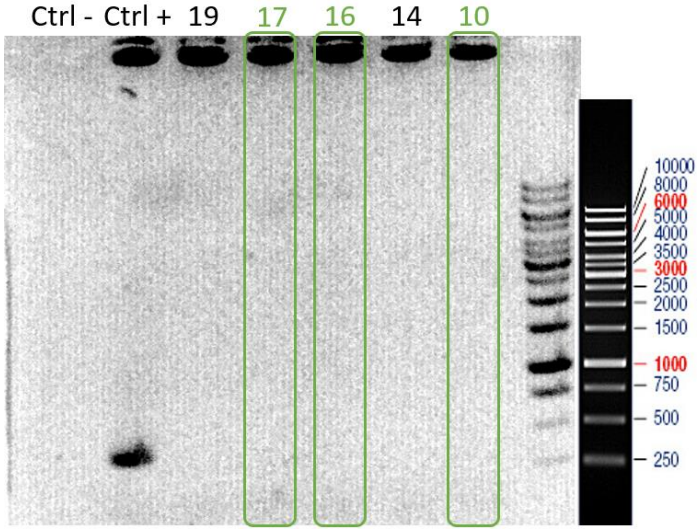

Figure 13 – *hos2* deletion verification. The presence of 405 bp band indicates presence of the *hos2* gene in the genome. Reaction without template was used as negative control (Ctrl-) and wild type strain with *hos2* gene present in the genome as a positive control (Ctrl+). PCR products were separated in 1% agarose gel and visualised by UV light (illuminator Azure biosystems c150). GeneRuler 1kb DNA Ladder (ThermoScientific) was loaded in the gel together with the PCR reactions. The DNA ladder is aligned to correctly estimate the size of desired DNA fragments. Numbers indicate the order of the colonies on the plate. Picked colonies for further use are marked with a green colour.

Example results for 5 clones are shown in the Figure 13. All 5 clones seem to lack the *hos2* gene in their genome. Glycerol stocks were therefore prepared from three clones randomly chosen and confirmed by fluorescent microscopy of both mCherry-*atb2* and *hht2*-GFP (using Nikon H-TIRF 2).

At this point, we have successfully created prototrophic HDAC deletion mutant strains of all 5 non-essential fission yeast HDACs with fluorescently tagged nuclear and spindle components. These strains will be used for further deletion of *cbf11* and as control strains for the upcoming experiments in this study.

6.1.2 Deletion of *cbf11*

Lithium-acetate transformation method of *Schizosaccharomyces pombe* was used to introduce the *cbf11* deletion in this study. The procedure was performed as described in the sub-chapter 3.2.3. The plasmid pMP91 (pCloneNat1, described in the sub-chapter 3.2) was linearised as described in the sub-chapter 3.2.2 and used as a transforming DNA for this

method. After the transformation procedure and one-day cultivation on non-selective YES plates, the biomass was replica plated on selective YES plates containing Nourseothricin antibiotic (100 µg/ml). After the sufficient growth of monocolonies (3-5 days), 20 randomly picked monocolonies were replated both on Nourseothricin selective YES plates and standard YES plates as a control of the procedure. Plates were further incubated at 32°C for 3 days until sufficient growth of biomass. A tiny amount (approximately 1 µg) of biomass of some randomly picked colonies was used for the PCR verification of *cbf11* deletion (as described in sub-chapter 3.2.5.2). The PCR products were loaded on a gel (as described in sub-chapter 3.2.6) and visualised. Two verified clones of every genotype were chosen for stock creation and further experiments. One of the *cbf11* deletion verification gels is shown in the Figure 14 as an example. The entire verification is to be found in the Supplementary materials chapter 10 of this study (Supplementary figure 1, Supplementary figure 2, Supplementary figure 3).

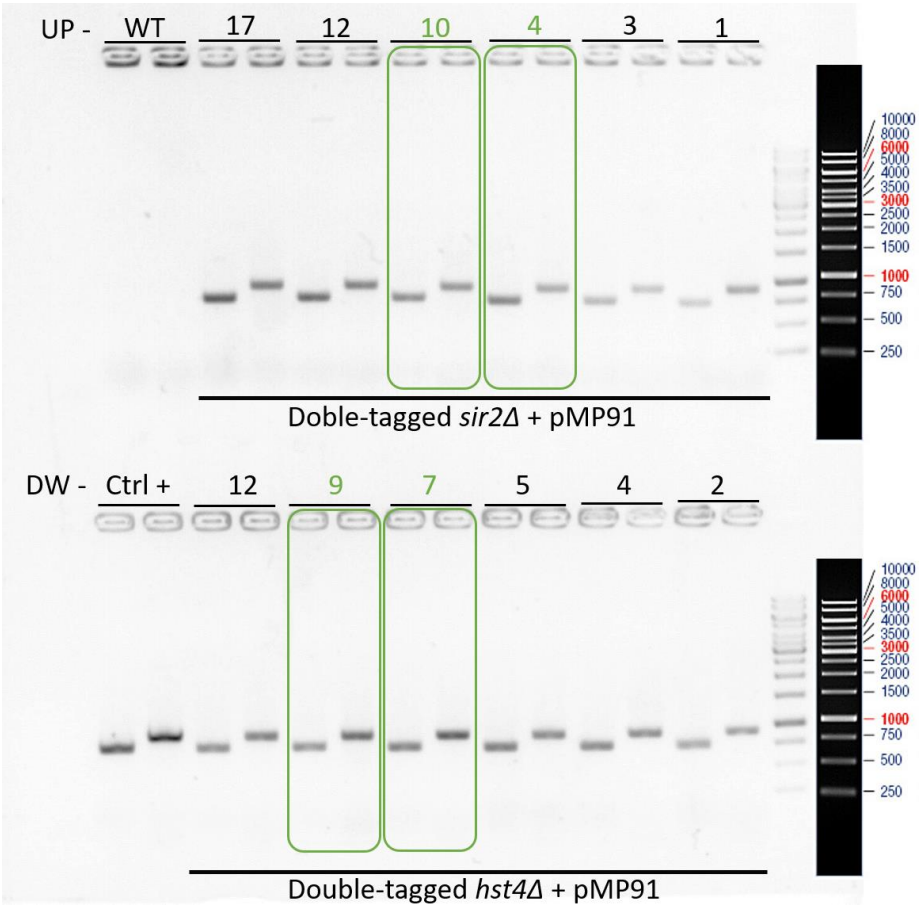

Figure 14 – *cbf11* deletion verification. The presence of both upstream and downstream plasmid integration regions is desired. The DNA fragment sizes of these regions are 953 bp and 823 bp respectively. Reaction without template was used as negative control for reactions of both upstream (UP -) and downstream (DW -) integration regions. *Cbf11Δ*

strain was used as a positive control (Ctrl+) for the reaction. PCR products were separated in 1.5% agarose gel and visualised by UV light (illuminator Azure biosystems c150). GeneRuler 1kb DNA Ladder (ThermoScientific) was loaded in the gel together with the PCR reactions. The DNA ladder is aligned to correctly estimate the size of desired DNA fragments. Numbers indicate the order of the colonies on the plate. The order of PCR reactions for every template is the reaction for the downstream region on the left and for the upstream region on the right. The colonies for further use are marked with a green colour.

The transformation method had to be repeated for the double-tagged *hst4Δ cbf11Δ*. The reason for the repetition was losing the GFP signal, which was discovered during the live-cell imaging experiments (described in the subchapter 6.3). The cause of this problem was identified by microscopy as a mixed parental double-tagged *hst4Δ* culture (strain MP851) with the presence of cells not emitting nuclear GFP signal in a stock (Figure 15). The other clone of this genotype created by the genetic crossing showed, however, unified nuclear signal emittance throughout the whole culture. The transformation was therefore repeated for both double-tagged *hst4Δ* clones. Also additional fluorescent microscopy was performed to select the correct transformants.

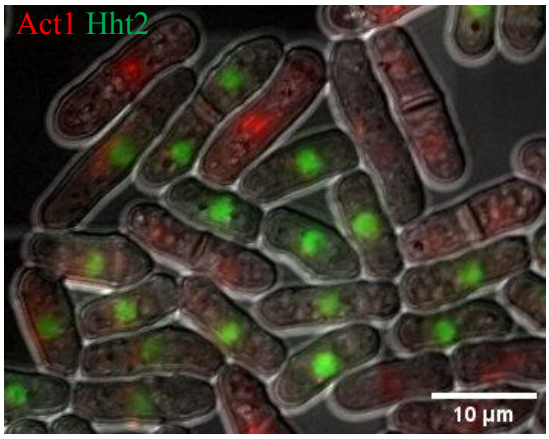

Figure 15 – Representative example of the double-tagged *hst4Δ* mixed culture. Overlayed image of DIC, green and red channels. Supposed genotype of the observed strain was *mCherry-atb2-HygR hht2-GFP:Ura4+ ura4-D18 hst4Δ::kanMX4.* Undesired cells with no nuclear signal are present in the culture.

Regarding our previous experience with the possibility of ectopic *cbf11* gene reintegration during the gene deletion procedure (not showed), we decided to test the *cbf11* deletion more. The outcome of such a scenario would be a strain with the verified deletion plasmid integration to the genome, but *cbf11* also still present. To be sure that *cbf11* gene is truly absent from the genome of transformant strains, we performed a PCR verification with the panel of primers designed to amplify 4 different regions inside the *cbf11* ORF as described in sub-chapter 3.2.5.3. To achieve maximum sensitivity, we have tested three different types

of templates for this type of reaction. We tested a template DNA isolated by quick lithium-acetate method, three different samples of template DNA isolated by phenol-chloroform method and direct insertion of biomass into the reaction as colony PCR.

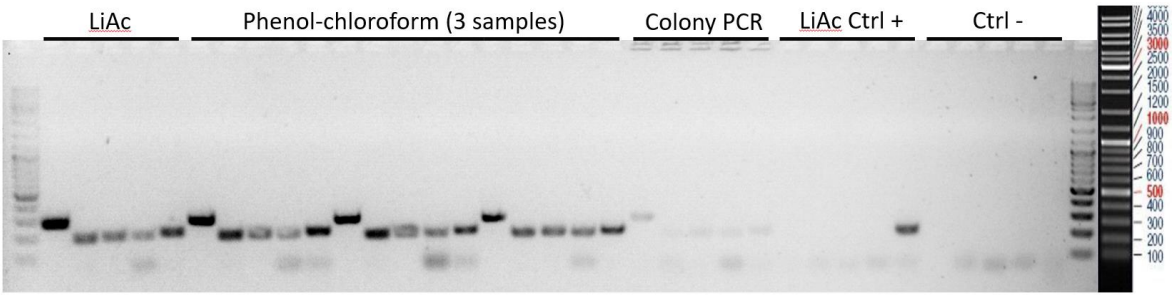

Figure 16 – Identification of the best DNA isolation method. 4 different primer pairs amplify regions inside the *cbf11* ORF during the PCR reaction with product sizes of 286, 190, 198 and 195 bp (respective order from left to right in the figure). Amplification of a fragment inside the *act1* gene ORF was used as a positive control of the reaction (fifth and the most right position of the panel). The reaction was performed for different types of template DNA from the wild type strain. Types of DNA template used from left to right: lithium-acetate isolated gDNA, three different samples (new from Anna Marešová, older from Anna Marešová and one from Viacheslav Zemlianski) of phenol-chloroform isolated gDNA and directly inserted tiny amount of biomass (approximately 1µg) as a colony PCR. Lithium-acetate isolated gDNA from *cbf11Δ* strain was used as a positive control of the reaction. Reaction without template was used as a negative control for each primer pair. PCR products were separated in 2% agarose gel and visualised by UV light (illuminator Azure biosystems c150). GeneRuler 1kb DNA Ladder (ThermoScientific) was loaded in the gel together with the PCR reactions. The DNA ladder is aligned to correctly estimate the size of desired DNA fragments.

Lithium-acetate chromosomal isolation method was picked as the most suitable method for the preparation of the template for *cbf11* deletion verification using a panel of primers. It is a significantly quicker method of DNA isolation than the phenol-chloroform method with comparable reaction efficiency in our scenario. The quickest colony PCR method cannot be used in this case because of a rather poor reaction efficiency.

For the cbf11 deletion verification using a panel of primers, chromosomal DNA was isolated from each *cbf11Δ* strain created in this study using the lithium-acetate method as described in the sub-chapter 3.2.4. 5 µl of isolated gDNA was used as a template for each PCR reaction. The PCR reaction was performed as described in the sub-chapter 3.2.5.3. Aliquots of PCR reactions were loaded on a gel and visualised (described in sub-chapter 3.2.6). The result of the experiment is shown in Figure 17.

At this point, all the necessary strains to observe the process of mitotic division in HDAC and *cbf11* deletion mutant background have been created and verified.

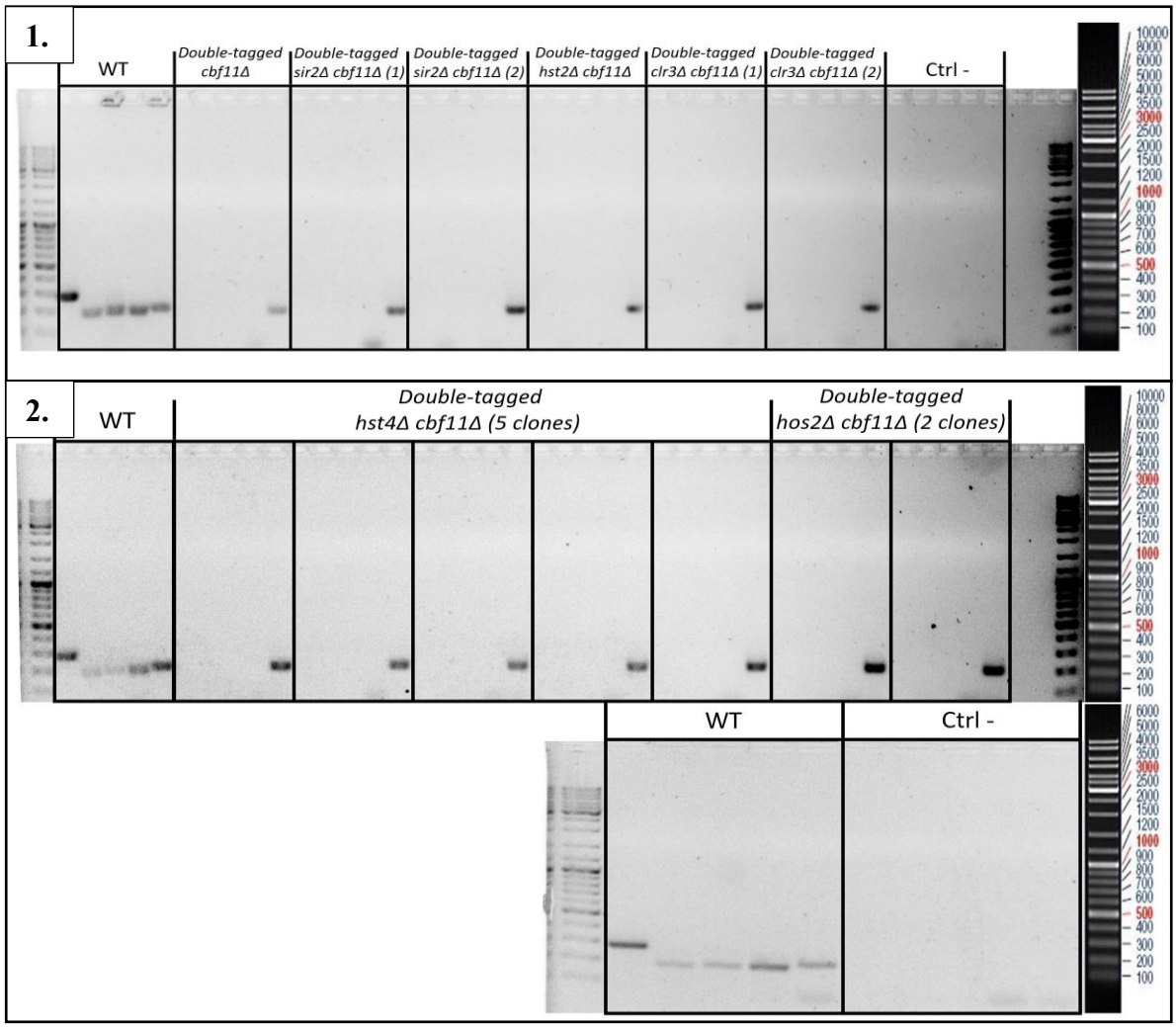

Figure 17 – *cbf11* deletion verification with panel of primers. 4 different primer pairs amplify regions inside the *cbf11* ORF during the PCR reaction with product sizes of 286, 190, 198 and 195 bp (respective order from left to right in the figure). Amplification of a fragment inside the *act1* gene ORF was used as a positive control of the reaction (fifth and the most right position of the panel). Reaction without template was used as negative control for the reaction of each primer pair. The panel verification was done in two separate experiments (numbered 1. and 2.) for every *cbf11* deletion mutant strain created in this study (5 reactions for every template). PCR products were separated in 2% agarose gel and visualised by UV light (Azure biosystems c150). GeneRuler 1kb DNA Ladder (ThermoScientific) was loaded in the gel together with the PCR reactions. The DNA ladder is aligned to correctly estimate the size of desired DNA fragments.

6.1.3 Doubling time measurement

To be able to correctly cultivate the newly created strains, their doubling times have to be determined. For this purpose, measurement on the VarioSkan microplate reader (Thermo Fisher Scientific) was performed as described in sub-chapter 3.1.7. The data was visualised in MS Excel using bar charts (Figure 18).

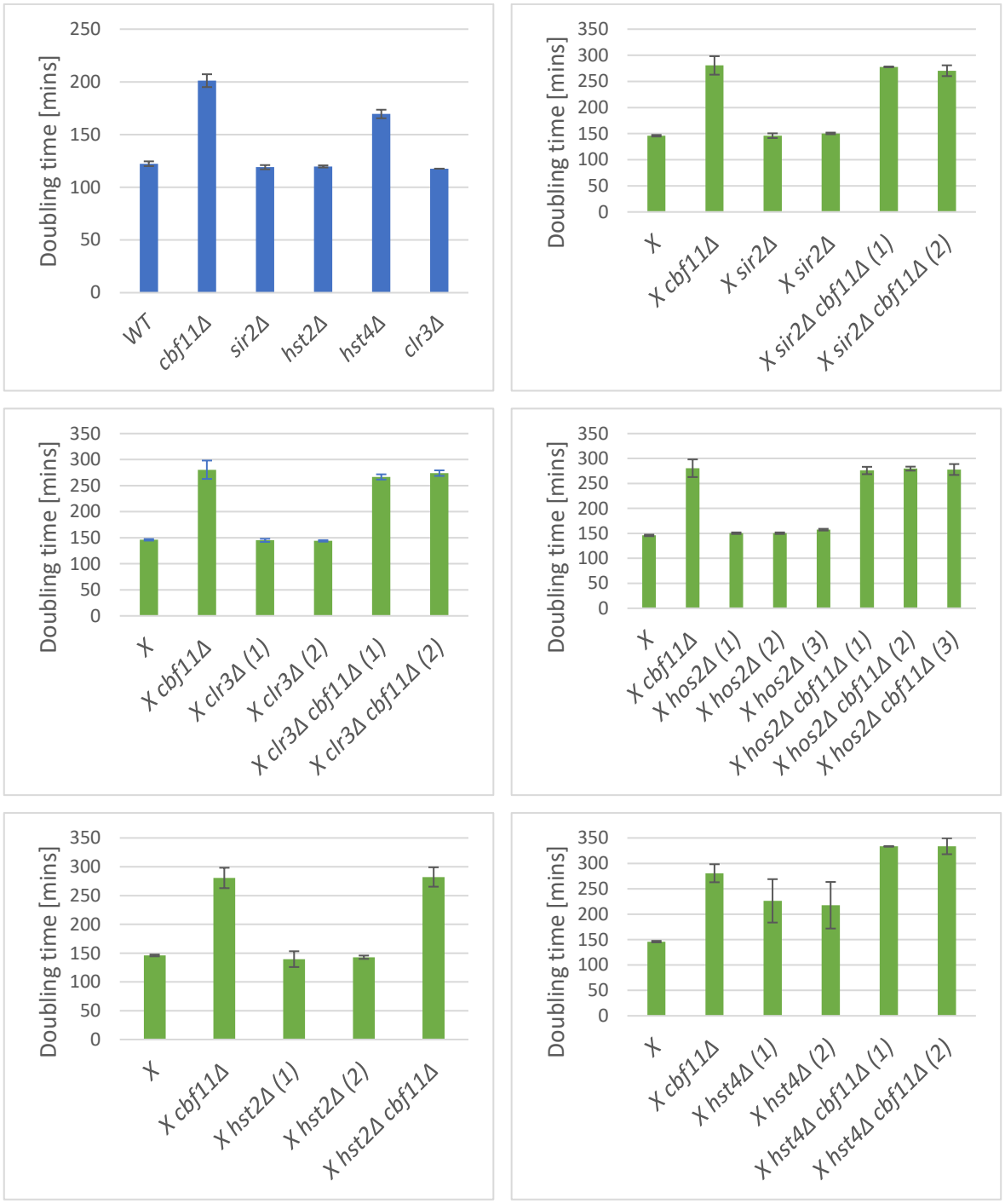

Figure 18 – Doubling time comparison between various genotypes of *S. pombe* strains. The chart in blue shows the doubling time data of control parental strains used for the creation of double-tagged mutant strains in this study. The charts in green show the doubling time data of double-tagged strains created in this study compared to the doubling time of the *cbf11Δ* strain with a known growth defect. The data shown are from 2 biological repeats. Bars represent mean values. Error bars represent standard deviation. X represents an abbreviation for the double-tagged genotype. If more clones have been created for a certain genotype, individual clones are distinguished by numbers in brackets.

The doubling time data show altered growth of strains after the introduction of mCherry and GFP fluorescent marks to some extent (~125 mins. for untagged wild type strain compared to ~145 mins. for double-tagged strain). This suggests that the addition of fluorescent protein tags may partially interfere with microtubule and/or histone dynamics. Overall, double-tagged HDACΔ strains show consistent growth comparable to the corresponding parental strain. The only exception is the double-tagged *hst4Δ* strain showing the growth phenotype comparable to the *cbf11Δ* strain. This is expected as the parental strain shows a growth phenotype to some extent. This phenotype got more pronounced with the introduction of fluorescent marks.

Cbf11Δ strains on the lower chart show also a more pronounced growth phenotype after the introduction of mCherry and GFP fluorescent marks used in this study. But the overall growth profile is again consistent between the strains with the exception of the strain with additional *hst4Δ* deletion.

In conclusion, the introduction of mCherry-*atb2* and *hht2*-GFP extends the overall doubling time of strains to some extent. The deletion of HDACs, on the other hand, has no significant effect on the strain growth (in both wild type and *cbf11Δ* background) with the exception of HDAC Hst4. The *hst4Δ* cells show slower and more variable growth compared to the other HDAC deletion mutants and this growth defects seems to be partially additive with the one conferred by deletion of cbf11.

6.2 CUT phenotype screening

One of the main goals of this study is to observe and describe the CUT phenotype during the mitotic division in *Schizosaccharomyces pombe* cells with different genetic backgrounds. Preliminary data by Akshay Vishwanatha show an interesting rescue in the CUT phenotype incidence in *HDACΔ cbf11Δ* strains (described in sub-chapter 5.5). These data were, however, obtained from strains with no fluorescent tags present in their genome. So, we decided to perform a screening of CUT phenotype incidence in each of the double-tagged strains created in the previous stages of this study (described in sub-chapter 6.1) to determine whether the mitotic phenotypes of the newly created strains are consistent with the preliminary data of Akshay Vishwanatha. The data for such screening is obtained by fluorescent microscopy of DAPI-stained fixed cells.

Fission yeast cells were cultured to the exponential phase of growth (as described in sub-chapter 3.1.3) with OD in a range of 0.4 – 0.7. Cells were then fixed with 70% ethanol as described in sub-chapter 3.1.5**Error! Reference source not found.** and stored at 4°C. Before the microscopic image acquisition, cells were stained with DAPI as described in sub-chapter 3.3. 2 µl of sedimented cell suspension was transferred on a microscopic slide and images were acquired by Leica microscope (Leica DM750 with Leica ICC50 W camera).

The image acquisition was done using the objective with 40x magnification for brightfield and blue channel (DAPI emitting blue light when excited by the UV light; maximal excitation wavelength – 358 nm; maximal emission wavelength – 461 nm). The pairs of images were overlayed and analysed using ImageJ software (as described in the sub-chapter 3.3.3.1). The data was further visualised using bar charts in MS Excel (Figure 19).

The results obtained differ from the preliminary data acquired by Akshay Vishwanatha (Figure 10). There was no apparent rescue of the CUT phenotype observed in either of the tested HDACΔ *cbf11Δ* mutant strains. These results prompted us to further test the strains used for preliminary data acquisition.

The method of *cbf11* deletion verification using a panel of ORF-spanning primers was developed only after the time of preliminary data acquisition by Akshay Vishwanatha. Therefore, we have decided to verify the *cbf11* deletion in his original strains using the panel of primers as described in sub-chapter 3.2.5.3 first. The verification of 4 strains used for preliminary data acquisition was performed by Jarmila Princová (other member of the group; Figure 20). The results show *cbf11* locus still present in two out of 4 tested strains used for preliminary data acquisition (*hos2Δ cbf11Δ* and *sir2Δ cbf11Δ* strains).

We decided to test the two problematic strains more and exclude the possibility of different cultivation and fixation conditions between the experiments performed for preliminary data acquisition and experiments performed during this study. We performed the CUT screening for the parental *hos2Δ* and *sir2Δ* strains, *hos2Δ cbf11Δ* and *sir2Δ cbf11Δ* strains used for preliminary data acquisition and double-tagged *hos2Δ*, *sir2Δ*, *hos2Δ cbf11Δ* and *sir2Δ cbf11Δ* created in this study. The cells were cultivated in the same conditions to OD_{600} equal to 0.45 – 0.6. Fixed cells were stained with DAPI (as described in sub-chapter 3.3), microscopic images were acquired and data analysed following the process described in this sub-chapter. The results of the experiment are shown in Figure 21. The results of this experiment are comparable to the preliminary data (Figure 10).

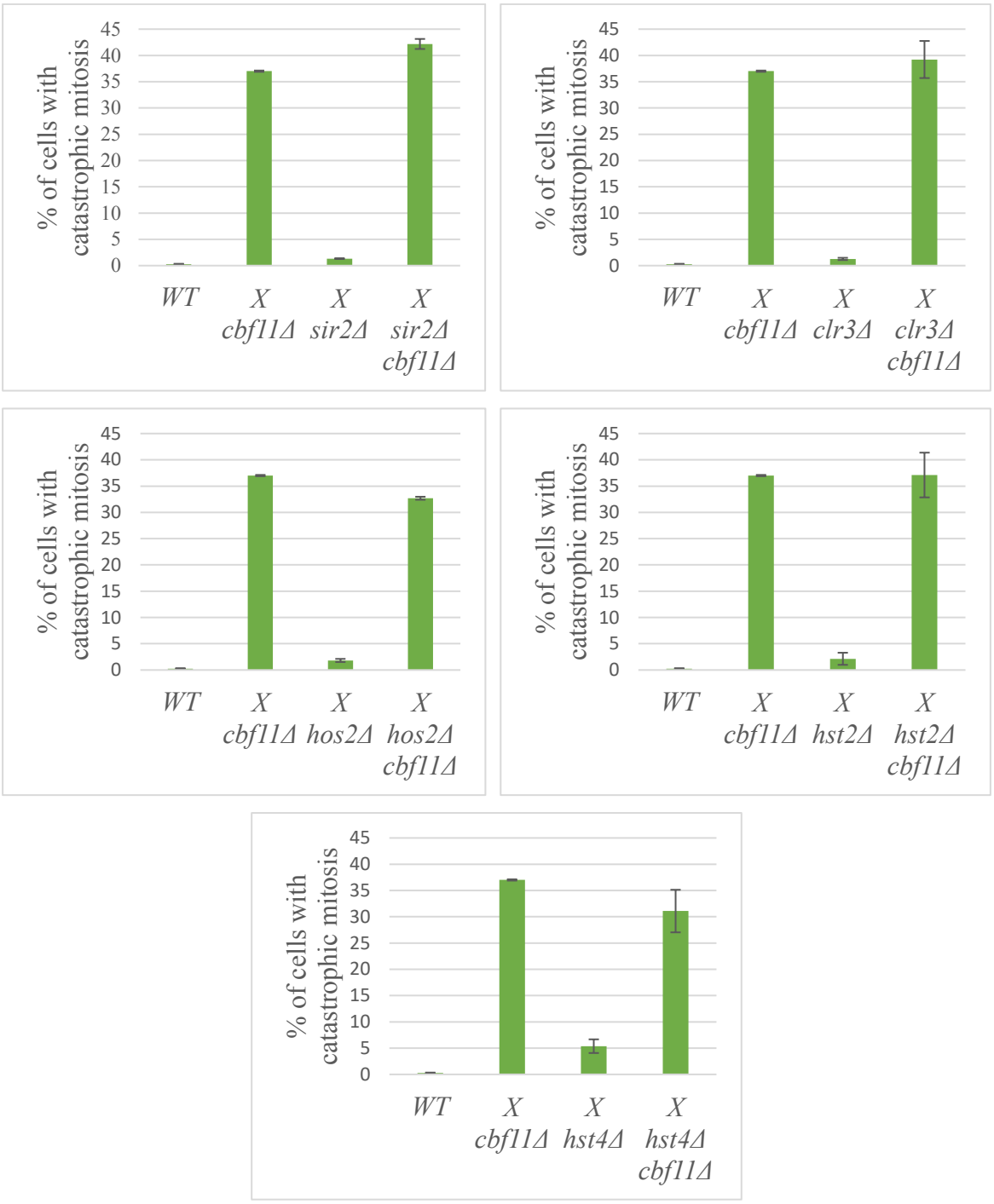

Figure 19 – Comparison of CUT phenotype incidence in different fission yeast HDAC mutants. Each panel shows the CUT phenotype incidence in a certain HDACΔ and HDACΔ*cbf11Δ* strains compared to the wild type and *cbf11Δ* strains. The same data for wild type and *cbf11Δ* strains is included in every panel for reference. Shown data are from 2 biological repeats. Bars represent mean values. Error bars represent standard deviation. X represents an abbreviation for the double-tagged genotype.

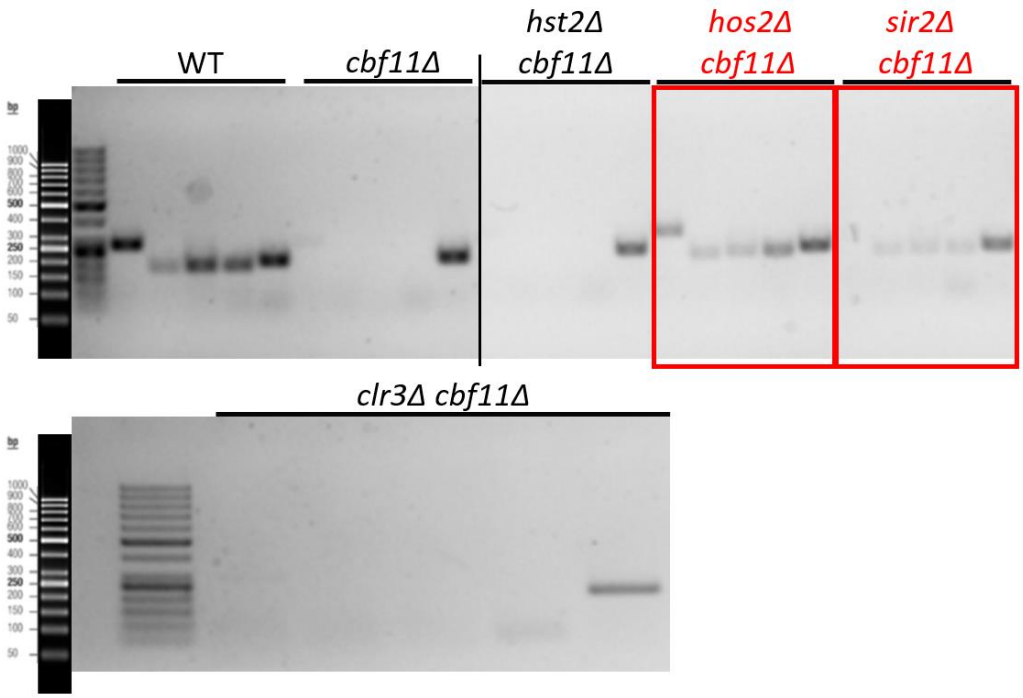

Figure 20 – cbf11 deletion verification in strains used for preliminary data acquisition using panel of primers. 4 different primer pairs amplify regions inside the *cbf11* ORF during the PCR reaction with product sizes of 286, 190, 198 and 195 bp (respective order from left to right in the figure). Amplification of a fragment inside the *act1* gene ORF was used as a positive control of the reaction (fifth and the most left position of the panel). Reaction without template was used as negative control for the reaction of each primer pair. PCR products were separated in 2% agarose gel and visualised by UV light (Azure biosystems c150). GeneRuler 50bp DNA Ladder (ThermoScientific) was loaded in the gel together with the PCR reactions. The DNA ladder is aligned to correctly estimate the size of desired DNA fragments. Incorrectly genotyped strains are marked with the red colour. Not relatable samples were cropped out of the gel (marked with the vertical line).

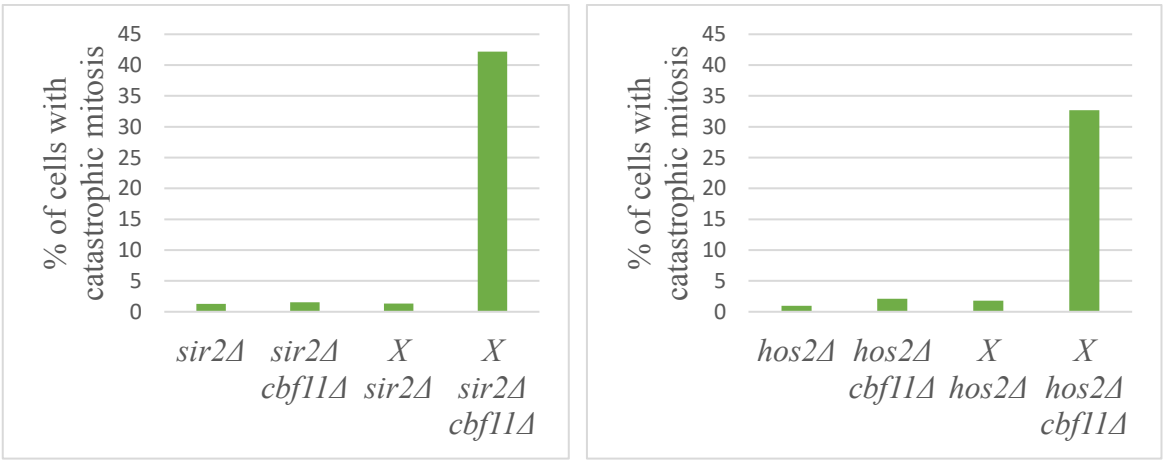

Figure 21 – Comparison of strains used in preliminary experiments with strains used in this study. The cells were cultivated together to OD_{600} equal 0.45 – 0.6. Shown data are from 1 biological repeat. X represents an abbreviation for the double-tagged genotype.

6.3 Live-cell imaging

The live-cell imaging was performed for all double-tagged strains created during this study as described in the sub-chapter 3.3.2, even though no rescue of CUT phenotype has been observed in any of the HDACΔ *cbf11Δ* strains. The protocol already contains optimization steps done by the author of this study, as optimization of the live-cell microscopy method was one of the goals of the study.

During the slide preparation, the first optimization of the method done by the author of this study (and suggested by Viacheslav Zemlianski, other member of the research group) was to let a cell suspension dry onto the YES + 4% agarose medium before the covering with the cover glass. The second optimization of the slide preparation process was taping the cover glass to the slide with the common office adhesive tape from sides.

The live-cell imaging pipeline for the Nikon H-TIRF 2 microscope was developed in the NIS-Elements software by the author of this study in collaboration with the Microscopy service facility of the Charles University and Viacheslav Zemlianski. In the beginning, the live-cell imaging pipeline was developed for one-slide setup. To be able to observe more cells with different genotypes in one run, the method was enhanced by the script to acquire microscopic images from two different slides.

In the live-cell imaging data, we managed to identify all three mitotic outcomes previously observed and described by Akshay Vishwanatha (described in sub-chapter 5.2):

1. Normal successful mitosis resulting in the formation of two daughter cells with equally segregated chromosomes.
2. Catastrophic CUT phenotype mitotic events with intersected nuclei and unequal chromosome segregation. Also, nuclear displacement occurred in some cases leading to the formation of a viable diploid daughter cell and a non-viable anucleate daughter cell.
3. The LSD phenotype with unequal chromosome segregation but no nuclear intersection.

The representative examples of the identified types of mitotic events are shown in the Figure 22.

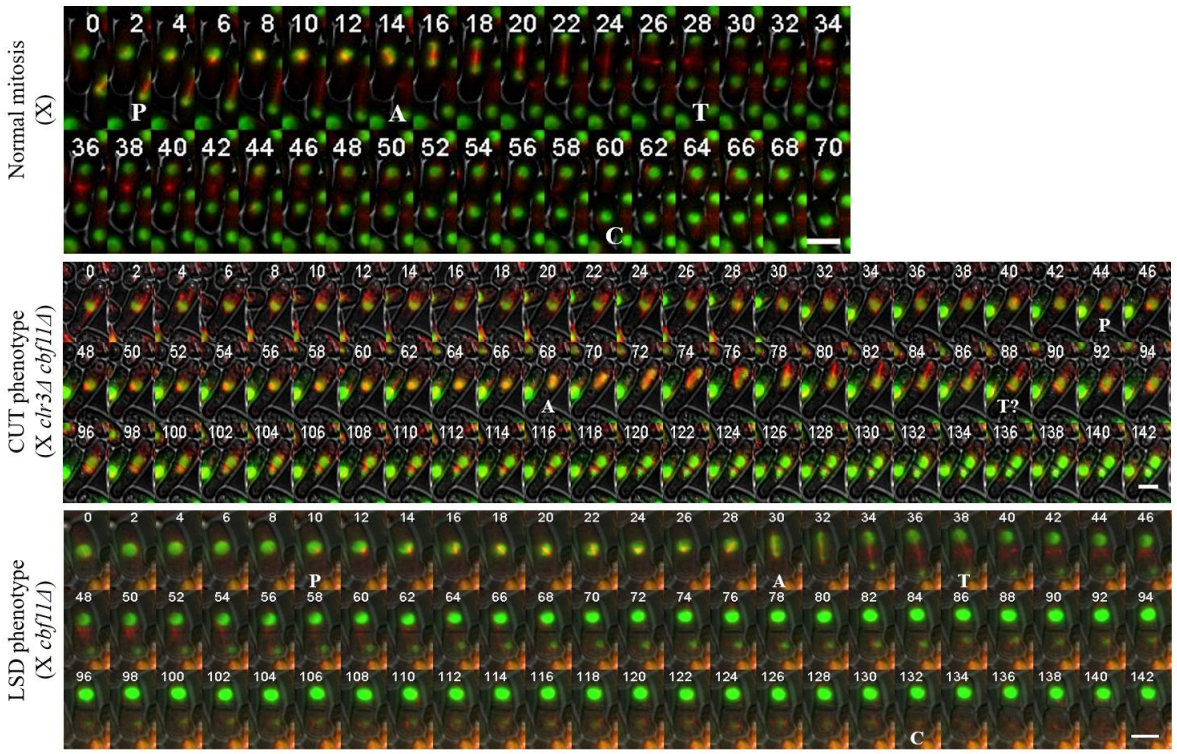

Figure 22 – Representative examples of the identified types of mitotic events. Three different types of mitotic events were identified by live-cell imaging in this study. The time-course examples in this figure show normal mitosis, CUT phenotype and LSD phenotype in double-tagged, double-tagged *clr3Δ cbf11Δ* and double-tagged *cbf11Δ* strains respectively. X represents an abbreviation for the double-tagged genotype. The numbers inside every individual picture indicate the exact time point in minutes. The letters inside particular time-frames indicate the beginning of respective mitotic phase (P = Prophase, A = Anaphase, T = Telophase, C = Cytokinesis)

6.3.1 Timing of mitotic phases

The analysis of duration of mitotic phases was done to better understand the defective mitotic process in *cbf11*Δ cells. In this setup of the analysis, there are three easily distinguishable mitotic phases:

- Prophase + metaphase – these two mitotic phases are impossible to distinguish from each other in this experimental setup, so their duration was merged and analysed together. The beginning of the prophase was set as the beginning of spindle formation. The end of the metaphase was set as the beginning of spindle elongation and nuclear division.
- Anaphase – The beginning of the anaphase was set as the beginning of spindle elongation and nuclear division. The end was set as the time point when the

nuclei reach the maximal distance between each other and the spindle reaches its maximal length.

- Telophase – The beginning of the telophase was set as the time point when the nuclei reach the maximal distance between each other and the spindle reaches its maximal length. The end was set as a time point when daughter cells are fully divided (cytokinesis).

The duration of these three identified mitotic phases was measured for all of the strains created in this study and compared with the results from preliminary experiments (described in the sub-chapter 5.3).

10 cells undergoing normal mitotic process were randomly picked for the analysis from each of the analysed strains with some exceptions. The first exception was *hos2Δ cbf11Δ* strain, in which only 5 mitotic cells had been observed. The other exceptions were the wild type strain and *cbf11Δ* strain, for which 30 cells undergoing normal mitotic process were randomly picked for more robust comparison of the analysis with the preliminary data. The telophase duration was measured only for cells successfully reaching cytokinesis during the experimental time frame with amounts varying through the used genotypes. Therefore, shown data on the telophase duration are just preliminary.

The results (Figure 23) show prolonged mitotic phases in each of the *cbf11Δ* strains compared to their respective double-tagged or double-tagged HDACΔ parental strains. Duration of the prophase + metaphase in the double-tagged strain was observed in the range of ~10-15 minutes with lower extreme measurements reaching 6 minutes duration time. In contrast, the duration of the same mitotic phase in the double-tagged *cbf11Δ* was longer in the range of ~12-16 minutes with higher extreme measurements reaching 20 minutes duration time. A similar shift of the mitotic phase duration is also seen for the anaphase. The duration of anaphase was even more variable in the double-tagged *cbf11Δ* strain ranging from ~8 to ~24 minutes. Obtained results also correspond with the preliminary findings described in sub-chapter 5.3 (Vishwanatha, unpublished).

Observed shift of the duration of mitotic phases is apparent in all of the studied genotypes. HDACΔ *cbf11Δ* strains show consistent shift in the timing of prophase + metaphase and anaphase mitotic phases compared to their respective HDACΔ parental strains similar to the double-tagged vs. double-tagged *cbf11Δ* comparison.

There was no rescue of mitotic defects apparent in any of the HDACΔ *cbf11Δ* double mutants compared to the *cbf11Δ* single mutant. Thus, there was no sense in performing statistical testing of results' significancy.

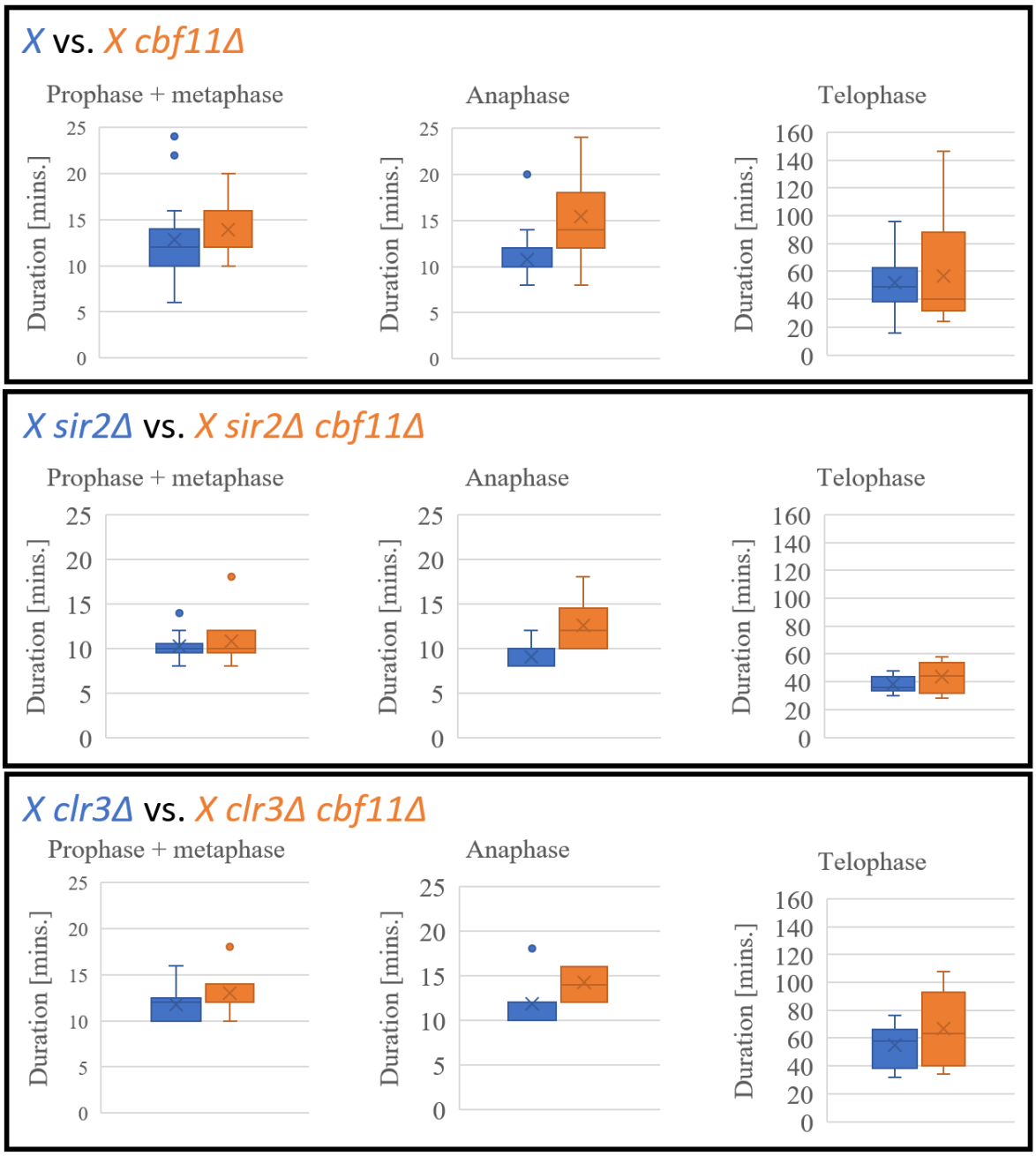

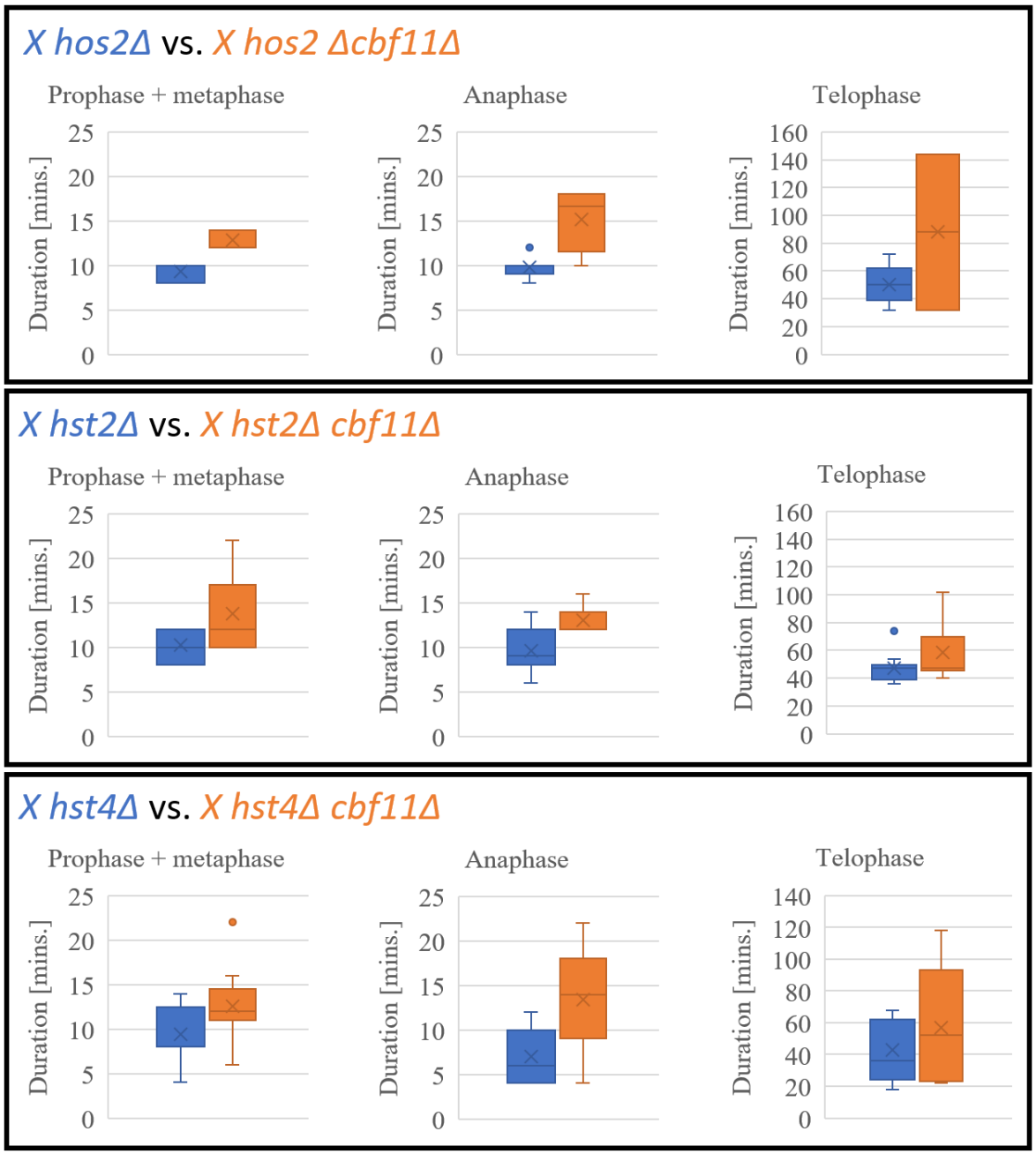

Figure 23 – Analysis of the timing of mitotic phases. Box and Whisker diagrams show the comparison of the timing of mitotic phases in *cbf11* deletion mutant strains and their respective parental strains. The duration of three mitotic phases was analysed: Prophase + metaphase, Anaphase and Telophase. X in the chart title represents an abbreviation for the double-tagged genotype. The cross inside the chart represents the mean value.

6.3.2 Nuclear distance during the mitotic progression

As described in the subchapter 4.3.1, during the fission yeast process of closed mitosis, the nucleus start to physically divide and forms a dumbbell structure with intact nuclear envelope. Two future daughter nuclei are pushed to the opposite poles of the cell by the spindle. The tension of the spindle finally separates two daughter nuclei located in the opposite poles of the cell.

We performed the analysis of nuclear distance, to better understand the process of nuclear division during the progression of closed mitosis. The analysis was performed using the processed green channel live-cell imaging data acquired by the method described in the sub-chapters 3.3.2 and 6.3. The pipeline for the analysis was developed in collaboration with Viacheslav Zemlianski using the ImageJ software (v1.53q; also available as an ImageJ macro at https://github.com/ViacheslavZemlianski/Mitotoc-dynamics):

1. Find and select the cell of interest using the "Rectangle" selection tool
2. Create a duplicate stack containing the selected cell of interest
3. Binarize the duplicate stack using the "Make Binary" ImageJ function (Process – Binary – Make Binary) – the method and background were set to "Default" and "Calculate threshold for each image" field ticked
4. The position of pixels was analysed using the "Analyze particles" ImageJ function (Analyze – Analyze particles) – Size: 0-Infinity, Circularity: 0.00-1.00, Show: "Bare outlines", "Exclude on edges" and "Include holes" fields ticked
5. The analysed position of pixels was saved as a .txt file using the "Save XY coordinates" ImageJ function (Analyze – Tools – Save XY Coordinates)

The created text file contains the coordinates of every analysed pixel from the analysed area. So, the most distant pixels (corresponding the most distant nuclear edges) were found using the Python script developed by Viacheslav Zemlianski (script available at https://github.com/ViacheslavZemlianski/Mitotoc-dynamics). The outcome of the script is a newly created .csv file containing the table of pixel distances between two identified most distant pixels for every picture (time point of the experiment). The values were then converted to metric distance values using the scale of the source images acquired during the live-cell imaging. The data series were then aligned by finding the exact point of nuclear division onset. Aligned data were plotted using standard line charts in MS Excel (Figure 24).

The analysis of nuclear distance during the mitosis was done for the double-tagged and double-tagged *cbf11Δ* strains. 10 cells undergoing normal mitotic division were plotted for both analysed genotypes. Additionally, 4 CUT phenotype cells and 2 LSD phenotype cells (described in the sub-chapter 5.2 and 6.3) were analysed for the double-tagged *cbf11Δ* strain. The results show relatively uniform nuclear distance dynamics during the mitotic progression in the double-tagged strain. In contrast, double-tagged *cbf11Δ* strain data show high variability in the nuclear distance during the mitotic progression in the cells undergoing the normal mitotic division. But the overall pattern of particular cells is comparable with the double-tagged strain data. The pattern of nuclear distance during the mitotic progression was not different for the analysed LSD phenotype cells. CUT phenotype cells, on the other hand, show an altered nuclear distance pattern compared to normally dividing cells. The chart shows a clear remerging of the dividing nucleus at some timepoint resulting in the nuclear distance similar to the starting positions.

In conclusion, we have managed to analyse the mitotic progression in the cells with perturbed lipid metabolism using quantitative data.

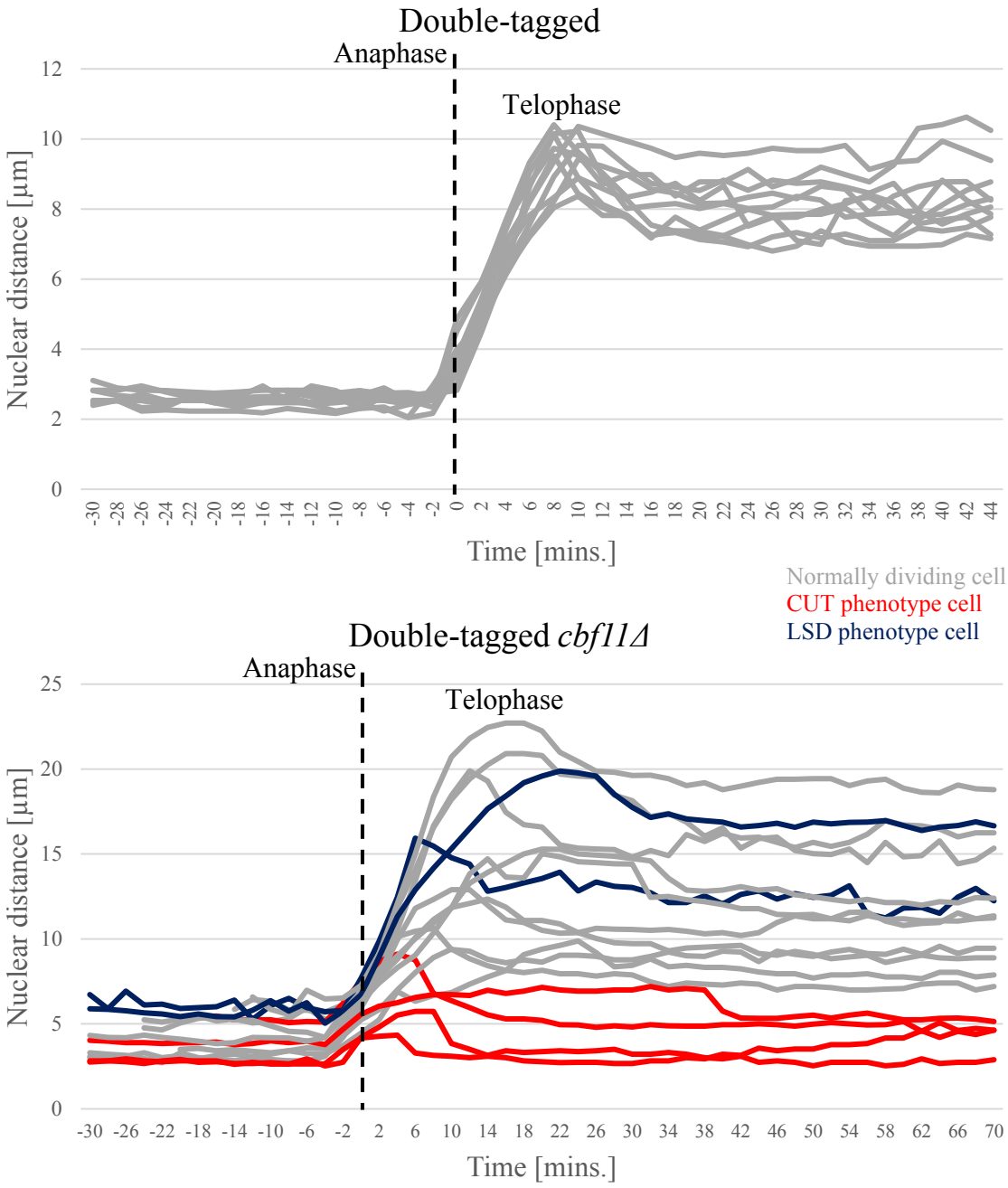

Figure 24 – Comparison of the nuclear distance during the progression of normal and catastrophic mitotic processes. The upper chart shows the nuclear distance during the mitotic progression in the double-tagged cells. The lower chart shows the nuclear distance during the mitotic progression in the double-tagged *cbf11Δ* cells. 10 cells undergoing normal mitotic division were plotted for both analysed genotypes (in grey). Additionally, 4 CUT phenotype cells (in red) and 2 LSD phenotype cells (in blue) were analysed for the double-tagged *cbf11Δ* strain. The anaphase onset was set as a timepoint 0 for both charts. The peaks represent the beginning of telophase (the daughter nuclei furthest from each other).

7 Discussion

7.1 Methodological summary

Methods used in this study are classical fission yeast and DNA manipulation methods used in the research of *Schizosaccharomyces pombe* with the exception of live-cell imaging. Despite the fact that live-cell imaging method is widely used to directly study in vivo cellular processes, it was not well established in our research group. In our research group, the live-cell imaging method was first introduced by Akshay Vishwanatha based on the published methodology by Lin *et al.* (Lin et al., 2017). It was used to uncover the details of mitotic cellular division in the cells with perturbed lipid metabolism (*cbf11Δ*). The experiments were however done using an auxotrophic strain acquired from a different laboratory (Lin et al., 2017).

Auxotrophic mutations can however alter various fission yeast cellular processes when cells are cultivated on a complex YES medium:

- Flocculation ability is increased in cells containing leucin, uracil and/or adenine auxotrophic mutations (Kwon et al., 2012)
- Cell wall integrity is perturbed in cells containing uracil auxotrophic mutation (Matsuo et al., 2013)
- Proliferation is inhibited and cell morphology is perturbed in cells containing adenine auxotrophic mutation (Kokina et al., 2014)
- There is strong genetic interaction between the auxotrophic mutations and deletion mutations of genes involved in the cellular respiration (Malecki et al., 2016)

Moreover, the effects of auxotrophic mutations on gene expression cannot be overcome by simple supplementation of cultivation medium with the respective nutrients (Alam et al., 2016). Therefore, it is recommended to avoid the auxotrophic mutations as much as possible to provide more reliable information on in vivo cellular processes. The auxotrophic mutations were successfully crossed-out of the *h^+ mCherry-atb2-HygR hht2-GFP:Ura4+ ade6-21? Leu1-32 ura4-D18* strain as described in the subchapters 3.1.6 and 6.1.1 and the created strain was used for further experiments of this study.

Also, the live-cell imaging method used for preliminary experiments by Akshay Vishwanatha was optimized for the older Olympus CellR inverted fluorescent microscope. Yet, before the beginning of this study, the more modern Nikon H-TIRF 2 inverted microscope became available to our research group. The crucial benefits of Nikon H-TIRF 2 microscope are its camera (CMOS Hamamatsu ORCA-flash4.0 LT) with wider field of view and its user-friendly controller software (NIS-Elements). The seemingly hard task of rebuilding the image acquisition pipeline for a new system turned out to be really straight-forward thanks to well-designed built-in functions of the NIS-Elements software. The pipeline was further enhanced by creating a script for the double-slide setup utilization.

The most crucial and decisive part of live-cell imaging turned out to be the slide preparation phase. The 4% agarose supplemented YES medium is really hard to manipulate with in small volumes. It needs to be melted at 94°C in a microcentrifuge tube and transferred to the prepared slide with Silicone Slide Spacer using a micropipette. Ideally, the transfer of the medium needs to be done in one take (taken volume ~350 µl; distributed ~175 µl per chamber of the Silicone Slide Spacer) because of the quick solidification of media. Experience is needed to be able to correctly and quickly distribute the medium into the chambers of the slide. When too little of medium is added inside the chamber of the Silicone Slide Spacer or bubbles occur, the cells would not be touching the cover-glass and it would be impossible to correctly focus the microscope. Another not less important step is to quickly cover both chambers containing still liquid medium with the 40 x 22 mm cover-glass. This ensures equal distribution of medium in the chambers and flattens the top surface of medium to be aligned with the width of Silicone Slide Spacer. Not aligned medium surface hampers the focusing of microscope or disrupts the adhesion of cover-glass to the Silicone Slide Spacer resulting in its movement during the image acquisition.

Other critical step of the slide preparation for live-cell imaging is letting the cell suspension dry when transferred onto the solidified YES + 4% agarose medium. This ensures cells' immobilization on the medium and eliminates the problem of cells floating out of the field of view during the image acquisition.

These optimizations are based on a number of failed live-cell imaging experiments during the study.

After the introduction of double-slide microscopic setup, two new challenges came up. Firstly, we needed to ensure the objective detachment during the movement between the

slides. This was managed by developing the script to be run during the image acquisition in the NIS Elements software. The other challenge was that the immersion oil used during the image acquisition was viscose enough to be able to detach the cover-glass from the slide when moving between two slides and ruin the experiment. The problem was effectively solved by simple taping the cover-glass to the slide. The best outcome was achieved using standard transparent office tape.

7.2 Results summary

7.2.1 CUT phenotype screening results

The screening of CUT phenotype incidence was performed as one of the main objectives of this study for each of the strains created during this study and the respective parental strains. The analysis was carried out as described in sub-chapter 6.2 and the results compared (Figure 19). Strikingly, the results of this analysis were in contrast with the results from preliminary experiments performed by Akshay Vishwanatha. Neither of the double-tagged HDACΔ *cbf11Δ* strains tested in this study showed a rescue of CUT phenotype as described in the preliminary results (sub-chapter 5.5). The only strain with seemingly lower percentage of catastrophic mitosis incidence compared to double-tagged *cbf11Δ* strain observed was the *hst4Δ cbf11Δ* strain displaying CUT phenotype occurrence even with the *cbf11* gene present in the genome. However more biological replicates are needed to formulate statistically significant conclusions. Hst4 regulates the acetylation of H3K56 at the site of DNA damage and thus regulates the DNA repair processes (Haldar & Kamakaka, 2008). The loss of Hst4 leads to slower growth compared to wild-type cells, elongated cell morphology, fragmented DNA, elevated chromosome loss rates and silencing defects at both telomeres and centromeres (Freeman-Cook et al., 1999). These effects can be linked with the CUT phenotype incidence.

In this study, we were more concerned about the inconsistencies between the preliminary results and results provided by this study. As a more thorough method of *cbf11* deletion verification was established in our research group only after the preliminary data acquisition, we tried to verify the *cbf11* deletion in these strains by using a panel of primers amplifying different regions inside the *cbf11* ORF. Notably, we have found *cbf11* locus still present in two out of four tested strains used for the preliminary data acquisition. But, Akshay

Vishwanatha's data show correct resistance cassette integration during the transformation method and thus successful *cbf11* deletion from its endogenous locus.

There are two possible reasons explaining this questionable outcome. Firstly, a genetic reintegration could occur during the transformation method as genetic information is destabilized and fission yeast genome contain multiple recombinogenic regions (Mani et al., 2009; Xu et al., 2014). In the scenario of genetic reintegration, the genome of the transformant strain would contain the inserted resistance cassette, but also the *cbf11* gene integrated elsewhere in the genome. The question is whether and to what extent the gene is active. The results obtained using such strain are, however, not trustworthy. Second reason for the incorrect genetic outcome of the transformant strain could be the mixed culture was used for the stock creation after finishing the transformation method. The plasmid insertion method used for the strains creation for preliminary experiments and also in this study uses the selection of transformant cells mediated by antibiotic Nourseothricin (based on the resistance cassette contained in the used plasmid, described in sub-chapter 3.2.3). Fission yeast cells are generally sensitive to the concentrations of antibiotics used for the selection and become resistant only after the successful integration and expression of the resistance cassette. However, despite the drug sensitivity, small fraction of un-transformed cells can still remain in the quiescent state. Quiescent un-transformed cells can then be picked from the plate together with the transformant for the stock preparation. The PCR verification would show successful transformation, but when grown in unselective conditions (complex YES medium with no addition of selective agent), the un-transformed cells with *cbf11* gene still functioning would gain a selective advantage and overgrow the *cbf11Δ* cells. Therefore, the culture would then behave as no deletion of *cbf11* gene had been introduced. The growth of the culture would not be altered as in the *cbf11* and CUT phenotype occurrence would resemble the parental strain used for the transformation. This is just a hypothesis which depends mainly on the number of generations of the culture used for the stock preparation and subsequent experiments. To test the hypothesis, the strain should be spread on the selective plate and cultivated at standard conditions. Only growth of monocolonies would confirm the hypothesis. The monocolonies should be then tested for *cbf11* deletion again because those could represent the correct transformants.

By these findings, we have disapproved the preliminary results of CUT phenotype rescue in *cbf11Δ* cells deficient in histone deacetylases. We have also managed to prevent the

submission of an incorrect part of a manuscript. However, the question about the connection of heterochromatin assembly and lipid metabolism in fission yeast had been reopened for further examination.

7.2.2 Study of the selected mitotic parameters

As rescue of CUT phenotype had been found after the deletion of HDACs in cells with perturbed lipid metabolism during the preliminary experiments (sub-chapter 5.5), we originally desired to identify particular mitotic parameters involved in this rescue by live-cell imaging method. Considering our expectation that the optimization of the live-cell imaging method would be rather time-consuming, we decided to proceed with it right after the strain creation procedure was completed. We wanted to acquire as much data as possible from the method and in the meantime, the cultivations and fixations for CUT phenotype screening were performed. The results from CUT phenotype screening indicating no CUT phenotype rescue were obtained only after the live-cell imaging method had been performed for all of the strains. Such order of experiments was incorrect and we are aware of our mistake in experimental planning. If we knew sooner about no rescue of CUT phenotype in double-tagged HDACΔ *cbf11Δ* strains, we would not proceed with the extensive live-cell imaging and rather dig deeper into the connection between lipid metabolism and histone modifications. However, as we already invested the time for the optimisation of live-cell imaging method and acquired the data from all of the created double-tagged strains, we decided to study and compare some of the strains' mitotic parameters.

The first and maybe the most prominent parameter studied was the timing of mitotic phases. Within the possibilities of the live-cell imaging method, timing of three different mitotic phases was measured: prophase + metaphase, anaphase and telophase (described in sub-chapter 6.3.1). The duration of all of the studied mitotic phases seems to be prolonged and more variable in all of the tested *cbf11Δ* mutant strains when compared with their respective counterparts with *cbf11* present. Although, as there was no rescue of mitotic defects apparent in any of the HDACΔ *cbf11Δ* double mutants compared to the *cbf11Δ* single mutant, there was no sense in performing statistical testing of results' significancy. These results together with the results from CUT phenotype screening suggest no major changes in the mitotic progression after HDAC deletion in fission yeast cells with perturbed lipid metabolism.

The second mitotic parameter studied was the distance between two most distant points of nucleus (or two daughter nuclei after the cytokinesis). We have described more variable nuclear division during mitotic progression in double-tagged *cbf11Δ* cells compared to double-tagged cells. We have also managed to visualise and measure the nuclear division in cells undergoing catastrophic mitosis (CUT and LSD phenotype). As the data obtained was comparable with the preliminary data and considering no major changes were discovered between HDAC-deletion and HDAC-non-deletion mutants, we expect the similar behaviour in case of nuclear division in HDAC-deletion mutant strains. So, we have decided not to proceed with the extensive analysis of the live-cell imaging data.

7.3 Future research suggestions

From all of the mentioned facts in this study, we can conclude the complexity of processes securing the correct segregation of genetic information during the mitosis in *Schizosaccharomyces pombe.* As we have studied only a small fraction of such a complex system, we would like to suggest possibilities in studying lipid metabolism involvement in the mitotic progression.

We have described no rescue of CUT phenotype in each of the double-tagged HDACΔ *cbf11Δ* strains but identified only two (*sir2Δ cbf11Δ* and *hos2Δ cbf11Δ*) incorrectly created *cbf11Δ* strains used in the preliminary experiments (Figure 20). Other two (*hst2Δ cbf11Δ* and *clr3Δ cbf11Δ*) seem to really be deficient in the *cbf11* gene and respective preliminary data show a rescue of catastrophic mitosis occurrence (Figure 10). To transparently resolve this situation, we suggest creating a new set of HDACΔ *cbf11Δ* with no fluorescent tag added. The CUT phenotype screening should be repeated using this new set of strains and compared with the data obtained using double-tagged strains.

We could also argue about the effects of introduced fluorescent tags on the CUT phenotype incidence, as we see an effect on the growth of the culture (Figure 18). In this study, we are using the strains with fluorescently tagged histone H3 and alpha tubulin, which are considered as the major components involved in the mitotic fidelity. Attaching rather large fluorescent proteins (GFP = 28 kDa (Hink et al., 2000), mCherry = 26.72 kDa (*MCherry :: Fluorescent Protein Database*, n.d.)) to the two major components of chromosome segregation process can alter the overall process and affect the data acquired using this system. As we are not interested in the segregation of particular chromosomes, rather the

segregation of nucleus as a whole, we would suggest using a strain with fluorescently tagged spindle pole body docking protein Cut11 (present in the nuclear membrane) and alpha tubulin (*h- cut11-GFP:NatR GFP-atb2:NatR ade6-21? Leu1-32 ura4-D18*) (Lin et al., 2017) for the same set of experiments as performed in this study. This strain, which is already available in our laboratory, has however both proteins tagged with the same fluorescent protein, so an appropriate swap of one of the fluorescent tags should be designed. The results should be then compared with the results of this study.

From the data presented in this study and also from the preliminary data by Akshay Vishwanatha, the apparent increased duration of mitotic phases in *cbf11Δ* fission yeast strains can be concluded. Strikingly, mitotic phases with no apparent connection to lipid metabolism (pre-anaphase mitotic period) are also affected. This fact prompted Vishwanatha *et al.* to investigate the role of the spindle assembly checkpoint (SAC) in mitotic fidelity. SAC monitors the proper attachment of all chromosomes to the spindle microtubules. Through the inactivation of anaphase-promoting complex/cyclosome, it inhibits premature sister chromatid separation (Musacchio, 2015). Vishwanatha *et al.* therefore hypothesised that after the deletion of mitotic spindle checkpoint kinase Bub1, mediating SAC activity silencing (Musacchio & Hardwick, 2002), the *cbf11Δ* cells would have more time to deal with any mitotic problems. In such conditions, the incidence of CUT phenotype could be decreased. However, no significant changes in the catastrophic mitosis incidence have been observed after the SAC inactivation by the deletion of *bub1* (Vishwanatha et al., unpublished).

At least partial suppression of catastrophic mitosis incidence was however discovered after the mutation of cohesin loader (Vishwanatha et al., unpublished). As described in sub-chapter 4.4.2, cohesin mediates tight physical cohesion of sister centromeres (Bernard et al., 2001). Its dynamics are however crucial during the process of mitosis. There are multiple factors involved in a successful cohesion loading or unloading in *S. pombe*. Namely it is cohesin loading factor Mis4 (adherin), cohesin N-acetyltransferase Eso1, mitotic and meiotic cohesin loader subunit Pds5 or cohesin loading/unloading factor (WAPL) Wpl1. A negative genetic interaction was found in a genetic screening between the *cbf11* deletion and mutations in Mis4 (*mis4-242*) and Eso1 (*eso1-G799D*) (Z. Chen et al., 2012). These findings suggest compromised sister chromatid cohesion and cohesin loading in *cbf11Δ* cells. In contrast, increased cohesin occupancy was found at the centromeric *dh/dg* repeats in the

cbf11Δ strain. As mentioned before, a fine balance between the cohesin loading and unloading must be established for the successful mitotic progression. Contributing to this fact, a rescue of otherwise lethal deletion of *eso1* had been discovered after the deletion of gene encoding the cohesin un/loading factor Wpl1 (Feytout et al., 2011). Strikingly, the deletion of *wpl1* rescued the CUT phenotype significantly in the *cbf11Δ* cells (Vishwanatha et al., unpublished). These results suggest the importance of the cohesin loading and unloading dynamics in the mitotic fidelity.

Although, the findings described in this study suggest no major role of SAC in mitotic fidelity, we would suggest to focus on the other processes during the pre-anaphase mitotic period and heterochromatin formation together with histone methylation processes. There are ongoing studies describing TOR-dependent rescue of CUT phenotype suggesting the importance of pre-anaphase mitotic processes in mitotic fidelity. In case of heterochromatin formation, there are two suggested models explaining how heterochromatin is formed over the outer repetitive sequences of centromere, both involving activity of RNAi machinery. Mutations in the RNAi machinery resulted in the reduction of H3K9me2 and loss of silencing over the centromeric outer repeats (Volpe et al., 2002). However, these RNAi mutants contained non-coding RNA (ncRNA) originating from centromeric outer repeats. Moreover, isolated ncRNAs were homologous to siRNAs naturally occurring in fission yeast (Reinhart & Bartel, 2002). siRNAs are generated after the cleavage of long non-coding double-stranded transcripts of centromeric regions mediated by the dicer (Dcr1) enzyme. siRNAs then guide the RNAi machinery to homologous loci and act to silence the respective region (Allshire & Ekwall, 2015).

The first model of heterochromatin establishment in *Schizosaccharomyces pombe* suggests the siRNA associated with RITS complex guides it onto the nascent transcript emerging from RNA polymerase II. There are also multiple possibilities how the initial siRNAs are formed. Either RNA polymerase II transcripts can be structured into double-stranded regions recognized and cleaved by Dcr1 (Djupedal et al., 2009), or primary siRNA could originate from dicer-independent RNA degradation processes (Halic & Moazed, 2010). Anyway, RITS is guided to the homologous region by the siRNA and recruits the chromatin-modifying complexes such as CLRC containing Clr4 histone methyl transferase.

A second model describes the requirement of H3K9 methylation to generate the siRNAs in *cis* through various RNA-processing activities (Noma et al., 2004; Sugiyama et al., 2005).

Also, experiments with mutants of RITS components suggest the requirement of H3K9 methylation before the production of siRNAs (Partridge et al., 2007).

These two models are however contradictory and more research is clearly needed to fully understand the process of heterochromatin establishment.

Negative genetic interaction between the deletions of *cbf11* and *sgf73* and higher frequency of catastrophic mitosis in *cbf11Δ sgf73Δ* strain (Guo et al., 2014) described in sub-chapter 4.4.3 suggest the possible involvement of lipid metabolism in the heterochromatin assembly mediated by RNAi. In this study, we have used the knowledge of the negative interaction between the deletions of *cbf11* and *sgf73* only from the perspective of Sgf73 contribution to the acetyl transferase activity of the SAGA complex (Guo et al., 2014). Sgf73 is however also involved in the assembly of the RITS complex (Deng et al., 2015). This proposes a potential connection between the lipid metabolism and RITS complex function.

Finally, we advise more research of the connection between lipid metabolism and heterochromatin stabilisation factors Swi6 and Chp2. Destabilised heterochromatin structure could lead to the rescue of catastrophic mitosis in the cells with perturbed lipid metabolism through easier sister chromatid segregation.

8 Conclusions

We have managed to achieve the objectives set in the beginning of this study:

- We have created the prototrophic strains with fluorescent tags allowing the *in vivo* observation of closed mitosis in the cells with normal and perturbed lipid metabolism. We have also created fluorescently tagged mutant strains with a deletion in each of the five non-essential HDACs and HDACΔ *cbf11Δ* strains to study the mitotic dynamics in the cells with altered epigenetic processes (described in sub-chapter 6.1).
- We have optimized the live-cell imaging method for a newer Nikon H-TIRF 2 microscopic system. The method was further optimized for the usage of two microscopic slides during a single experimental run for the maximal utilization of the system.
- We have established a data analysis pipeline for live-cell imaging data. The pipeline was further optimised in collaboration with Viacheslav Zemlianski (other member of the research group) by implementing custom scripts to make the data analysis process more efficient and consistent for further use.
- Two of the mitotic parameters were studied and characterised in the strains used in this study. The first and most prominent studied mitotic parameter was the timing of mitotic phases. Cells with perturbed lipid metabolism (double-tagged *cbf11Δ*) show longer mitotic phases with higher variability when compared with the cells with unperturbed lipid metabolism (double-tagged). The similar shift of timing of mitotic phases was observed when HDACΔ cells were compared with their respective HDACΔ *cbf11Δ* counterparts (described in sub-chapter 6.3.1). Secondly, the distance between the two furthest poles of nucleus was analysed. The nuclear division of double-tagged *cbf11Δ* cells was again more variable when compared with the parental double-tagged cells. Also, the nuclear division of CUT and LSD phenotype cells was described (described in sub-chapter 6.3.2). Lastly, the CUT phenotype screening was done for all of the strains used in this study. Interestingly, we have found no rescue of CUT phenotype after the deletion of HDACs in cells with perturbed lipid metabolism. These findings are in contrast with the preliminary data provided by Akshay Vishwanatha (former

member of the research group). After further analysis, we have identified genotype discrepancies in the strains used for the preliminary experiments (described in sub-chapter 6.2).

Based on the results provided by this study, we refuse the hypothesis that deletion of histone deacetylases can rescue the catastrophic mitosis of the prototrophic *Schizosaccharomyces pombe* cells with perturbed lipid metabolism. However, the exact mechanisms linking mitotic fidelity with lipid metabolism need to be studied more to fully understand the process of closed mitosis.

9 References

Alam, M. T., Zelezniak, A., Mülleder, M., Shliaha, P., Schwarz, R., Capuano, F., Vowinckel, J., Radmaneshfar, E., Krüger, A., Calvani, E., Michel, S., Börno, S., Christen, S., Patil, K. R., Timmermann, B., Lilley, K. S., & Ralser, M. (2016). The metabolic background is a global player in Saccharomyces gene expression epistasis. *Nature Microbiology*, *1*(3), 15030. https://doi.org/10.1038/NMICROBIOL.2015.30

Allshire, R. C., & Ekwall, K. (2015). Epigenetic Regulation of Chromatin States in Schizosaccharomyces pombe. *Cold Spring Harbor Perspectives in Biology*, *7*(7), a018770. https://doi.org/10.1101/CSHPERSPECT.A018770

Allshire, R. C., Nimmo, E. R., Ekwall, K., Javerzat, J. P., & Cranston, G. (1995). Mutations derepressing silent centromeric domains in fission yeast disrupt chromosome segregation. *Genes & Development*, *9*(2), 218–233. https://doi.org/10.1101/GAD.9.2.218

Alper, B. J., Job, G., Yadav, R. K., Shanker, S., Lowe, B. R., & Partridge, J. F. (2013). Sir2 is required for Clr4 to initiate centromeric heterochromatin assembly in fission yeast. *The EMBO Journal*, *32*(17), 2321–2335. https://doi.org/10.1038/EMBOJ.2013.143

Arnone, J. T., Walters, A. D., & Cohen-Fix, O. (2013). The dynamic nature of the nuclear envelope: lessons from closed mitosis. *Nucleus (Austin, Tex.)*, *4*(4). https://doi.org/10.4161/NUCL.25341

Bannister, A. J., Zegerman, P., Partridge, J. F., Miska, E. A., Thomas, J. O., Allshire, R. C., & Kouzarides, T. (2001). Selective recognition of methylated lysine 9 on histone H3 by the HP1 chromo domain. *Nature*, *410*(6824), 120–124. https://doi.org/10.1038/35065138

Bernard, P., Maure, J. F., Partridge, J. F., Genier, S., Javerzat, J. P., & Allshire, R. C. (2001). Requirement of heterochromatin for cohesion at centromeres. *Science (New York, N.Y.)*, *294*(5551), 2539–2542. https://doi.org/10.1126/SCIENCE.1064027

Bimboim, H. C., & Doly, J. (1979). A rapid alkaline extraction procedure for screening recombinant plasmid DNA. *Nucleic Acids Research*, *7*(6), 1513–1523. https://doi.org/10.1093/NAR/7.6.1513

Bjerling, P., Silverstein, R. A., Thon, G., Caudy, A., Grewal, S., & Ekwall, K. (2002). Functional Divergence between Histone Deacetylases in Fission Yeast by Distinct Cellular Localization and In Vivo Specificity. *Molecular and Cellular Biology*, *22*(7), 2170. https://doi.org/10.1128/MCB.22.7.2170-2181.2002

Boettcher, B., & Barral, Y. (2013). The cell biology of open and closed mitosis., 160–165. https://doi.org/10.4161/NUCL.24676

Bray, S. J. (2006). Notch signalling: a simple pathway becomes complex. *Nature Reviews. Molecular Cell Biology*, *7*(9), 678–689. https://doi.org/10.1038/NRM2009

Castagnetti, S., Božič, B., & Svetina, S. (2015). Mechanical and molecular basis for the symmetrical division of the fission yeast nuclear envelope. *Physical Chemistry Chemical Physics*, *17*(24), 15629–15636. https://doi.org/10.1039/C5CP01243K

Chen, E. S., Zhang, K., Nicolas, E., Cam, H. P., Zofall, M., & Grewal, S. I. S. (2008). Cell cycle control of centromeric repeat transcription and heterochromatin assembly. *Nature*, *451*(7179), 734–737. https://doi.org/10.1038/NATURE06561

Chen, Z., McCroskey, S., Guo, W., Li, H., & Gerton, J. L. (2012). A genetic screen to discover pathways affecting cohesin function in Schizosaccharomyces pombe identifies chromatin effectors. *G3: Genes, Genomes, Genetics*, *2*(10), 1161–1168. https://doi.org/10.1534/G3.112.003327/-/DC1

Choi, H. S., Su, W. M., Morgan, J. M., Han, G. S., Xu, Z., Karanasios, E., Siniossoglou, S., & Carman, G. M. (2011). Phosphorylation of phosphatidate phosphatase regulates its membrane association and physiological functions in Saccharomyces cerevisiae: identification of SER(602), THR(723), AND SER(744) as the sites phosphorylated by CDC28 (CDK1)-encoded cyclin-dependent kinase. *The Journal of Biological Chemistry*, *286*(2), 1486–1498. https://doi.org/10.1074/JBC.M110.155598

Clarke, L., Amstutz, H., Fishel, B., & Carbon, J. (1986). Analysis of centromeric DNA in the fission yeast Schizosaccharomyces pombe. *Proceedings of the National Academy of Sciences of the United States of America*, *83*(21), 8253–8257. https://doi.org/10.1073/PNAS.83.21.8253

Daněk, P. (2015). *Molekulární mechanismus účasti proteinů rodiny CSL v odpovědi na oxidativní stress u Schizosaccharomyces pombe.*

Deng, X., Zhou, H., Zhang, G., Wang, W., Mao, L., Zhou, X., Yu, Y., & Lu, H. (2015). Sgf73, a subunit of SAGA complex, is required for the assembly of RITS complex in fission yeast. *Scientific Reports*, *5*. https://doi.org/10.1038/srep14707

Djupedal, I., Kos-Braun, I. C., Mosher, R. A., Söderholm, N., Simmer, F., Hardcastle, T. J., Fender, A., Heidrich, N., Kagansky, A., Bayne, E., Wagner, E. G. H., Baulcombe, D. C., Allshire, R. C., & Ekwall, K. (2009). Analysis of small RNA in fission yeast; centromeric siRNAs are potentially generated through a structured RNA. *The EMBO Journal*, *28*(24), 3832–3844. https://doi.org/10.1038/EMBOJ.2009.351

Dubots, E., Cottier, S., Péli-Gulli, M. P., Jaquenoud, M., Bontron, S., Schneiter, R., & de Virgilio, C. (2014). TORC1 Regulates Pah1 Phosphatidate Phosphatase Activity via the Nem1/Spo7 Protein Phosphatase Complex. *PLOS ONE*, *9*(8), e104194. https://doi.org/10.1371/JOURNAL.PONE.0104194

Durand-Dubief, M., Sinha, I., Fagerström-Billai, F., Bonilla, C., Wright, A., Grunstein, M., & Ekwall, K. (2007). Specific functions for the fission yeast Sirtuins Hst2 and Hst4 in gene regulation and retrotransposon silencing. *The EMBO Journal*, *26*(10), 2477–2488. https://doi.org/10.1038/SJ.EMBOJ.7601690

Egel, R. (2004). *The molecular biology of Schizosaccharomyces pombe: Genetics, genomics and beyond.* Springer.

Egel, R., Beach, D. H., & Klar, A. J. S. (1984). Genes required for initiation and resolution steps of mating-type switching in fission yeast. *Proceedings of the National Academy of Sciences of the United States of America*, *81*(11), 3481–3485. https://doi.org/10.1073/PNAS.81.11.3481

Egel Richard. (2004). The Molecular Biology of Schizosaccharomyces pombe. *The Molecular Biology of Schizosaccharomyces Pombe*. https://doi.org/10.1007/978-3-662-10360-9

Ekwall, K., Javerzat, J. P., Lorentz, A., Schmidt, H., Cranston, G., & Allshire, R. (1995). The chromodomain protein Swi6: a key component at fission yeast centromeres. *Science (New York, N.Y.)*, *269*(5229), 1429–1431. https://doi.org/10.1126/SCIENCE.7660126

Feytout, A., Vaur, S., Genier, S., Vazquez, S., & Javerzat, J.-P. (2011). Psm3 Acetylation on Conserved Lysine Residues Is Dispensable for Viability in Fission Yeast but Contributes to Eso1-Mediated Sister Chromatid Cohesion by Antagonizing Wpl1. *Molecular and Cellular Biology*, *31*(8), 1771–1786. https://doi.org/10.1128/MCB.01284-10/ASSET/DF36B7A9-6D6C-4993-8699-F46636FC7E76/ASSETS/GRAPHIC/ZMB9991090190008.JPEG

Freeman-Cook, L. L., Sherman, J. M., Brachmann, C. B., Allshire, R. C., Boeke, J. D., & Pillus, L. (1999). The Schizosaccharomyces pombe hst4+ gene is a SIR2 homologue

with silencing and centromeric functions. *Molecular Biology of the Cell*, *10*(10), 3171–3186. https://doi.org/10.1091/mbc.10.10.3171

Funabiki, H., Kumada, K., & Yanagida, M. (1996). Fission yeast Cut1 and Cut2 are essential for sister chromatid separation, concentrate along the metaphase spindle and form large complexes. *The EMBO Journal*, *15*(23), 6617. https://doi.org/10.1002/j.1460-2075.1996.tb01052.x

Gazave, E., Lapébie, P., Richards, G. S., Brunet, F., Ereskovsky, A. v., Degnan, B. M., Borchiellini, C., Vervoort, M., & Renard, E. (2009). Origin and evolution of the Notch signalling pathway: an overview from eukaryotic genomes. *BMC Evolutionary Biology*, *9*(1). https://doi.org/10.1186/1471-2148-9-249

Gregan, J., Rabitsch, P. K., Rumpf, C., Novatchkova, M., Schleiffer, A., & Nasmyth, K. (2006). High-throughput knockout screen in fission yeast. *Nature Protocols*, *1*(5), 2457–2464. https://doi.org/10.1038/NPROT.2006.385

Grewal, C., Hickmott, J., Rentas, S., & Karagiannis, J. (2012). A conserved histone deacetylase with a role in the regulation of cytokinesis in Schizosaccharomyces pombe. *Cell Division*, *7*(1), 1–14. https://doi.org/10.1186/1747-1028-7-13/FIGURES/6

Grewal, S. I. S., Bonaduce, M. J., & Klar, A. J. S. (1998). Histone deacetylase homologs regulate epigenetic inheritance of transcriptional silencing and chromosome segregation in fission yeast. *Genetics*, *150*(2), 563–576. https://doi.org/10.1093/GENETICS/150.2.563

Grunstein, M., & Gasser, S. M. (2013). Epigenetics in Saccharomyces cerevisiae. *Cold Spring Harbor Perspectives in Biology*, *5*(7). https://doi.org/10.1101/CSHPERSPECT.A017491

Guo, Y., Lei, B., Deng, X., Yu, Y., & Lv, H. (2014). Large scale screening of genetic interaction with sgf73(+) in fission yeast. *Yi Chuan = Hereditas*, *36*(7), 723–731. https://doi.org/10.3724/SP.J.1005.2014.0723

Güttinger, S., Laurell, E., & Kutay, U. (2009). Orchestrating nuclear envelope disassembly and reassembly during mitosis. *Nature Reviews Molecular Cell Biology 2009 10:3*, *10*(3), 178–191. https://doi.org/10.1038/nrm2641

Haldar, D., & Kamakaka, R. T. (2008). Schizosaccharomyces pombe Hst4 functions in DNA damage response by regulating histone H3 K56 acetylation. *Eukaryotic Cell*, *7*(5), 800–813. https://doi.org/10.1128/EC.00379-07/SUPPL_FILE/SUPPL_FIG_LEGEND.DOC

Halic, M., & Moazed, D. (2010). Dicer-independent primal RNAs trigger RNAi and heterochromatin formation. *Cell*, *140*(4), 504–516. https://doi.org/10.1016/J.CELL.2010.01.019

Han, G. S., O'Hara, L., Carman, G. M., & Siniossoglou, S. (2008). An Unconventional Diacylglycerol Kinase That Regulates Phospholipid Synthesis and Nuclear Membrane Growth. *The Journal of Biological Chemistry*, *283*(29), 20433. https://doi.org/10.1074/JBC.M802903200

Hink, M. A., Griep, R. A., Borst, J. W., van Hoek, A., Eppink, M. H. M., Schots, A., & Visser, A. J. W. G. (2000). Structural Dynamics of Green Fluorescent Protein Alone and Fused with a Single Chain Fv Protein *. *Journal of Biological Chemistry*, *275*(23), 17556–17560. https://doi.org/10.1074/JBC.M001348200

Hori, K., Sen, A., & Artavanis-Tsakonas, S. (2013). Notch signaling at a glance. *Journal of Cell Science*, *126*(Pt 10), 2135–2140. https://doi.org/10.1242/JCS.127308

Hsieh, L. S., Su, W. M., Han, G. S., & Carman, G. M. (2015). Phosphorylation regulates the ubiquitin-independent degradation of yeast pah1 phosphatidate phosphatase by the

20S proteasome. *Journal of Biological Chemistry*, *290*(18), 11467–11478. https://doi.org/10.1074/JBC.M115.648659
Imai, S. I., Armstrong, C. M., Kaeberlein, M., & Guarente, L. (2000). Transcriptional silencing and longevity protein Sir2 is an NAD-dependent histone deacetylase. *Nature*, *403*(6771), 795–800. https://doi.org/10.1038/35001622
Jorgensen, P., Edgington, N. P., Schneider, B. L., Rupeš, I., Tyers, M., & Futcher, B. (2007). The Size of the Nucleus Increases as Yeast Cells Grow. *Molecular Biology of the Cell*, *18*(9), 3523. https://doi.org/10.1091/MBC.E06-10-0973
Kanoh, J., Sadaie, M., Urano, T., & Ishikawa, F. (2005). Telomere binding protein Taz1 establishes Swi6 heterochromatin independently of RNAi at telomeres. *Current Biology : CB*, *15*(20), 1808–1819. https://doi.org/10.1016/J.CUB.2005.09.041
Kniola, B., O'Toole, E., McIntosh, J. R., Mellone, B., Allshire, R., Mengarelli, S., Hultenby, K., & Ekwall, K. (2001). The domain structure of centromeres is conserved from fission yeast to humans. *Molecular Biology of the Cell*, *12*(9), 2767–2775. https://doi.org/10.1091/MBC.12.9.2767/ASSET/IMAGES/LARGE/MK0911591007.JPEG
Kokina, A., Kibilds, J., & Liepins, J. (2014). Adenine auxotrophy--be aware: some effects of adenine auxotrophy in Saccharomyces cerevisiae strain W303-1A. *FEMS Yeast Research*, *14*(5), 697–707. https://doi.org/10.1111/1567-1364.12154
Kopan, R., & Ilagan, M. X. G. (2009). The canonical Notch signaling pathway: unfolding the activation mechanism. *Cell*, *137*(2), 216–233. https://doi.org/10.1016/J.CELL.2009.03.045
Kwon, E. J. G., Laderoute, A., Chatfield-Reed, K., Vachon, L., Karagiannis, J., & Chua, G. (2012). Deciphering the transcriptional-regulatory network of flocculation in Schizosaccharomyces pombe. *PLoS Genetics*, *8*(12). https://doi.org/10.1371/JOURNAL.PGEN.1003104
Lin, L., Chen, L., & Tran, P. T. (2017). *Fission yeast neddylation ligase Dcn1 facilitates cohesin cleavage and chromosome segregation at anaphase*. https://doi.org/10.1242/bio.021238
Lõoke, M., Kristjuhan, K., & Kristjuhan, A. (2011). Extraction of genomic DNA from yeasts for PCR-based applications. *BioTechniques*, *50*(5), 325–328. https://doi.org/10.2144/000113672
Louvi, A., & Artavanis-Tsakonas, S. (2012). Notch and disease: a growing field. *Seminars in Cell & Developmental Biology*, *23*(4), 473–480. https://doi.org/10.1016/J.SEMCDB.2012.02.005
Makarova, M., Gu, Y., Chen, J. S., Beckley, J. R., Gould, K. L., & Oliferenko, S. (2016). Temporal Regulation of Lipin Activity Diverged to Account for Differences in Mitotic Programs. *Current Biology*, *26*(2), 237. https://doi.org/10.1016/J.CUB.2015.11.061
Malecki, M., Bitton, D. A., Rodríguez-López, M., Rallis, C., Calavia, N. G., Smith, G. C., & Bähler, J. (2016). Functional and regulatory profiling of energy metabolism in fission yeast. *Genome Biology*, *17*(1), 1–18. https://doi.org/10.1186/S13059-016-1101-2/FIGURES/8
Mani, P., Yadav, V. K., Das, S. K., & Chowdhury, S. (2009). Genome-Wide Analyses of Recombination Prone Regions Predict Role of DNA Structural Motif in Recombination. *PLOS ONE*, *4*(2), e4399. https://doi.org/10.1371/JOURNAL.PONE.0004399
Matsuo, Y., Nishino, K., Mizuno, K., Akihiro, T., Toda, T., Matsuo, Y., Kaino, T., & Kawamukai, M. (2013). Polypeptone induces dramatic cell lysis in ura4 deletion

mutants of fission yeast. *PloS One*, *8*(3). https://doi.org/10.1371/JOURNAL.PONE.0059887

mCherry :: Fluorescent Protein Database. (n.d.). Retrieved April 21, 2022, from https://www.fpbase.org/protein/mcherry/

Meyers, A., Chourey, K., Weiskittel, T. M., Pfiffner, S., Dunlap, J. R., Hettich, R. L., & Dalhaimer, P. (2017). The protein and neutral lipid composition of lipid droplets isolated from the fission yeast, Schizosaccharomyces pombe. *Journal of Microbiology (Seoul, Korea)*, *55*(2), 112–122. https://doi.org/10.1007/S12275-017-6205-1

Musacchio, A. (2015). The Molecular Biology of Spindle Assembly Checkpoint Signaling Dynamics. *Current Biology*, *25*(20), R1002–R1018. https://doi.org/10.1016/J.CUB.2015.08.051

Musacchio, A., & Hardwick, K. G. (2002). The spindle checkpoint: structural insights into dynamic signalling. *Nature Reviews. Molecular Cell Biology*, *3*(10), 731–741. https://doi.org/10.1038/NRM929

Nagao, K., & Yanagida, M. (2006). Securin can have a separase cleavage site by substitution mutations in the domain required for stabilization and inhibition of separase. *Genes to Cells : Devoted to Molecular & Cellular Mechanisms*, *11*(3), 247–260. https://doi.org/10.1111/J.1365-2443.2006.00941.X

Nakayama, J., Rice, J. C., Strahl, B. D., Allis, C. D., & Grewal, S. I. S. (2001). Role of histone H3 lysine 9 methylation in epigenetic control of heterochromatin assembly. *Science (New York, N.Y.)*, *292*(5514), 110–113. https://doi.org/10.1126/SCIENCE.1060118

Nguyen, B. C., Lefort, K., Mandinova, A., Antonini, D., Devgan, V., Gatta, G. della, Koster, M. I., Zhang, Z., Wang, J., di Vignano, A. T., Kitajewski, J., Chiorino, G., Roop, D. R., Missero, C., & Dotto, G. P. (2006). Cross-regulation between Notch and p63 in keratinocyte commitment to differentiation. *Genes & Development*, *20*(8), 1028. https://doi.org/10.1101/GAD.1406006

Noma, K. I., Sugiyama, T., Cam, H., Verdel, A., Zofall, M., Jia, S., Moazed, D., & Grewal, S. I. S. (2004). RITS acts in cis to promote RNA interference-mediated transcriptional and post-transcriptional silencing. *Nature Genetics*, *36*(11), 1174–1180. https://doi.org/10.1038/NG1452

O'Hara, L., Han, G. S., Sew, P. C., Grimsey, N., Carman, G. M., & Siniossoglou, S. (2006). Control of phospholipid synthesis by phosphorylation of the yeast lipin Pah1p/Smp2p Mg2+-dependent phosphatidate phosphatase. *The Journal of Biological Chemistry*, *281*(45), 34537–34548. https://doi.org/10.1074/JBC.M606654200

Olins, D. E., & Olins, A. L. (2003). Chromatin history: our view from the bridge. *Nat. Rev. Mol. Cell Biol.*, *4*(10), 809–814. https://doi.org/10.1038/nrm1225

Oravcová, M., Teska, M., Půta, F., Folk, P., & Převorovský, M. (2013). Fission Yeast CSL Proteins Function as Transcription Factors. *PLOS ONE*, *8*(3), e59435. https://doi.org/10.1371/JOURNAL.PONE.0059435

Park, S. Y., & Kim, J. S. (2020). A short guide to histone deacetylases including recent progress on class II enzymes. *Experimental & Molecular Medicine 2020 52:2*, *52*(2), 204–212. https://doi.org/10.1038/s12276-020-0382-4

Partridge, J. F., DeBeauchamp, J. L., Kosinski, A. M., Ulrich, D. L., Hadler, M. J., & Noffsinger, V. J. P. (2007). Functional separation of the requirements for establishment and maintenance of centromeric heterochromatin. *Molecular Cell*, *26*(4), 593–602. https://doi.org/10.1016/J.MOLCEL.2007.05.004

Penton, A. L., Leonard, L. D., & Spinner, N. B. (2012). Notch signaling in human development and disease. *Seminars in Cell & Developmental Biology*, *23*(4), 450–457. https://doi.org/10.1016/J.SEMCDB.2012.01.010

Pérez, P., Cortés, J. C. G., Martín-García, R., & Ribas, J. C. (2016). Overview of fission yeast septation. *Cellular Microbiology*, *18*(9), 1201–1207. https://doi.org/10.1111/CMI.12611

Pidoux, A. L., & Allshire, R. C. (2004). Kinetochore and heterochromatin domains of the fission yeast centromere. *Chromosome Research 2004 12:6*, *12*(6), 521–534. https://doi.org/10.1023/B:CHRO.0000036586.81775.8B

PomBase - Ontology term - - histone deacetylase activity. (n.d.). Retrieved March 19, 2022, from https://www.pombase.org/term/GO:0004407

Převorovský, M., Groušl, T., Staňurová, J., Ryneš, J., Nellen, W., Půta, F., & Folk, P. (2009). Cbf11 and Cbf12, the fission yeast CSL proteins, play opposing roles in cell adhesion and coordination of cell and nuclear division. *Experimental Cell Research*, *315*(8), 1533–1547. https://doi.org/10.1016/J.YEXCR.2008.12.001

Převorovský, M., Oravcová, M., Tvarůžková, J., Zach, R., Folk, P., Půta, F., & Bähler, J. (2015). Fission Yeast CSL Transcription Factors: Mapping Their Target Genes and Biological Roles. *PloS One*, *10*(9). https://doi.org/10.1371/JOURNAL.PONE.0137820

Převorovský, M., Oravcová, M., Zach, R., Jordáková, A., Bähler, J., Půta, F., & Folk, P. (2016). CSL protein regulates transcription of genes required to prevent catastrophic mitosis in fission yeast. *Cell Cycle*, *15*(22), 3082. https://doi.org/10.1080/15384101.2016.1235100

Převorovský, M., Půta, F., & Folk, P. (2007). Fungal CSL transcription factors. *BMC Genomics*, *8*, 233. https://doi.org/10.1186/1471-2164-8-233

Raben, D. M., & Barber, C. N. (2017). Phosphatidic acid and neurotransmission. *Advances in Biological Regulation*, *63*, 15. https://doi.org/10.1016/J.JBIOR.2016.09.004

Reinhart, B. J., & Bartel, D. P. (2002). Small RNAs correspond to centromere heterochromatic repeats. *Science (New York, N.Y.)*, *297*(5588), 1831. https://doi.org/10.1126/SCIENCE.1077183

Roche, B., Arcangioli, B., & Martienssen, R. A. (2016). RNA interference is essential for cellular quiescence. *Science*, *354*(6313). https://doi.org/10.1126/SCIENCE.AAH5651/SUPPL_FILE/AAH5651-ROCHE-SM.PDF

Romila, C. A., Townsend, S., Malecki, M., Kamrad, S., Rodríguez-López, M., Hillson, O., Cotobal, C., Ralser, M., & Bähler, J. (2021). Barcode sequencing and a high-throughput assay for chronological lifespan uncover ageing-associated genes in fission yeast. *Microbial Cell (Graz, Austria)*, *8*(7), 146–160. https://doi.org/10.15698/mic2021.07.754

Rundlett, S. E., Carmen, A. A., Kobayashi, R., Bavykin, S., Turner, B. M., & Grunstein, M. (1996). HDA1 and RPD3 are members of distinct yeast histone deacetylase complexes that regulate silencing and transcription. *Proceedings of the National Academy of Sciences of the United States of America*, *93*(25), 14503–14508. https://doi.org/10.1073/PNAS.93.25.14503

Sabatinos, S. A., & Forsburg, S. L. (2010). Molecular genetics of Schizosaccharomyces pombe. *Methods in Enzymology*, *470*(C), 759–795. https://doi.org/10.1016/S0076-6879(10)70032-X

Sadaie, M., Iida, T., Urano, T., & Nakayama, J. I. (2004). A chromodomain protein, Chp1, is required for the establishment of heterochromatin in fission yeast. *The EMBO Journal*, *23*(19), 3825–3835. https://doi.org/10.1038/SJ.EMBOJ.7600401

Saitoh, S., Takahashi, K., Nabeshima, K., Yamashita, Y., Nakaseko, Y., Hirata, A., & Yanagida, M. (1996). Aberrant mitosis in fission yeast mutants defective in fatty acid synthetase and acetyl CoA carboxylase. *The Journal of Cell Biology*, *134*(4), 949–961. https://doi.org/10.1083/JCB.134.4.949

Saka, Y., Sutani, T., Yamashita, Y., Saitoh, S., Takeuchi, M., Nakaseko, Y., & Yanagida, M. (1994). Fission yeast cut3 and cut14, members of a ubiquitous protein family, are required for chromosome condensation and segregation in mitosis. *The EMBO Journal*, *13*(20), 4938. https://doi.org/10.1002/j.1460-2075.1994.tb06821.x

Samejima, I., Matsumoto, T., Nakaseko, Y., Beach, D., & Yanagida, M. (1993). Identification of seven new cut genes involved in Schizosaccharomyces pombe mitosis. *Journal of Cell Science*, *105 (Pt 1)*(1), 135–143. https://doi.org/10.1242/JCS.105.1.135

Santos-Rosa, H., Leung, J., Grimsey, N., Peak-Chew, S., & Siniossoglou, S. (2005). The yeast lipin Smp2 couples phospholipid biosynthesis to nuclear membrane growth. *The EMBO Journal*, *24*(11), 1931–1941. https://doi.org/10.1038/SJ.EMBOJ.7600672

Schneider, C. A., Rasband, W. S., & Eliceiri, K. W. (2012). NIH Image to ImageJ: 25 years of image analysis. *Nature Methods*, *9*(7), 671–675. https://doi.org/10.1038/NMETH.2089

Schroeter, E. H., Kisslinger, J. A., & Kopan, R. (1998). Notch-1 signalling requires ligand-induced proteolytic release of intracellular domain. *Nature 1998 393:6683*, *393*(6683), 382–386. https://doi.org/10.1038/30756

Siniossoglou, S., Santos-Rosa, H., Rappsilber, J., Mann, M., & Hurt, E. (1998). A novel complex of membrane proteins required for formation of a spherical nucleus. *The EMBO Journal*, *17*(22), 6449. https://doi.org/10.1093/EMBOJ/17.22.6449

Stolz, J. (2003). Isolation and characterization of the plasma membrane biotin transporter from Schizosaccharomyces pombe. *Yeast (Chichester, England)*, *20*(3), 221–231. https://doi.org/10.1002/YEA.959

Su, W. M., Han, G. S., Casciano, J., & Carman, G. M. (2012). Protein kinase A-mediated phosphorylation of Pah1p phosphatidate phosphatase functions in conjunction with the Pho85p-Pho80p and Cdc28p-cyclin B kinases to regulate lipid synthesis in yeast. *The Journal of Biological Chemistry*, *287*(40), 33364–33376. https://doi.org/10.1074/JBC.M112.402339

Sugiyama, T., Cam, H., Verdel, A., Moazed, D., & Grewal, S. I. S. (2005). RNA-dependent RNA polymerase is an essential component of a self-enforcing loop coupling heterochromatin assembly to siRNA production. *Proceedings of the National Academy of Sciences of the United States of America*, *102*(1), 152–157. https://doi.org/10.1073/PNAS.0407641102

Syrovatkina, V., & Tran, P. T. (2015). Loss of kinesin-14 results in aneuploidy via kinesin-5-dependent microtubule protrusions leading to chromosome cut. *Nature Communications 2015 6:1*, *6*(1), 1–8. https://doi.org/10.1038/ncomms8322

Takemoto, A., Kawashima, S. A., Li, J. J., Jeffery, L., Yamatsugu, K., Elemento, O., & Nurse, P. (2016). Nuclear envelope expansion is crucial for proper chromosomal segregation during a closed mitosis. *Journal of Cell Science*, *129*(6), 1250–1259. https://doi.org/10.1242/JCS.181560

Tange, Y., Hirata, A., & Niwa, O. (2002). An evolutionarily conserved fission yeast protein, Ned1, implicated in normal nuclear morphology and chromosome stability,

interacts with Dis3, Pim1/RCC1 and an essential nucleoporin. *Journal of Cell Science*, *115*(Pt 22), 4375–4385. https://doi.org/10.1242/JCS.00135
Tarnowski, B. I., Spinale, F. G., & Nicholson, J. H. (1991). DAPI as a useful stain for nuclear quantitation. *Biotechnic and Histochemistry*, *66*(6), 296–302. https://doi.org/10.3109/10520299109109990
Tashiro, S., Asano, T., Kanoh, J., & Ishikawa, F. (2013). Transcription-induced chromatin association of RNA surveillance factors mediates facultative heterochromatin formation in fission yeast. *Genes to Cells : Devoted to Molecular & Cellular Mechanisms*, *18*(4), 327–339. https://doi.org/10.1111/GTC.12038
Tinline-Purvis, H., Savory, A. P., Cullen, J. K., Davé, A., Moss, J., Bridge, W. L., Marguerat, S., Bähler, J., Ragoussis, J., Mott, R., A Walker, C., & Humphrey, T. C. (2009). Failed gene conversion leads to extensive end processing and chromosomal rearrangements in fission yeast. *The EMBO Journal*, *28*(21), 3400–3412. https://doi.org/10.1038/EMBOJ.2009.265
Tran, P. T., Paoletti, A., & Chang, F. (2004). Imaging green fluorescent protein fusions in living fission yeast cells. *Methods*, *33*(3), 220–225. https://doi.org/10.1016/J.YMETH.2003.11.017
Tun, T., Hamaguchi, Y., Matsunami, N., Furukawa, T., Honjo, T., & Kawaichi, M. (1994). Recognition sequence of a highly conserved DNA binding protein RBP-J kappa. *Nucleic Acids Research*, *22*(6), 965–971. https://doi.org/10.1093/NAR/22.6.965
Tvarůžková, J. (2015). *The role of CSL proteins in oxidative stress response of Schizosaccharomyces pombe.*
Uemura, T., Ohkura, H., Adachi, Y., Morino, K., Shiozaki, K., & Yanagida, M. (1987). DNA topoisomerase II is required for condensation and separation of mitotic chromosomes in S. pombe. *Cell*, *50*(6), 917–925. https://doi.org/10.1016/0092-8674(87)90518-6
Uemura, T., & Tanagida, M. (1986). Mitotic spindle pulls but fails to separate chromosomes in type II DNA topoisomerase mutants: uncoordinated mitosis. *The EMBO Journal*, *5*(5), 1003. https://doi.org/10.1002/j.1460-2075.1986.tb04315.x
VanDussen, K. L., Carulli, A. J., Keeley, T. M., Patel, S. R., Puthoff, B. J., Magness, S. T., Tran, I. T., Maillard, I., Siebel, C., Kolterud, Å., Grosse, A. S., Gumucio, D. L., Ernst, S. A., Tsai, Y. H., Dempsey, P. J., & Samuelson, L. C. (2012). Notch signaling modulates proliferation and differentiation of intestinal crypt base columnar stem cells. *Development (Cambridge, England)*, *139*(3), 488–497. https://doi.org/10.1242/DEV.070763
Volpe, T. A., Kidner, C., Hall, I. M., Teng, G., Grewal, S. I. S., & Martienssen, R. A. (2002). Regulation of heterochromatic silencing and histone H3 lysine-9 methylation by RNAi. *Science (New York, N.Y.)*, *297*(5588), 1833–1837. https://doi.org/10.1126/SCIENCE.1074973
Watts, B. R., Wittmann, S., Wery, M., Gautier, C., Kus, K., Birot, A., Heo, D. H., Kilchert, C., Morillon, A., & Vasiljeva, L. (2018). Histone deacetylation promotes transcriptional silencing at facultative heterochromatin. *Nucleic Acids Research*, *46*(11), 5426–5440. https://doi.org/10.1093/NAR/GKY232
West, R. R., Vaisberg, E. v., Ding, R., Nurse, P., & Richard McIntosh, J. (1998). cut11(+): A gene required for cell cycle-dependent spindle pole body anchoring in the nuclear envelope and bipolar spindle formation in Schizosaccharomyces pombe. *Molecular Biology of the Cell*, *9*(10), 2839–2855. https://doi.org/10.1091/MBC.9.10.2839
Wirén, M., Silverstein, R. A., Sinha, I., Walfridsson, J., Lee, H. M., Laurenson, P., Pillus, L., Robyr, D., Grunstein, M., & Ekwall, K. (2005). Genome wide analysis of

nucleosome density histone acetylation and HDAC function in fission yeast. *The EMBO Journal*, *24*(16), 2906–2918. https://doi.org/10.1038/SJ.EMBOJ.7600758

Xhemalce, B., & Kouzarides, T. (2010). A chromodomain switch mediated by histone H3 Lys 4 acetylation regulates heterochromatin assembly. *Genes & Development*, *24*(7), 647–652. https://doi.org/10.1101/GAD.1881710

Xu, Q. R., Yan, L., Lv, Q. Z., Zhou, M., Sui, X., Cao, Y. B., & Jiang, Y. Y. (2014). Molecular genetic techniques for gene manipulation in Candida albicans. *Virulence*, *5*(4), 507. https://doi.org/10.4161/VIRU.28893

Yam, C., He, Y., Zhang, D., Chiam, K. H., & Oliferenko, S. (2011). Divergent strategies for controlling the nuclear membrane satisfy geometric constraints during nuclear division. *Current Biology : CB*, *21*(15), 1314–1319. https://doi.org/10.1016/J.CUB.2011.06.052

Yamashita, Y. M., Nakaseko, Y., Kumada, K., Nakagawa, T., & Yanagida, M. (1999). Fission yeast APC/cyclosome subunits, Cut20/Apc4 and Cut23/Apc8, in regulating metaphase-anaphase progression and cellular stress responses. *Genes to Cells : Devoted to Molecular & Cellular Mechanisms*, *4*(8), 445–463. https://doi.org/10.1046/J.1365-2443.1999.00274.X

Yang, X., Klein, R., Tian, X., Cheng, H. T., Kopan, R., & Shen, J. (2004). Notch activation induces apoptosis in neural progenitor cells through a p53-dependent pathway. *Developmental Biology*, *269*(1), 81–94. https://doi.org/10.1016/J.YDBIO.2004.01.014

Yuasa, T., Hayashi, T., Ikai, N., Katayama, T., Aoki, K., Obara, T., Toyoda, Y., Maruyama, T., Kitagawa, D., Takahashi, K., Nagao, K., Nakaseko, Y., & Yanagida, M. (2004). An interactive gene network for securin-separase, condensin, cohesin, Dis1/Mtc1 and histones constructed by mass transformation. *Genes to Cells : Devoted to Molecular & Cellular Mechanisms*, *9*(11), 1069–1082. https://doi.org/10.1111/J.1365-2443.2004.00790.X

Zach, R. (2018). *The phenomenon of lipid metabolism " cut " mutants*. *July*, 631–637. https://doi.org/10.1002/yea.3358

Zach, R., Tvarůžková, J., Schätz, M., Tupa, O., Grallert, B., & Převorovský, M. (2018). Mitotic defects in fission yeast lipid metabolism "cut" mutants are suppressed by ammonium chloride. *FEMS Yeast Research*, *18*(6). https://doi.org/10.1093/FEMSYR/FOY064

Zhang, K., Mosch, K., Fischle, W., & Grewal, S. I. S. (2008). Roles of the Clr4 methyltransferase complex in nucleation, spreading and maintenance of heterochromatin. *Nature Structural & Molecular Biology*, *15*(4), 381–388. https://doi.org/10.1038/NSMB.1406

Zhu, Q., Zheng, F., Liu, A. P., Qian, J., Fu, C., & Lin, Y. (2016). Shape Transformation of the Nuclear Envelope during Closed Mitosis. *Biophysical Journal*, *111*(10), 2309–2316. https://doi.org/10.1016/J.BPJ.2016.10.004

10 Supplementary materials

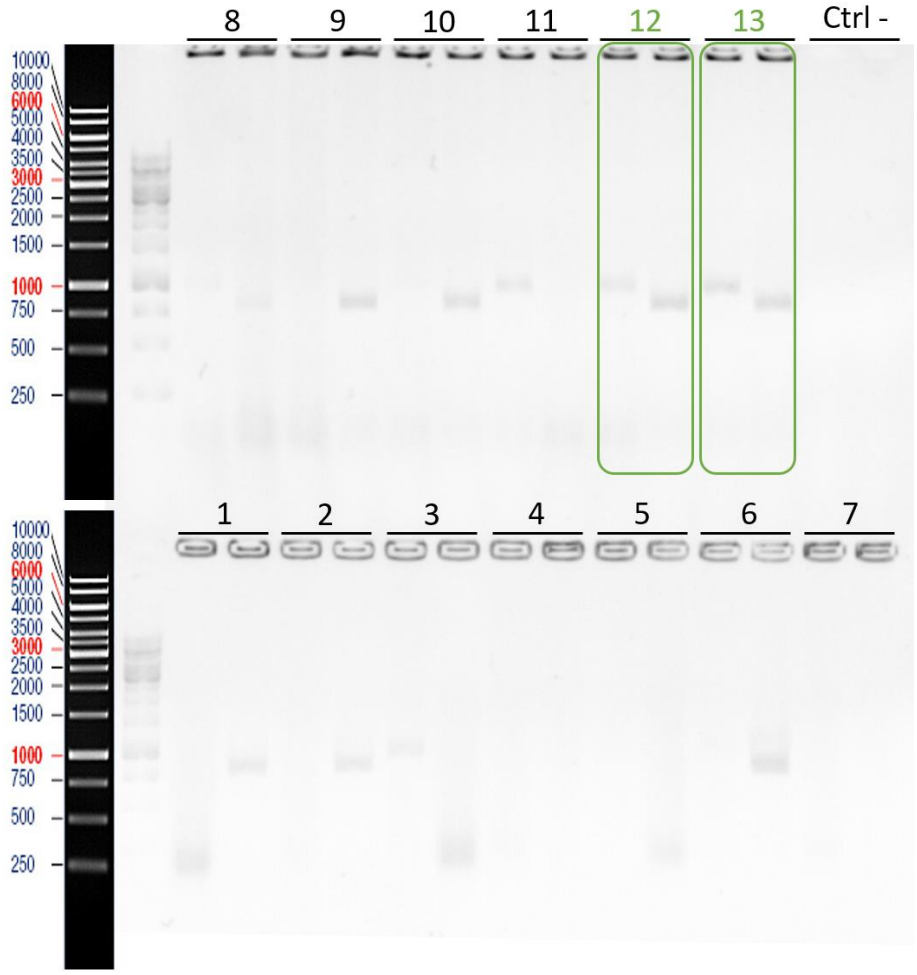

Supplementary figure 1 - Verification of *cbf11* deletion in double-tagged strain. Presence of both upstream and downstream plasmid integration regions is desired. The DNA fragment sizes of these regions are 953 bp and 823 bp respectively. Reaction without template was used as negative control for reactions of both upstream and downstream integration regions (Ctrl-). PCR products were separated in 1.5% agarose gel and visualised by UV light (illuminator Azure biosystems c150). GeneRuler 1kb DNA Ladder (ThermoScientific) was loaded in the gel together with the PCR reactions. The DNA ladder is aligned to correctly estimate the size of desired DNA fragments. Numbers indicate the order of the colonies on the plate. The order of PCR reactions for every template is reaction for downstream region on the left and upstream region on the right. Picked colonies for further use are marked with the green colour.

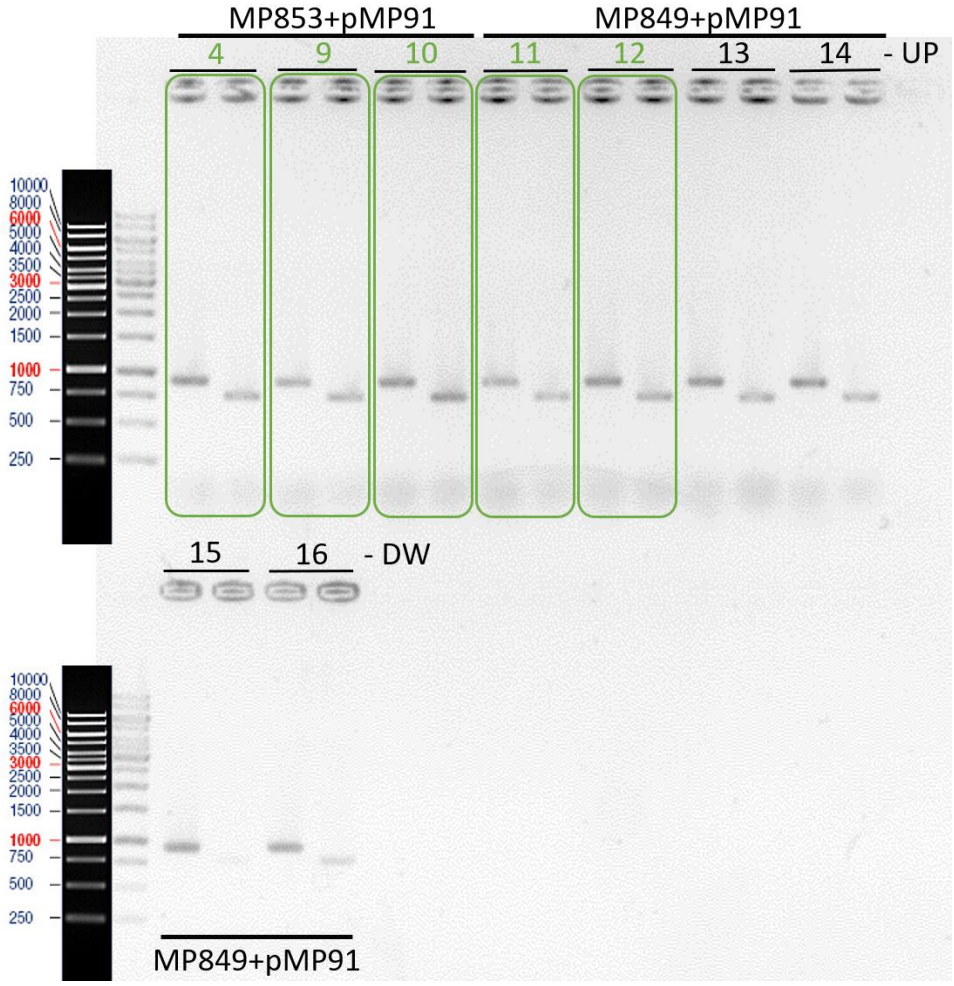

Supplementary figure 2 - Verification of *cbf11* deletion in *hst2Δ* and *clr3Δ* strains. Presence of both upstream and downstream plasmid integration regions is desired. The DNA fragment sizes of these regions are 953 bp and 823 bp respectively. Reaction without template was used as negative control for reactions of both upstream (UP -) and downstream (DW -) integration regions. PCR products were separated in 1.5% agarose gel and visualised by UV light (illuminator Azure biosystems c150). GeneRuler 1kb DNA Ladder (ThermoScientific) was loaded in the gel together with the PCR reactions. The DNA ladder is aligned to correctly estimate the size of desired DNA fragments. Numbers indicate the order of the colonies on the plate. The order of PCR reactions for every template is the reaction for the downstream region on the left and the upstream region on the right. Picked colonies for further use are marked with a green colour.

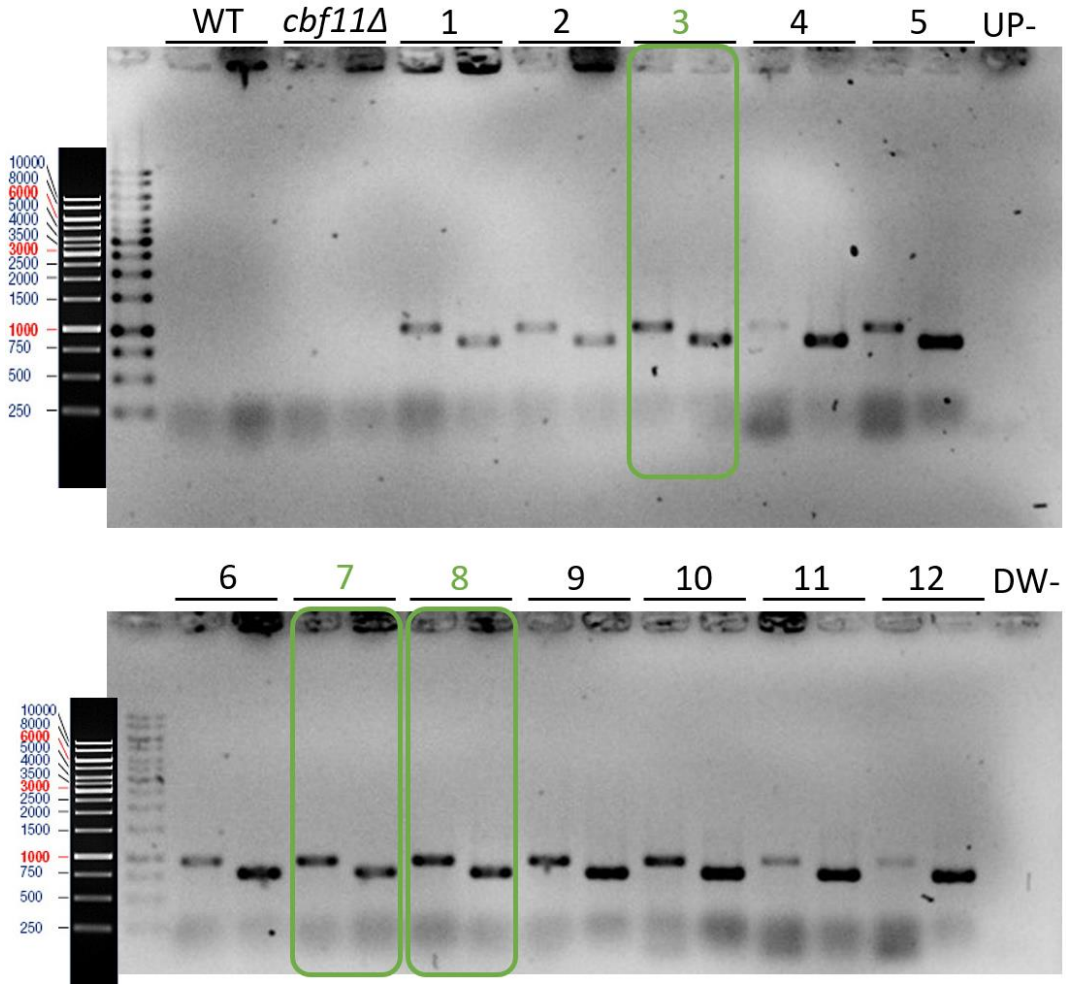

Supplementary figure 3 - Verification of *cbf11* deletion in *hos2Δ* strain. The presence of both upstream and downstream plasmid integration regions is desired. The DNA fragment sizes of these regions are 953 bp and 823 bp respectively. A reaction without a template was used as negative control for reactions of both upstream (UP -) and downstream (DW -) integration regions. PCR products were separated in 1.5% agarose gel and visualised by UV light (illuminator Azure biosystems c150). GeneRuler 1kb DNA Ladder (ThermoScientific) was loaded in the gel together with the PCR reactions. The DNA ladder is aligned to correctly estimate the size of desired DNA fragments. Numbers indicate the order of the colonies on the plate. The order of PCR reactions for every template is the reaction for the downstream region on the left and the upstream region on the right. Picked colonies for further use are marked with a green colour.